USL Report No. 827

The Acoustic Field in a Closed Space Behind a Rectangular Simply Supported Plate Excited By Boundary Layer Turbulence

WAYNE A. STRAWDERMAN
Special Developments Branch
Submarine Sonar Division

11 May 1967

Distribution of this document is unlimited.

U. S. Navy Underwater Sound Laboratory
Fort Trumbull, New London, Connecticut

ABSTRACT

An analytic solution is obtained for the acoustic pressure statistics in a closed rectangular shaped cavity behind a simply supported, rectangular plate excited by boundary layer turbulence. The contribution of the cavity acoustic pressure is neglected as contributing to the plate excitation, leaving only the turbulent pressure fluctuations as the exciting force. The mathematical model for the turbulent pressure statistics is based on that of Corcos, which agrees well with experiment. A byproduct of this analysis is an analytic solution for the turbulent flow excited plate vibration velocity statistics. The plate velocity and cavity acoustic pressure statistics are expressed in the form of cross power spectral densities and power spectral densities. Dimensionless forms of the plate velocity spectral density and cavity acoustic pressure spectral density are developed.

The dimensionless plate velocity spectral density and dimensionless cavity acoustic pressure spectral density were computed, by means of a digital computer, for selected values of dimensionless input parameters. From these computed dimensionless spectra, the effects of major parameters on the plate velocity spectral density and the cavity acoustic pressure spectral density were determined.

A "peak spectrum," constructed by connecting the major spectral peaks in the plate velocity or cavity acoustic pressure spectra, proved to be a useful engineering concept. Knowledge of the "peak spectrum" is equivalent to knowledge of the maximum plate velocity or cavity acoustic pressure spectral levels for a particular set of input parameters. Based on the computed dimensionless spectra, mathematical expressions are derived for the dimensionless plate velocity "peak spectral density" and the cavity acoustic pressure "peak spectral density" over a limited range of dimensionless frequency. The computed simply supported plate velocity "peak spectrum" compares well with the plate velocity "peak spectrum" constructed from experimental measurements on a fixed edge plate above the first plate natural frequency. No experimental data exists for the cavity acoustic pressure.

Comparison of the computed dimensionless cavity acoustic pressure spectral density at the plate and the dimensionless turbulent pressure spectral density allowed formulation of criteria under which the cavity acoustic pressure was negligible compared to the turbulent pressure. As this analysis assumed the cavity acoustic pressure to be negligible compared to the turbulent pressure, the aforementioned criteria are, in effect, limits of applicability of this analysis.

ADMINISTRATIVE INFORMATION

This study was originally prepared as a dissertation in partial fulfillment of the requirements for the degree Doctor of Philosophy in Applied Mechanics at the University of Connecticut. The work was accomplished under USL Project No. 7-1-052-00-00 and the Navy Subproject and Task No. ZR 011 01 01.

The author wishes to express his gratitude to Dr. Ronald Brand for his guidance in the accomplishment of this work. Dr. Wendell Davis, Dr. Norman Small, and Professor Victor Scottron were of assistance in the preparation of the manuscript. The assistance of Donald Kass, Arthur Yacubian, and Marvin Goldstein, of the U. S. Navy Underwater Sound Laboratory, and Mrs. Sharon Good, of the David Taylor Model Basin, in the programming of this analysis for digital computer is gratefully acknowledged. The computations were performed at the Underwater Sound Laboratory and at the David Taylor Model Basin. Finally, the author wishes to express his gratitude to the Underwater Sound Laboratory for supporting this work.

REVIEWED AND APPROVED: 11 May 1967

H. E. Nash
H. E. Nash
Technical Director

R L Corkran Jr
R. L. Corkran, Jr., Captain, USN
Commanding Officer and Director

TABLE OF CONTENTS

Chapter			Page
	4.3.2	Cavity Acoustic Pressure Cross Correlation. .	37
	4.3.3	Cavity Acoustic Pressure Cross Spectral Density	41
	4.3.4	Cavity Acoustic Pressure Spectral Density . .	45
	4.4	Non-Dimensional Spectra	47
	4.4.1	Dimensionless Plate Velocity Spectral Density .	47
	4.4.2	Dimensionless Cavity Acoustic Pressure Spectral Density	51
V.	RESULTS		54
	5.1	Results of Plate Velocity Spectral Density Computations.	55
	5.1.1	Comparison with Existing Experimental Data .	55
	5.1.2	Effect of Major Parameters on Plate Velocity Spectrum	59
	5.1.2.1	Effect of Plate Coordinates	60
	5.1.2.2	Effect of Plate Damping	62
	5.1.2.3	Effect of Plate Rigidity	64
	5.1.3	Dimensionless Plate Velocity "Peak Spectral Density"	65
	5.2	Results of Cavity Acoustic Pressure Spectral Density Computations	69
	5.2.1	Effect of Major Parameters on the Cavity Acoustic Pressure Spectrum	70
	5.2.1.1	Effect of Cavity Coordinates	72
	5.2.1.2	Effect of Speed of Sound of Cavity Fluid . . .	74
	5.2.1.3	Effects of Damping and Frequency	77
	5.2.1.4	Effect of Plate Rigidity	78
	5.2.1.5	Dimensionless Cavity Acoustic Pressure "Peak Spectrum"	82
	5.2.2	Limits of Applicability of Theory	85
VI.	SUMMARY AND CONCLUSIONS		91
BIBLIOGRAPHY	. . . .		96

LIST OF TABLES

LIST OF ILLUSTRATIONS

Figure		Page

Figure		Page

SYMBOLS

a	Plate and acoustic cavity dimension in x-coordinate (longitudinal) direction
b	Plate and acoustic cavity dimension in y-coordinate (lateral) direction
b^{+}	Dimensionless plate and acoustic cavity dimension defined in equation (4.129)
c	Speed of sound in acoustic medium
c^{+}	Dimensionless speed of sound defined in equation (4.140)
d	Acoustic cavity dimension in z-coordinate (depth) direction
db	Decibel $[10 \log_{10} \Phi(\omega)]$
d^{+}	Dimensionless cavity dimension defined in equation (4.140)
$f_{qrst}(\Omega)$	Defined by equation (4.110)
$g_{jkmn}(z_1, z_2, \omega)$	Defined by equation (4.113)
$h(x, x', y, y', \theta)$	Plate displacement response to a unit impulsive force
i	Square root of minus one
k	Acoustic wave number defined in equation (4.78)
k_x	Acoustic wave number in the x-coordinate direction
k_y	Acoustic wave number in the y-coordinate direction
$k_{z_{jk}}(\omega)$	Acoustic wave number in the z-coordinate direction

$k^+_{z_{jk}}(\omega^+)$	Dimensionless acoustic wave number in the z-coordinate direction
p_t	Turbulent boundary layer wall pressure
p_a	Cavity acoustic pressure
r	Effective plate damping coefficient per unit area
$r_{c_{mn}}$	Critical plate damping coefficient for the m-n*th* mode
r^+	Dimensionless plate damping coefficient defined in equation (4.129)
$r^+_{c_{mn}}$	Dimensionless critical plate damping coefficient for the m-n*th* mode
t	Time coordinate
t'	Time at which impulsive force occurs
$\vec{u}$	Acoustic phase velocity vector
u_x	Acoustic phase velocity in the x-coordinate direction
u_y	Acoustic phase velocity in the y-coordinate direction
u_z	Acoustic phase velocity in the z-coordinate direction
w	Plate displacement in the z-coordinate direction
x	Longitudinal spacial coordinate
x^+	Dimensionless longitudinal spacial coordinate defined by equation (4.130)
y	Lateral spacial coordinate
y^+	Dimensionless lateral spacial coordinate defined by equation (4.130)

z^+	Dimensionless spacial coordinate defined by equation (4.141)
A	Defined in equation (4.40)
$A(\omega\xi/U_c)$	Functional dependence of the turbulent boundary layer wall pressure cross spectral density on the longitudinal coordinate
$B(\omega\eta/U_c)$	Functional dependence of the turbulent boundary layer wall pressure cross spectral density on the lateral coordinate
C_j	Arbitrary constants
D	Plate flexural rigidity
D^+	Dimensionless plate flexural rigidity
$E[\ ]$	Denotes ensemble average
$F_{qrst}(x_1, x_2, y_1, y_2)$	Defined by equation (4.109)
G_{ns}	Defined by equation (4.54)
$G^+_{mn}(\omega^+)$	Defined by equation (4.134)
$G_{jkmn}(x_1, x_2, y_1, y_2)$	Defined by equation (4.112)
$H(x, x', y, y', \omega)$	Complex frequency response of plate
$I_{1_{mq}}$	Defined by equation (4.40)
$I_{2_{ns}}$	Defined by equation (4.41)
$K_{jkmnqrst}$	Defined by equation (4.119)
M	Dimensionless fluid mass defined by equation (4.129)
P_n	Defined by equation (4.55)
$P^+_n(\omega^+)$	Defined by equation (4.135)

$Q_{\phi\phi}(x_1,x_2,y_1,y_2,t_1,t_2)$	Plate velocity cross correlation
$Q_{aa}(x_1,x_2,y_1,y_2,z_1,z_2,t_1,t_2)$	Cavity acoustic pressure cross correlation
R_m	Defined by equation (4.146)
$R_m^+(\omega^+)$	Defined by equation (4.131)
$S_{\phi\phi}(x_1,x_2,y_1,y_2,\omega)$	Plate velocity cross spectral density
$S_{aa}(x_1,x_2,y_1,y_2,z_1,z_2,\omega)$	Cavity acoustic pressure cross spectral density
$S_{pp}(\xi,\eta,\omega)$	Turbulent wall pressure cross spectral density
T_{mn}	Defined by equation (4.57)
$T_{mn}^+(\omega^+)$	Defined by equation (4.136)
U_o	Free stream velocity of flowing fluid in x-coordinate direction
U_c	Mean convection velocity of turbulent boundary layer
U^+	Dimensionless free stream velocity defined by equation (4.129)
$U_{jkmn}^+(\omega^+)$	Defined by equation (4.143)
V_{mnqs}	Defined by equation (4.59)
W_{mnqs}	Defined by equation (4.67)
$W_{mnqs}^+(\omega^+)$	Defined by equation (4.137)
$X_{j\ell}(\omega)$	Defined by equation (4.85)
$Y_{j\ell}(\omega)$	Defined by equation (4.89)
a	A dimensionless constant
$a_{mn}(x,y)$	Plate normalized natural mode shapes
$\delta_{j\ell}$	Kronecker delta
$\delta(\omega-\Omega)$	Dirac delta function

δ^*	Turbulent boundary layer displacement thickness
δ^+	Dimensionless turbulent boundary layer displacement thickness defined by equation (4.129)
$\zeta(x, x', y, y', \theta)$	Plate velocity response to a unit impulsive force
η	Relative lateral coordinate $(y - y')$
θ	Relative time coordinate $(t - t')$
λ_{mn}	Phase angle defined by equation (4.52)
μ	Effective mass of plate per unit area
ν_m	Phase angle defined by equation (4.43)
ξ	Relative longitudinal coordinate $(x - x')$
ρ_f	Mass density of flowing fluid
ρ_{a_o}	Time average mass density of acoustic medium
ρ_a	Instantaneous mass density of acoustic medium
τ	Time difference $(t_2 - t_1)$
ϕ	Plate velocity
ψ	Acoustic velocity potential
ω	Radial frequency
ω^+	Dimensionless radial frequency
ω_{mn}	Natural frequency of m-n mode of plate
ω^+_{mn}	Dimensionless natural frequency of m-n mode of plate
∇^4	Biharmonic operator
$\Phi(\omega)$	Turbulent wall pressure spectral density
$\Phi^+(\omega)$	Dimensionless turbulent wall pressure spectral density
$\Phi_\phi(x, y, \omega)$	Plate velocity spectral density

$\Phi^+_{\phi}(x^+, y^+, \omega^+)$	Dimensionless plate velocity spectral density
$\Phi_a(x, y, z, \omega)$	Cavity acoustic pressure spectral density
$\Phi^+_a(x^+, y^+, z^+, \omega^+)$	Dimensionless cavity acoustic pressure spectral density
$\Phi_{\phi_p}(x, y, \omega)$	Plate velocity "peak spectral density"
$\Phi^+_{\phi_p}(x^+, y^+, \omega^+)$	Dimensionless plate velocity "peak spectral density"
$\Phi^+_{a_p}(x^+, y^+, z^+, \omega^+)$	Dimensionless cavity acoustic pressure "peak spectral density"
$X(\omega)$	Defined by equation (4.111)
Ω	Radial frequency

I

INTRODUCTION

Flow induced noise is largely responsible for limiting submarine and surface ship sonar performance, producing objectionable noise levels inside high speed aircraft, and producing relatively high vibration levels in the propulsion systems of modern spacecraft which increase the probability of failure of system components. Because of this wide variety of problems, theoretical and experimental research in flow noise and flow induced noise has increased in the past decade. The research in flow noise has been aimed at defining a statistical model for the turbulent boundary layer pressure and/or velocity which provides the excitation to the mechanical system. The research in flow induced noise has been primarily aimed at theoretical solutions for the response characteristics of various systems using mathematically tractable approximations to the turbulent boundary layer excitation. Certain experimental studies of flow induced noise in simple systems have also been performed.

To date, although there is general agreement in the measurements of boundary layer pressure statistics, there is not complete agreement as to the mathematical model of these statistics. Also, although a wide variety of elementary flow induced noise problems have been studied, few have used any of the existing, experimentally based, mathematical models for the boundary layer excitation.

It is the purpose of this study to add to the understanding of flow induced noise by investigating the effects of major parameters on the sound field produced in a closed space behind a simply supported plate excited by boundary layer turbulence utilizing an existing, experimentally based mathematical model of the turbulent wall pressure.

II
OBJECTIVES

The objective of this study is to provide the submarine sonar systems designer with information concerning: (1) the acoustic environment of sonar transducers; and (2) the major parameters which may affect this environment.

The above objective has been attacked by means of an analytical study of the acoustic field in a closed space behind a simply supported, rectangular, flat plate which is excited by turbulent boundary layer pressure fluctuations. The closed space is bounded by five rigid walls and the flexible plate. A sketch of the model used in this analysis is shown in Figure 1. This model provides a fair representation of the acoustic environment of sonar transducers in submarines.

III

TECHNICAL APPROACH

3.1 Technical Background

The purpose of this section is twofold. First, it summarizes work in the field of flow and flow induced noise. Secondly, it provides justification for certain assumptions made in the analysis to follow.

3.1.1 Theoretical Studies in Flow Induced Noise

Early theoretical studies in the field of flow induced noise were directed toward a prediction of noise in aircraft fuselages [1, 2]. The mathematical models of the turbulent boundary layer in these studies were not based on experimental evidence. During this same period, Lyon [3] studied the response of strings to random excitation, Eringen [4] derived expressions for the response of beams and plates to random pressure fields, and Kraichnan [5] studied the free radiation of sound from turbulent excitation of a series of thin, stiff flat plates. Again, the excitation, although characteristic of boundary layer turbulence in certain respects, was not compatible with experimental data.

Dyer [6] was one of the first to study the coupled plate vibration-acoustic radiation problem. He assumed the boundary layer pressure correlation function to be the product of a convected spacial delta function, a fixed spacial delta function, an amplitude, and a decaying function of time. Although the delta functions were relatively poor approximations to the actual longitudinal and lateral pressure correlations, the convection and time decay were phenomena which agreed with experiments. The above excitation was used in a normal mode approach to the prediction of the acoustic field in a closed space behind a simply supported, flow excited, flat plate. The walls enclosing the space were pressure release surfaces. Although Dyer's input was not precise, it provided insight into the behavior of the model considered and encouraged further work utilizing normal mode theory.

A short time layer, Dyer [7] used the same model of the turbulent pressure correlation to calculate the displacement correlation function of a turbulence excited flat plate. About this same time, Strasberg [8] used a mathematical model of the turbulent pressure correlation based on the data of Harrison [9] to predict the displacement spectral density of plates and membrances. This was one of the first cases where experimentally based inputs were used.

Powell [10] investigated the fatigue of structures excited by random pressure fields and indicated that the response cross spectral density is maximized when the incident pressure correlation matches the modal wavelength. Although this is a possible condition in spacecraft because of their high speeds, it is not likely to occur in submarines.

Maidanik and Lyon [11] studied the response of strings to moving noise fields using the Dyer delta function model for the pressure correlation.

From 1960 to the present, an extensive research program in flow noise and flow induced noise has been conducted at the University of Southampton. This program yielded a recent paper by Mercer [12] in the response of multi-supported beams to a random pressure field.

Tack and Lambert [13] derived general expressions for the response of plates and bars to boundary layer turbulence.

A recent paper by White [14] used an experimentally based expression for the turbulent pressure cross spectral density to predict the response and consequent sound radiation from a rectangular flat plate. The response of the plate and the acoustic radiation are averaged over frequency bands so that the details of the response are bypassed, and only the effect of such gross parameters as panel modal density and boundary layer characteristics are investigated. White obtains very good agreement between theory and experiment within these assumptions.

Bull et al. [15], as a part of the University of Southampton effort, calculated the displacement spectral density of flat plates due to turbulent excitation. They used a normal mode approach to the plate problem and an experimentally based expression for the turbulent pressure correlation as input. Collier [16], using an approximation to the turbulent pressure correlation function, calculated the plate acceleration correlation functions and acoustic pressure field radiated from the plate into an infinite fluid space at rest.

Pretlove [17] presents the theory, from a normal mode approach, for calculating the displacement spectral density of a simply supported panel, backed by a rectangular closed cavity. In the forcing function for the plate, he makes provision for both the turbulent pressure and the resultant acoustic pressure in the cavity. He does not, however, solve this problem for any particular model of the turbulent pressure. From his theory, however, he states that the effect of the backing cavity is most severe in the cases of thin panels covering shallow cavities.

3.1.2 Experimental Studies in Flow Induced Noise

Few experimental studies of flow induced noise appear in the literature. El Baroudi, Ludwig, and Ribner [18] experimentally investigated the displacement correlation properties of a flow excited plate and the resultant total sound power radiated into a reverberant room. In a related effort, el Baroudi [19] measured the displacement correlation properties and displacement spectral density of thin flat plates excited by turbulent boundary layers.

Bull et al. [15] measured the displacement spectra of thin flat plates due to turbulent excitation. The plates were effectively mounted in a fixed manner, and the experimental results were compared to the theoretically predicted spectra for the simply supported case using an experimentally based model for pressure correlation as input. As might be expected, agreement between theoretical and experimental results was not good.

Maestrello [20] measured the sound power spectra radiated into a reverberation chamber from turbulence-excited plates. In another paper [21] he measured the plate displacement correlation function for turbulence excited plates.

3.1.3 Theoretical Studies of Flow Noise

Flow noise, as used in this study, refers to the wall pressure fluctuations produced by a turbulent boundary layer. The mathematical theory of pressure fluctuations in homogeneous, isotropic turbulence is well developed [22, 23, 24, 25, 26]. However, because of its extreme complexity, the problem of pressure fluctuations produced by a turbulent boundary layer has not been treated extensively.

Kraichnan [27, 28], Lilley and Hodgson [29], and Sternberg [30] have made theoretical studies aimed at computing the mean of the turbulent wall pressure, but the space-time correlation properties (or their Fourier transform) are required in order to treat flow induced noise problems.

Two attempts have been made to predict the correlation properties of turbulent wall pressure fluctuations. Gardner [31], starting with the Navier-Stokes equations, attempted to predict the wall pressure correlation by assuming forms for the various velocity correlations occurring in his expressions. His results were in sharp disagreement with experiment. White [32], claiming that Gardner's approach was sound and that mathematical errors were the cause of the discrepancy between theory and experiment, attacked the same problem through Gardner's approach. White calculated the turbulent wall pressure cross correlation function, lateral and longitudinal cross spectral densities, and convection velocity. White's predictions agree reasonably well with experiment except in the case of the wall spectral density where there is a large discrepancy between predicted and experimental results. White shows that the pressure cross spectral density is approximately equal to the product of the lateral and longitudinal cross spectral densities, which bears out a previous empirical prediction by Corcos [33].

3.1.4 Experimental Studies in Flow Noise

The first reliable measurements of turbulent boundary layer pressure statistics were made by Willmarth [34] in 1956. Harrison [9] in 1958 published the first measurements of the wall pressure cross spectral density. Since these measurements, many experimenters have measured the turbulent wall pressure cross spectral density and correlation functions. Extensive bibliographies of this work are presented by White [35] and Bull et al. [15], and only selected references will be presented in this study.

Bakewell et al. [36] published extensive data of mean square pressure, pressure spectral densities, and pressure correlation functions from experiments in a 3-1/2-inch-diameter turbulent air flow facility.

Using both theoretical arguments and data obtained at the Ordnance Research Laboratory at Pennsylvania State University, Skudrzyk and Haddle [37] derived the following semi-empirical expression for the turbulent wall pressure spectrum as measured with very small transducers:

$$\begin{aligned} \Phi(\omega) &= 0.75 \times 10^{-5} a^2 \rho_f^2 U_o^3 \delta^* & \omega &\leq 1.256 \frac{U_o}{\delta^*} \\ \Phi(\omega) &= 1.5 \times 10^{-5} a^2 \frac{\rho_f^2 U_o^6}{\omega^3 \delta^{*2}} & \omega &> 1.256 \frac{U_o}{\delta^*} \end{aligned} \tag{3.1}$$

where a is a constant which takes on different values for different fluids. For water,

$$a \cong 1.0$$

and for air,

$$a \cong 3.0 \tag{3.2}$$

Although this expression is not in exact agreement with experimental data in shape because of the discontinuous nature of (3.1), it shows good agreement with experimental data in both amplitude and shape at frequencies above the discontinuity and a reasonable approximation to the amplitude at frequencies below the discontinuity. The agreement between (3.1) and experimental data will be discussed further in Section 4.1.

Willmarth and Wooldridge [38] reported further measurements in 1962, designed to provide more detailed statistical properties of the wall pressure fields. About this same time, Serafini [39] published new data of wall pressure measurements.

Corcos [33, 40], using the data of Willmarth, Bakewell, and Serafini, stated that the turbulent wall pressure cross spectral density function could be expressed as

$$S_{pp}(\xi,\eta,\omega) = \Phi(\omega)\, A\left(\frac{\omega\xi}{U_c}\right) B\left(\frac{\omega\eta}{U_c}\right) e^{-i(\omega\xi/U_c)}. \qquad (3.3)$$

Plots of $A(\omega\xi/U_c)$ and $B(\omega\eta/U_c)$ are also included in Corcos' work and are reproduced in Figures 2 and 3. Corcos went on to predict the error resulting from the measurement of the turbulent wall pressure field with finite-size transducers and presented a means of correcting measurements for this error.

Researchers at the University of Southampton have made extensive measurements of the turbulent wall pressure statistics. The resulting reports are summarized in the 1963 report by Bull et al.[15]. Willmarth and Roos [41], incorporating Bull's data, reattacked the problem of resolution by finite-size transducers on the basis that Corcos' similarity form for the cross spectral density, equation (3.3), although accurate over a wide frequency range, failed to provide accurate hydrophone size corrections at high frequencies. Willmarth indicates that the reason for this limitation is that (3.3) is inaccurate at small spacial separations. However, as Willmarth points out, wall pressure correlation measurements at small spacial separations have never been made because of experimental difficulties. He therefore does not propose an alternate form to (3.3).

Some of the data mentioned above have been obtained at the walls of circular pipes and others at the surfaces of flat plates. The lack of any significant difference between the pressure spectra obtained in both cases is indicated in a recent work by Schloemer [42], who measured turbulent wall pressure data in the presence of favorable and adverse pressure gradients.

IV

THEORETICAL DEVELOPMENT

The model treated in this analysis was a simply supported, rectangular, flat plate mounted in an infinite rigid baffle and backed by a rectangular cavity with rigid walls. Fluid flows over the top of the rigid baffle and plate, and the cavity is filled with an acoustic fluid. A graphic representation of this model is presented in Figure 1.

In order to determine the acoustic pressure field within the cavity, it would ordinarily be necessary to determine the vibration of the plate due to the combined turbulent and cavity acoustic pressure excitations. The cavity acoustic phase velocity at the plate would then be equated to the plate velocity, resulting in an integral equation for the acoustic velocity potential. The various constants resulting from the solution of this integral equation would be determined by the remaining boundary conditions, which require that the acoustic phase velocity be zero on the rigid cavity walls. Pretlove [17] used an approach similar to the above in computing the plate displacement spectral density for a model identical to that described above. However, Pretlove discovered that the cavity acoustic pressure had little effect on the plate displacement spectral density except in cases of thin plates covering shallow cavities. For submarine applications, the plates covering the cavities are not thin and, therefore, in accordance with Pretlove's results, it is assumed in this analysis that the cavity acoustic pressure provides negligible excitation to the plate; that is, the only forces exciting plate vibrations are those associated with the turbulent boundary layer pressure fluctuations.

The above assumption simplifies the problem considerably. To compute the cavity acoustic pressure field, it is now merely necessary to compute the plate vibration velocity due to the turbulent boundary layer excitation and to equate this result to the cavity acoustic phase velocity at the plate. The resulting acoustic velocity potential must also satisfy the zero velocity condition at the rigid walls. Hence, it is only necessary to determine a model for the turbulent boundary layer pressure statistics in order to solve the above problem.

Since the turbulent boundary layer pressure is a random phenomenon, the cavity acoustic pressure resulting from the boundary layer excitation of the plate will also be a random phenomenon. Random processes are usually treated in terms of their space-time correlations or in terms of their spectral properties in the frequency domain. Collier's recent work [16] on the vibration and acoustic radiation of turbulence excited plates indicated certain computational difficulties arising from treatment of the statistical properties in the time domain. Therefore, in this analysis, random variables will be described in terms of their spectral properties in the frequency domain.

4.1 Mathematical Model of the Turbulent Wall Pressure Cross Spectral Density

The mathematical model of the turbulent wall pressure cross spectral density selected for use in this analysis was that of Corcos [33], which is given by (3.3) and is repeated here for reference.

$$S_{pp}(\xi,\eta,\omega) = \Phi(\omega)\, A\left(\frac{\omega\xi}{U_c}\right) B\left(\frac{\omega\eta}{U_c}\right) e^{-i(\omega\xi/U_c)}. \tag{3.3}$$

Corcos' model was selected for two reasons. First, its mathematical form is such that space variables are separated, thereby easing computational difficulties. Secondly, Corcos' model was used to theoretically predict transducer size corrections which agree well with measurements over a wide range of frequencies. Thus, subject to the limitation at high frequencies discussed in Section 3.1.4, Corcos' model of the turbulent wall pressure cross spectral density provided a realistic and mathematically attractive model for this analysis.

Before proceeding further, it is necessary to discuss the limitations in applicability of equation (3.3). Since ξ and η are relative coordinates, equation (3.3) tacitly assumes homogeneous stationary turbulence. Therefore, Corcos' model of the cross spectral density is strictly applicable only to the case of a flow having zero pressure gradient and constant boundary layer thickness. However, equation (3.3) can be used with good accuracy for turbulent flows in which slow boundary layer growth and small pressure gradients occur. In this analysis, the flow is assumed to have the following characteristics:

a. constant boundary layer thickness over the plate,

b. zero pressure gradient.

Corcos [33] also shows that the convection velocity is a function of the Strouhal Number $\omega\delta^*/U_0$. This relationship is shown in Figure 4. Since the variation of the convection velocity is not large over a wide range of Strouhal Number, it is further assumed in this analysis that the convection velocity is a constant given by

$$U_c = 0.65\, U_o . \tag{4.1}$$

Figures 2 and 3 present curve fits to experimental data for the functions $A(\omega\xi/U_c)$ and $B(\omega\eta/U_c)$ contained in (3.3). From these figures, the following expressions have been selected to represent the A and B functions based on a balance of curve fit and mathematical simplicity:

$$A\left(\frac{\omega\xi}{U_c}\right) = e^{-0.115|\omega\xi/U_c|} \tag{4.2}$$

and

$$B\left(\frac{\omega\eta}{U_c}\right) = e^{-0.7|\omega\eta/U_c|} . \tag{4.3}$$

Note that equation (4.2) fits the measured value of $A(\omega\xi/U_c)$ very well, whereas equation (4.3) sacrifices some accuracy in fitting the experimental data in favor of mathematical simplicity. The expression

$$B\left(\frac{\omega\eta}{U_c}\right) = \frac{1}{1 + 1.4\left|\frac{\omega\eta}{U_c}\right|}$$

provides a much better fit to the experimental data than does equation (4.3), but its use in the analysis to follow greatly increased the mathematical complexity. Hence, equation (4.3) was selected to represent $B(\omega\eta/U_c)$.

It remains to select an expression for $\Phi(\omega)$ in equation (3.3) in order to completely specify the mathematical form of the turbulent wall pressure cross spectral density. Lilley and Hodgson [29], and Skudrzyk and Haddle [37] have proposed expressions designed to describe the turbulent wall pressure spectral density. The agreement of the Skudrzyk and Haddle expression with experimental results is much better than the Lilley and Hodgson expression. Further, the mathematical form of the Skudrzyk and Haddle model is quite simple. Hence, the Skudrzyk and Haddle expression for the turbulent wall pressure spectral density (equations (3.1) and (3.2)) was used in this model and is repeated here for reference:

$$\Phi(\omega) = 0.75 \times 10^{-5} a^2 \rho_f^2 U_o^3 \delta^* \qquad \omega \leq 1.256 \frac{U_o}{\delta^*}$$
$$\Phi(\omega) = 1.5 \times 10^{-5} a^2 \frac{\rho_f^2 U_o^6}{\omega^3 \delta^{*2}} \qquad \omega > 1.256 \frac{U_o}{\delta^*} , \tag{3.1}$$

where

a = 1.0 for water

a = 3.0 for air .

Figure 5 presents a comparison of the experimental data of Bakewell [36], Schloemer [42], and Bull [15] with the Skudrzyk and Haddle model. The data are for air rather than water because of the greater availability of air data. The agreement between the experimental data and the Skudrzyk and Haddle expression is poor at low non-dimensional frequencies but improves considerably above the cutoff frequency. Although the data of Schloemer and Bull were obtained on flat plates and those of Bakewell in a pipe flow facility, the Skudrzyk and Haddle non-dimensional form brings these data into excellent agreement. It may therefore be assumed that the parametric form of equation (3.1) is valid, but the values of the constants and cutoff frequency could be considerably improved. For this analysis, however. equation (3.1) was used in the original form to describe the turbulent wall pressure spectral density.

Combining equations (3.3), (4.2), (4.3), and (3.1), the turbulent wall pressure cross spectral density may be described by

$$S_{pp}(\xi,\eta,\omega) = 0.75 \times 10^{-5} a^2 \rho_f^2 U_o^3 \delta^* \left[e^{-0.115|\omega\xi/U_c|}\right]\left[e^{-0.7|\omega\eta/U_c|}\right] e^{-i(\omega\xi/U_c)}$$

$$\omega \leq 1.256 \frac{U_o}{\delta^*} ,$$

$$S_{pp}(\xi,\eta,\omega) = 1.5 \times 10^{-5} a^2 \frac{\rho_f^2 U_o^6}{\omega^3 \delta^{*2}} \left[e^{-0.115|\omega\xi/U_c|}\right]\left[e^{-0.7|\omega\eta/U_c|}\right] e^{-i(\omega\xi/U_c)}$$

$$\omega > 1.256 \frac{U_o}{\delta^*} . \tag{4.4}$$

Equation (4.4) is the mathematical model of the turbulent wall pressure cross spectral density used in the analysis to follow. For convenience of reference, the assumptions pertinent to equation (4.4) are summarized as follows:

a. constant boundary layer thickness over the plate,

b. small pressure gradients.

It is further assumed that the ratio of the convection velocity to the free stream velocity is constant as presented in equation (4.1).

4.2 Development of the Plate Velocity Cross Spectral Density

4.2.1 Plate Velocity Response to a Deterministic Pressure

The differential equation governing the displacement of the plate due to the turbulent boundary layer pressure excitation on the plate surface is

$$D\nabla^4 w + r\frac{\partial w}{\partial t} + \mu\frac{\partial^2 w}{\partial t^2} = p_t(x,y,t), \tag{4.5}$$

where

D is the flexural rigidity,

r is the effective damping coefficient per unit area, and

μ is the effective mass per unit area.

The terms "effective mass" and "effective damping" as used above denotes the mass and damping due to the combined effect of the plate and water. In this treatment, for lack of detailed information concerning the effect of the water on mass and damping, the effective mass and the effective damping coefficient are assumed to be constants. It is further tacitly assumed in equation (4.5) that the turbulent pressure field is not affected by the plate motion. The effects of cavity acoustic pressure on the plate and neglected, and the forcing function is only the turbulent pressure.

The solution to equation (4.5) for any arbitrary deterministic pressure field can be determined by a superposition of the normal modes of vibration of the corresponding free-undamped plate, governed by

$$D\nabla^4 w + \mu \frac{\partial^2 w}{\partial t^2} = 0. \tag{4.6}$$

The solutions to equation (4.6) satisfying the simply supported edge conditions shown in Figure 1 are given by

$$w(x,y,t) = a_{mn}(x,y) \sin \omega_{mn} t, \tag{4.7}$$

where the mode shapes and corresponding natural frequencies are given by

$$a_{mn}(x,y) = \frac{2}{\sqrt{ab}} \sin \frac{m\pi y}{a} \sin \frac{n\pi x}{b} \tag{4.8}$$

and

$$\omega_{mn} = \sqrt{\frac{D}{\mu}} \left[\left(\frac{m\pi}{a}\right)^2 + \left(\frac{n\pi}{b}\right)^2\right] \tag{4.9}$$

The normal modes, a_{mn}, form a complete set of orthonormal functions: that is,

$$\int_0^b \int_0^a a_{mn}(x,y)\, a_{qr}(x,y)\, dx\, dy = \delta_{mq}\delta_{nr}. \tag{4.10}$$

It is now assumed that the solution to equation (4.5), for any deterministic pressure, can be written as a sum of the normal modes, each multiplied by a function of time: that is,

$$w(x,y,t) = \sum_{\substack{m=1\\n=1}}^{\infty} \alpha_{mn}(x,y)\,T_{mn}(t). \tag{4.11}$$

where T_{mn} is to be determined.

Substituting (4.11) into (4.5) and utilizing (4.10), one finds that $T_{mn}(t)$ must satisfy

$$\frac{d^2T_{mn}}{dt^2} + \frac{r}{\mu}\frac{dT_{mn}}{dt} + \omega_{mn}^2 T_{mn} = \frac{1}{\mu}\int_0^b\int_0^a p_t(x,y,t)\,\alpha_{mn}(x,y)\,dx\,dy\,. \tag{4.12}$$

At this point, it is convenient to solve equation (4.5) by means of equations (4.11) and (4.12) for two special cases. For the first case, let

$$p_t(x,y,t) = \delta(x-x')\,\delta(y-y')\,e^{i\omega t}, \tag{4.13}$$

that is, a concentrated load applied at (x',y') varying sinusoidally in time. Assume the solution can be written as

$$w(x,y,t) = H(x,x',y,y',\omega)\,e^{i\omega t}. \tag{4.14}$$

Equation (4.14) is the defining statement for $H(x,x',y,y',\omega)$, which is termed the complex frequency response. Solution of (4.12) with $p_t(x,y,t)$ defined by (4.13) results in the following solution via (4.11):

$$w(x,y,t) = \sum_{\substack{m=1\\n=1}}^{\infty} \frac{\alpha_{mn}(x,y)\,\alpha_{mn}(x',y')}{\mu\left[(\omega_{mn}^2 - \omega^2) + \dfrac{ir\omega}{\mu}\right]}\,e^{i\omega t}\,. \tag{4.15}$$

Hence, comparison of (4.15) and (4.14) yields the following solution for the complex frequency response:

$$H(x,x',y,y',\omega) = \frac{1}{\mu} \sum_{\substack{m=1 \\ n=1}}^{\infty} \frac{a_{mn}(x,y)a_{mn}(x',y')}{\left[(\omega_{mn}^2 - \omega^2) + \frac{ir\omega}{\mu}\right]} . \tag{4.16}$$

As the second special case, consider the impulsive loading at (x',y') occurring at time t':

$$p_t(x,y,t) = \delta(x - x')\,\delta(y - y')\,\delta(t - t') \tag{4.17}$$

and, define:

$$\theta = t - t'$$

$$h(x,x',y,y',\theta) = \begin{cases} w(x,y,t) & \theta > 0 \\ 0 & \theta \leqq 0 . \end{cases} \tag{4.18}$$

The solution of equation (4.12), when p_t is as given by (4.17), is

$$T_{mn}(t) = e^{-r\theta/2\mu}\left[C_1 \sin\sqrt{\omega_{mn}^2 - \left(\frac{r}{2\mu}\right)^2}\,\theta + C_2 \cos\sqrt{\omega_{mn}^2 - \left(\frac{r}{2\mu}\right)^2}\,\theta\right]. \tag{4.19}$$

The constants C_1 and C_2 may be evaluated by applying initial conditions appropriate to an impulsive loading, with the following result:

$$T_{mn}(t) = \frac{e^{-r\theta/2\mu}}{\mu\sqrt{\omega_{mn}^2 - \left(\frac{r}{2\mu}\right)^2}}\, a_{mn}(x',y') \sin\sqrt{\omega_{mn}^2 - \left(\frac{r}{2\mu}\right)^2}\,\theta . \tag{4.20}$$

Hence, from (4.11) and (4.18)

$$h(x,x',y,y',\theta) = \frac{e^{-r\theta/2\mu}}{\mu} \sum_{\substack{m=1 \\ n=1}}^{\infty} \frac{a_{mn}(x,y)a_{mn}(x',y')}{\sqrt{\omega_{mn}^2 - \left(\frac{r}{2\mu}\right)^2}} \sin\sqrt{\omega_{mn}^2 - \left(\frac{r}{2\mu}\right)^2}\,\theta \tag{4.21}$$

$$\theta \geqq 0 .$$

By use of (4.21) and the principal of superposition for linear systems, the plate response for any deterministic pressure excitation may be constructed. This is accomplished by considering the excitation pressure field to be the superposition (or summation) of an infinite number of impulses in time and space. Hence, for any deterministic pressure field, the response may be written:

$$w(x,y,t) = \int_{-\infty}^{t}\int_{0}^{b}\int_{0}^{a} p_t(x',y',t')\,h(x,x',y,y',\theta)\,dx'\,dy'\,dt' . \tag{4.22}$$

However, as $\theta = t - t'$, (4.22) may be rewritten as

$$w(x,y,t) = \int_{0}^{\infty}\int_{0}^{b}\int_{0}^{a} p_t(x',y',t-\theta)\,h(x,x',y,y',\theta)\,dx'\,dy'\,d\theta \tag{4.23}$$

In the acoustic problem, the velocity of the plate (rather than the displacement) will be required for the boundary value. Hence, defining

$$\zeta(x,x',y,y',\theta) = \frac{\partial h(x,x',y,y',\theta)}{\partial t} \tag{4.24}$$

as the velocity response of the plate to an impulsive loading, from (4.24) and (4.21) the velocity response is found to be

$$\zeta(x,x',y,y',\theta) = \frac{e^{-r\theta/2\mu}}{\mu} \sum_{\substack{m=1 \\ n=1}}^{\infty} \frac{\alpha_{mn}(x,y)\,\alpha_{mn}(x',y')}{\sqrt{\omega_{mn}^2 - \left(\frac{r}{2\mu}\right)^2}} \left\{ \sqrt{\omega_{mn}^2 - \left(\frac{r}{2\mu}\right)^2} \cos \sqrt{\omega_{mn}^2 - \left(\frac{r}{2\mu}\right)^2}\,\theta - \frac{r}{2\mu} \sin \sqrt{\omega_{mn}^2 - \left(\frac{r}{2\mu}\right)^2}\,\theta \right\}$$

$$\theta \geqq 0 . \tag{4.25}$$

Defining the velocity field of the plate as

$$\phi(x,y,t) = \frac{\partial w(x,y,t)}{\partial t} . \tag{4.26}$$

one may express the velocity response of the plate to a deterministic pressure excitation via (4.25) and (4.26) as

$$\phi(x,y,t) = \int_0^\infty \int_0^b \int_0^a p_t(x',y',t-\theta)\,\zeta(x,x',y,y',\theta)\,dx'\,dy'\,d\theta . \tag{4.27}$$

4.2.2 Plate Velocity Cross Correlation

The plate velocity cross correlation is defined as

$$Q_{\phi\phi}(x_1,x_2,y_1,y_2,t_1,t_2) = E\,[\phi(x_1,y_1,t_1)\,\phi(x_2,y_2,t_2)] \tag{4.28}$$

and the turbulent wall pressure cross correlation as

$$Q_{pp}\,(x_1,x_2,y_1,y_2,t_1,t_2) = E\,[p_t(x_1,y_1,t_1)\,p_t(x_2,y_2,t_2)] , \tag{4.29}$$

where E denotes the ensemble average.

From (4.27) and (4.28),

$$Q_{\phi\phi}(x_1,x_2,y_1,y_2,t_1,t_2) = E\left[\int_0^b\int_0^a\int_0^b\int_0^a\int_0^\infty\int_0^\infty p_t(x_1',y_1',t_1-\theta_1)\,p_t(x_2',y_2',t_2-\theta_2)\right.$$
$$\left.\zeta(x_1,x_1',y_1,y_1',\theta_1)\,\zeta(x_2,x_2',y_2,y_2',\theta_2)\,d\theta_1\,d\theta_2\,dx_1'\,dy_1'\,dx_2'\,dy_2'\right]. \tag{4.30}$$

However, the plate velocity impulse response is not a random quantity; hence the ensemble average applies only to the turbulent pressure field. Thus, from (4.30) and (4.29), the plate velocity cross correlation may be written as

$$Q_{\phi\phi}(x_1,x_2,y_1,y_2,t_1,t_2) = \int_0^b\int_0^a\int_0^b\int_0^a\int_0^\infty\int_0^\infty Q_{pp}\,(x_1',x_2',y_1',y_2',t_1-\theta_1,t_2-\theta_2)$$
$$\zeta(x_1,x_1',y_1,y_1',\theta_1)\,\zeta(x_2,x_2',y_2,y_2',\theta_2)\,d\theta_1\,d\theta_2\,dx_1'\,dy_1'\,dx_2'\,dy_2' \cdot \tag{4.31}$$

From Section 4.1, the turbulent boundary layer pressure is assumed to be a homogeneous, stationary random process. Therefore, the turbulent pressure cross correlation is a function of the difference between the spacial and temporal coordinates rather than the coordinates themselves. Hence, (4.31) may be written:

$$Q_{\phi\phi}(x_1,x_2,y_1,y_2,\tau) = \int_0^b\int_0^a\int_0^b\int_0^a\int_0^\infty\int_0^\infty Q_{pp}(\xi',\eta',\tau+\theta_1-\theta_2)\zeta(x_1,x_1',y_1,y_1',\theta_1)$$

$$\zeta(x_2,x_2',y_2,y_2',\theta_2)\,d\theta_1\,d\theta_2\,dx_1'\,dy_1'\,dx_2'\,dy_2' \, . \tag{4.32}$$

4.2.3 Plate Velocity Cross Spectral Density

The cross spectral density is defined as the Fourier Transform of the cross-correlation function. Hence, the plate velocity cross spectral density is defined as

$$S_{\phi\phi}(x_1,x_2,y_1,y_2,\omega) = \frac{1}{\sqrt{2\pi}}\int_{-\infty}^{\infty} Q_{\phi\phi}(x_1,x_2,y_1,y_2,\tau)\,e^{-i\omega\tau}\,d\tau. \tag{4.33}$$

Multiplying and dividing equation (4.32) by $e^{-i\omega(\theta_1-\theta_2)}$ and substituting into (4.33) gives the following expression for the plate velocity cross spectral density:

$$S_{\phi\phi}(x_1,x_2,y_1,y_2,\omega) = \int_0^b\int_0^a\int_0^b\int_0^a\int_0^\infty\int_0^\infty \left\{\frac{1}{\sqrt{2\pi}}\int_{-\infty}^{\infty} Q_{pp}(\xi',\eta',\tau+\theta_1-\theta_2)\,e^{-i\omega(\tau+\theta_1-\theta_2)}\,d(\tau+\theta_1-\theta_2)\right\}$$

$$\zeta(x_1,x_1',y_1,y_1',\theta_1)\,e^{i\omega\theta_1}\,\zeta(x_2,x_2',y_2,y_2',\theta_2)\,e^{-i\omega\theta_2}\,d\theta_1\,d\theta_2\,dx_1'\,dy_1'\,dx_2'\,dy_2' \tag{4.34}$$

However, the term in brackets is easily recognized as $S_{pp}(\xi',\eta',\omega)$; therefore, (4.34) may be rewritten:

$$S_{\phi\phi}(x_1,x_2,y_1,y_2,\omega) = \int_0^b\int_0^a\int_0^b\int_0^a S_{pp}(\xi',\eta',\omega) \int_0^\infty \zeta(x_1,x_1',y_1,y_1',\theta_1)\, e^{i\omega\theta_1}\, d\theta_1$$

$$\int_0^\infty \zeta(x_2,x_2',y_2,y_2',\theta_2)\, e^{-i\omega\theta_2}\, d\theta_2\, dx_1'\, dy_1'\, dx_2'\, dy_2' \,. \tag{4.35}$$

Since $\zeta(x,x',y,y',\omega)$ is zero for $\theta \leq 0$, the semi-infinite limits in θ_1 and θ_2 may be replaced by infinite limits. It is easily shown that

$$\int_{-\infty}^\infty \zeta(x_2,x_2',y_2,y_2',\theta_2)\, e^{-i\omega\theta_2}\, d\theta_2 = i\omega H(x_2,x_2',y_2,y_2',\omega) \tag{4.36}$$

and that

$$\int_{-\infty}^\infty \zeta(x_1,x_1',y_1,y_1',\theta_1)\, e^{i\omega\theta_1}\, d\theta_1 = -i\omega H(x_1,x_1',y_1,y_1',-\omega) \ . \tag{4.37}$$

Hence,

$$S_{\phi\phi}(x_1,x_2,y_1,y_2,\omega) = \int_0^b\int_0^a\int_0^b\int_0^a \omega^2 S_{pp}(\xi',\eta',\omega)\, H(x_1,x_1',y_1,y_1',-\omega)$$

$$H(x_2,x_2',y_2,y_2',\omega)\, dx_1'\, dy_1'\, dx_2'\, dy_2' \,, \tag{4.38}$$

where $H(x,x',y,y',\omega)$ is as defined in equation (4.16).

The expression for $S_{pp}(\xi',\eta',\omega)$ was presented in equation (4.4). Combination of (4.4), (4.38), and (4.16) results in

$$S_{\phi\phi}(x_1,x_2,y_1,y_2,\omega) = A\omega^2 \sum_{\substack{m=1\\n=1}}^{\infty} \sum_{\substack{q=1\\s=1}}^{\infty} \frac{a_{mn}(x_1,y_1)\, a_{qs}(x_2,y_2)}{\left[(\omega_{mn}^2 - \omega^2) - \frac{ir\omega}{\mu}\right]\left[(\omega_{qs}^2 - \omega^2) + \frac{ir\omega}{\mu}\right]}$$

$$\left\{ \int_0^b\int_0^a\int_0^b\int_0^a e^{-0.115(\omega/U_c)(|x_2'-x_1'|)}\, e^{-i(\omega/U_c)(x_2'-x_1')}\, e^{-0.7(\omega/U_c)(|y_2'-y_1'|)} \right.$$

$$\left. a_{mn}(x_1',y_1')\, a_{qs}(x_2',y_2')\, dx_1'\, dy_1'\, dx_2'\, dy_2' \right\}$$

$$\omega \leq 1.256\, \frac{U_o}{\delta^*} \,,$$

$$S_{\phi\phi}(x_1,x_2,y_1,y_2,\omega) = 2A\omega^2\left(\frac{\omega\delta^*}{U_o}\right)^{-3}\sum_{\substack{m=1\\n=1}}^{\infty}\sum_{\substack{q=1\\s=1}}^{\infty}\frac{a_{mn}(x_1,y_1)\,a_{qs}(x_2,y_2)}{\left[(\omega_{mn}^2-\omega^2)-\frac{ir\omega}{\mu}\right]\left[(\omega_{qs}^2-\omega^2)+\frac{ir\omega}{\mu}\right]}$$

$$\left\{\int_0^b\int_0^a\int_0^b\int_0^a e^{-0.115(\omega/U_c)(|x_2'-x_1'|)}e^{-i(\omega/U_c)(x_2'-x_1')}e^{-0.7(\omega/U_c)(|y_2'-y_1'|)}\right.$$

$$\left. a_{mn}(x_1',y_1')\,a_{qs}(x_2',y_2')\,dx_1'\,dy_1'\,dx_2'\,dy_2'\right\}$$

$$\omega > 1.256\,\frac{U_o}{\delta^*}\,, \qquad (4.39)$$

where

$$A = 0.75\times10^{-5}\,a^2\rho_f^2U_o^3\delta^*\,. \qquad (4.40)$$

Equation (4.39) may be rewritten by recalling the definition of $a_{mn}(x,y)$ from equation (4.8) and defining

$$I_{1_{mq}} = \int_0^a\int_0^a e^{-0.115(\omega/U_c)(|x_2'-x_1'|)}e^{-i(\omega/U_c)(x_2'-x_1')}\sin\frac{m\pi x_1'}{a}\sin\frac{q\pi x_2'}{a}\,dx_1'\,dx_2' \qquad (4.41)$$

and

$$I_{2_{ns}} = \int_0^b\int_0^b e^{-0.7(\omega/U_c)(|y_2'-y_1'|)}\sin\frac{n\pi y_1'}{b}\sin\frac{s\pi y_2'}{b}\,dy_1'\,dy_2'\ : \qquad (4.42)$$

$$S_{\phi\phi}(x_1,x_2,y_1,y_2,\omega) = \frac{16A\omega^2}{\mu^2a^2b^2}\sum_{\substack{m=1\\n=1}}^{\infty}\sum_{\substack{q=1\\s=1}}^{\infty}\frac{\sin\frac{m\pi x_1}{a}\sin\frac{n\pi y_1}{b}\sin\frac{q\pi x_2}{a}\sin\frac{s\pi y_2}{b}}{\left[(\omega_{mn}^2-\omega^2)-\frac{ir\omega}{\mu}\right]\left[(\omega_{qs}^2-\omega^2)+\frac{ir\omega}{\mu}\right]}\,I_{1_{mq}}I_{2_{ns}}$$

$$\omega \leqq 1.256\,\frac{U_o}{\delta^*}\,,$$

$$S_{\phi\phi}(x_1,x_2,y_1,y_2,\omega) = \frac{32A\omega^2}{\mu^2a^2b^2}\left(\frac{\omega\delta^*}{U_o}\right)^{-3}\sum_{\substack{m=1\\n=1}}^{\infty}\sum_{\substack{q=1\\s=1}}^{\infty}\frac{\sin\frac{m\pi x_1}{a}\sin\frac{n\pi y_1}{b}\sin\frac{q\pi x_2}{a}\sin\frac{s\pi y_2}{b}}{\left[(\omega_{mn}^2-\omega^2)-\frac{ir\omega}{\mu}\right]\left[(\omega_{qs}^2-\omega^2)+\frac{ir\omega}{\mu}\right]}\,I_{1_{mq}}I_{2_{ns}}$$

$$\omega > 1.256\,\frac{U_o}{\delta^*}$$

(4.43)

It remains to evaluate $I_{1_{mq}}$ and $I_{2_{ns}}$ in order to complete the solution for the plate velocity case spectral density.

From (4.41), $I_{1_{mq}}$ is defined as

$$I_{1_{mq}} = \int_0^a\int_0^a e^{-0.115(\omega/U_c)(|x_2'-x_1'|)} e^{-i(\omega/U_c)(x_2'-x_1')} \sin\frac{m\pi x_1'}{a} \sin\frac{q\pi x_2'}{a}\, dx_1' dx_2' \,. \tag{4.41}$$

Note that the integrand depends on the absolute value of $x_2' - x_1'$, and thus the integration must be performed over limits as shown in Figure 6. The appropriate values of the term containing the absolute value for each area of integration are also presented in this figure. Thus, by utilizing Figure 6, equation (4.41) becomes

$$\begin{aligned} I_{1_{mq}} = {} & \int_0^a e^{-(\omega/U_c)(0.115-i)x_1'} \sin\frac{m\pi x_1'}{a} \left\{\int_0^{x_1'} e^{(\omega/U_c)(0.115-i)x_2'} \sin\frac{q\pi x_2'}{a}\, dx_2'\right\} dx_1' \\ & + \int_0^a e^{-(\omega/U_c)(0.115+i)x_2'} \sin\frac{q\pi x_2'}{a} \left\{\int_0^{x_2'} e^{(\omega/U_c)(0.115+i)x_1'} \sin\frac{m\pi x_1'}{a}\, dx_1'\right\} dx_2' \,. \end{aligned} \tag{4.44}$$

The above integral may easily be evaluated from standard integral tables, and after extensive, but routine, simplification, (4.44) becomes

$$\begin{aligned} I_{1_{mq}} = \frac{1}{R_m R_q} \Bigg\{ & \delta_{mq}\, 1.0066\, \frac{\omega a}{U_c} R_m \cos(\nu_m - 0.463\pi) \\ & + [1-\delta_{mq}] \frac{mq\pi^2}{a^2} \frac{[(-1)^m(-1)^q - 1]}{\left[\left(\frac{m\pi}{a}\right)^2 - \left(\frac{q\pi}{a}\right)^2\right]} [R_m e^{i\nu_q} - R_q e^{-i\nu_m}] + 2\frac{mq\pi^2}{a^2} \cos(\nu_q + \nu_m) \\ & - \frac{mq\pi^2}{a^2} e^{-0.115(\omega a/U_c)} [(-1)^m e^{i(\omega a/U_c + \nu_q + \nu_m)} + (-1)^q e^{-i(\omega a/U_c + \nu_q + \nu_m)}] \Bigg\} , \end{aligned} \tag{4.45}$$

where

$$R_m = \sqrt{\left[\left(\frac{m\pi}{a}\right)^2 - 0.987\left(\frac{\omega}{U_c}\right)^2\right]^2 + 0.0529\left(\frac{\omega}{U_c}\right)^4} \,, \tag{4.46}$$

$$R_q = \sqrt{\left[\left(\frac{q\pi}{a}\right)^2 - 0.987\left(\frac{\omega}{U_c}\right)^2\right]^2 + 0.0529\left(\frac{\omega}{U_c}\right)^4}\ , \tag{4.47}$$

$$\nu_m = \tan^{-1}\frac{0.23\left(\frac{\omega}{U_c}\right)^2}{\left[\left(\frac{m\pi}{a}\right)^2 - 0.987\left(\frac{\omega}{U_c}\right)^2\right]}\ , \tag{4.48}$$

$$\nu_q = \tan^{-1}\frac{0.23\left(\frac{\omega}{U_c}\right)^2}{\left[\left(\frac{q\pi}{a}\right)^2 - 0.987\left(\frac{\omega}{U_c}\right)^2\right]}\ , \tag{4.49}$$

and δ_{mq} is the Kronecker delta.

From (4.42), $I_{2_{ns}}$ is defined:

$$I_{2_{ns}} = \int_0^b\int_0^b e^{-0.7(\omega/U_c)(|y_2'-y_1'|)} \sin\frac{n\pi y_1'}{b} \sin\frac{s\pi y_2'}{b}\, dy_1'\, dy_2'\ . \tag{4.42}$$

Again, because of the appearance of the absolute value of the difference of the variables of integration in the integrand, the integration must be performed over limits as shown in Figure 7. By applying arguments similar to those used in calculating $I_{1_{mq}}$ one can show that

$$I_{2_{ns}} = \frac{1}{\left[\left(0.7\frac{\omega}{U_c}\right)^2 + \left(\frac{n\pi}{b}\right)^2\right]\left[\left(0.7\frac{\omega}{U_c}\right)^2 + \left(\frac{s\pi}{b}\right)^2\right]}\left\{0.35\frac{\omega b}{U_c}\delta_{ns}\left[2\left(0.7\frac{\omega}{U_c}\right)^2 + \left(\frac{n\pi}{b}\right)^2 + \left(\frac{s\pi}{b}\right)^2\right]\right.$$
$$\left. + \frac{ns\pi^2}{b^2}\left[(-1)^n(-1)^s - 1\right]\left[1 - \delta_{ns}\right] + \frac{ns\pi^2}{b^2}\left[2 - \left[(-1)^n + (-1)^s\right]e^{-0.7(\omega b/U_c)}\right]\right\}. \tag{4.50}$$

Here again, δ_{ns} is the Kronecker delta. It shouldbe noted that the Kronecker delta was used in equations (4.45) and (4.50) to conserve space rather than writing separate expressions for $m = q$ and $m \neq q$ in (4.45) and, similarly, for $n = s$ and $n \neq s$ in (4.50). Hence, in order that no confusion arise in evaluating $I_{1_{mq}}$ and $I_{2_{ns}}$, the effect of the Kronecker delta should be considered first.

Combining (4.43), (4.45), and (4.50), one finds

$$S_{\phi\phi}(x_1,x_2,y_1,y_2,\omega) = \frac{16A\omega^2}{\mu^2 a^2 b^2} \sum_{\substack{m=1\\n=1}}^{\infty} \sum_{\substack{q=1\\s=1}}^{\infty} \frac{\sin\frac{m\pi x_1}{a} \sin\frac{n\pi y_1}{b} \sin\frac{q\pi x_2}{a} \sin\frac{s\pi y_2}{b}}{\left[(\omega_{mn}^2 - \omega^2) - \frac{ir\omega}{\mu}\right]\left[(\omega_{qs}^2 - \omega^2) + \frac{ir\omega}{\mu}\right]}$$

$$\frac{1}{R_m R_q}\Bigg\{\delta_{mq}\, 1.0066\, \frac{\omega a}{U_c} R_m \cos(\nu_m - 0.463\pi)$$

$$+ (1-\delta_{mq}) \frac{mq\pi^2}{a^2} \frac{[(-1)^m(-1)^q - 1]}{\left[\left(\frac{m\pi}{a}\right)^2 - \left(\frac{q\pi}{a}\right)^2\right]}[R_m e^{i\nu_q} - R_q e^{-i\nu_m}] + \frac{2mq\pi^2}{a^2}\cos(\nu_q + \nu_m)$$

$$- \frac{mq\pi^2}{a^2} e^{-0.115(\omega a/U_c)}[(-1)^m e^{i(\omega a/U_c + \nu_q + \nu_m)} + (-1)^q e^{-i(\omega a/U_c + \nu_q + \nu_m)}]\Bigg\}$$

$$\frac{1}{\left[\left(0.7\frac{\omega}{U_c}\right)^2 + \left(\frac{n\pi}{b}\right)^2\right]\left[\left(0.7\frac{\omega}{U_c}\right)^2 + \left(\frac{s\pi}{b}\right)^2\right]}\Bigg\{0.35\frac{\omega b}{U_c}\delta_{ns}\left[2\left(0.7\frac{\omega}{U_c}\right)^2 + \left(\frac{n\pi}{b}\right)^2 + \left(\frac{s\pi}{b}\right)^2\right]$$

$$+ \frac{ns\pi^2}{b^2}[(-1)^n(-1)^s - 1][1-\delta_{ns}] + \frac{ns\pi^2}{b^2}\left[2 - [(-1)^n + (-1)^s]e^{-0.7(\omega b/U_c)}\right]\Bigg\}$$

$$\omega \leqq 1.256\frac{U_o}{\delta^*},$$

$$S_{\phi\phi}(x_1,x_2,y_1,y_2,\omega) = \frac{32A\omega^2}{\mu^2 a^2 b^2}\left(\frac{\omega\delta^*}{U_o}\right)^{-3} \sum_{\substack{m=1\\n=1}}^{\infty} \sum_{\substack{q=1\\s=1}}^{\infty} \frac{\sin\frac{m\pi x_1}{a} \sin\frac{n\pi y_1}{b} \sin\frac{q\pi x_2}{a} \sin\frac{s\pi y_2}{b}}{\left[(\omega_{mn}^2 - \omega^2) - \frac{ir\omega}{\mu}\right]\left[(\omega_{qs}^2 - \omega^2) + \frac{ir\omega}{\mu}\right]}$$

$$\frac{1}{R_m R_q}\Bigg\{\delta_{mq}\, 1.0066\, \frac{\omega a}{U_c} R_m \cos(\nu_m - 0.463\pi)$$

$$+ (1-\delta_{mq}) \frac{mq\pi^2}{a^2} \frac{[(-1)^m(-1)^q - 1]}{\left[\left(\frac{m\pi}{a}\right)^2 - \left(\frac{q\pi}{a}\right)^2\right]}[R_m e^{i\nu_q} - R_q e^{-i\nu_m}] + \frac{2mq\pi^2}{a^2}\cos(\nu_q + \nu_m)$$

$$- \frac{mq\pi^2}{a^2} e^{-0.115(\omega a/U_c)}[(-1)^m e^{i(\omega a/U_c + \nu_q + \nu_m)} + (-1)^q e^{-i(\omega a/U_c + \nu_q + \nu_m)}]\Bigg\}$$

$$\frac{1}{\left[\left(0.7\frac{\omega}{U_c}\right)^2 + \left(\frac{n\pi}{b}\right)^2\right]\left[\left(0.7\frac{\omega}{U_c}\right)^2 + \left(\frac{s\pi}{b}\right)^2\right]}\Bigg\{0.35\frac{\omega b}{U_c}\delta_{ns}\left[2\left(0.7\frac{\omega}{U_c}\right)^2 + \left(\frac{n\pi}{b}\right)^2 + \left(\frac{s\pi}{b}\right)^2\right]$$

$$+ \frac{ns\pi^2}{b^2}[(-1)^n(-1)^s - 1][1-\delta_{ns}] + \frac{ns\pi^2}{b^2}\left[2 - [(-1)^n + (-1)^s]e^{-0.7(\omega b/U_c)}\right]\Bigg\}$$

$$\omega > 1.256\frac{U_o}{\delta^*}.$$

(4.51)

By defining

$$\lambda_{mn} = \tan^{-1} \frac{\frac{r\omega}{\mu}}{[\omega_{mn}^2 - \omega^2]} , \tag{4.52}$$

$$\lambda_{qs} = \tan^{-1} \frac{\frac{r\omega}{\mu}}{[\omega_{qs}^2 - \omega^2]} , \tag{4.53}$$

$$G_{ns} = 0.35 \frac{\omega b}{U_c} \delta_{ns} \left[2\left(0.7 \frac{\omega}{U_c}\right)^2 + \left(\frac{n\pi}{b}\right)^2 + \left(\frac{s\pi}{b}\right)^2 \right] + \frac{ns\pi^2}{b^2} [1 - \delta_{ns}] [(-1)^n (-1)^s - 1]$$
$$+ \frac{ns\pi^2}{b^2} \left\{ 2 - [(-1)^n + (-1)^s] e^{-0.7(\omega b/U_c)} \right\} , \tag{4.54}$$

$$P_n = \left(0.7 \frac{\omega}{U_c}\right)^2 + \left(\frac{n\pi}{b}\right)^2 , \tag{4.55}$$

$$P_s = \left(0.7 \frac{\omega}{U_c}\right)^2 + \left(\frac{s\pi}{b}\right)^2 , \tag{4.56}$$

$$T_{mn} = \sqrt{(\omega_{mn}^2 - \omega^2)^2 + \left(\frac{r\omega}{\mu}\right)^2} , \tag{4.57}$$

$$T_{qs} = \sqrt{(\omega_{qs}^2 - \omega^2)^2 + \left(\frac{r\omega}{\mu}\right)^2} , \tag{4.58}$$

$$V_{mnqs} = \Bigg\{ \delta_{mq}\, 1.0066 \frac{\omega a}{U_c} R_m \cos(\nu_m - 0.463\pi)$$
$$+ (1 - \delta_{mq}) \frac{mq\pi^2}{a^2} \frac{[(-1)^m (-1)^q - 1]}{\left[\left(\frac{m\pi}{a}\right)^2 - \left(\frac{q\pi}{a}\right)^2\right]} [R_m e^{i\nu_q} - R_q e^{-i\nu_m}] + \frac{2mq\pi^2}{a^2} \cos(\nu_q + \nu_m)$$
$$- \frac{mq\pi^2}{a^2} e^{-0.115(\omega a/U_c)} [(-1)^m e^{i(\omega a/U_c + \nu_q + \nu_m)} + (-1)^q e^{-i(\omega a/U_c + \nu_q + \nu_m)}] \Bigg\} e^{i(\lambda_{mn} - \lambda_{qs})} , \tag{4.59}$$

equation (4.51) may be simplified further. The resulting expression for the plate velocity cross spectral density is given by

$$S_{\dot\phi\dot\phi}(x_1,x_2,y_1,y_2,\omega) = \frac{16A\omega^2}{\mu^2a^2b^2}\sum_{\substack{m=1\\n=1}}^{\infty}\sum_{\substack{q=1\\s=1}}^{\infty}\frac{\sin\frac{m\pi x_1}{a}\sin\frac{n\pi y_1}{b}\sin\frac{q\pi x_2}{a}\sin\frac{s\pi y_2}{b}}{T_{mn}T_{qs}P_nP_sR_mR_q}G_{ns}V_{mnqs}$$

$$\omega \leq 1.256\frac{U_o}{\delta^*},$$

$$S_{\dot\phi\dot\phi}(x_1,x_2,y_1,y_2,\omega) = \frac{32A\omega^2}{\mu^2a^2b^2}\left(\frac{\omega\delta^*}{U_o}\right)^{-1}\sum_{\substack{m=1\\n=1}}^{\infty}\sum_{\substack{q=1\\s=1}}^{\infty}\frac{\sin\frac{m\pi x_1}{a}\sin\frac{n\pi y_1}{b}\sin\frac{q\pi x_2}{a}\sin\frac{s\pi y_2}{b}}{T_{mn}T_{qs}P_nP_sR_mR_q}G_{ns}V_{mnqs}$$

$$\omega > 1.256\frac{U_o}{\delta^*}.$$

(4.60)

4.2.4 Plate Velocity Spectral Density

The power spectrum of the plate velocity, $\Phi_{\dot\phi}(x,y,\omega)$, may be defined in terms of the plate velocity cross spectral density as follows:

$$\Phi_{\dot\phi}(x_1,y_1,\omega) = S_{\dot\phi\dot\phi}(x_1,x_1,y_1,y_1,\omega)\,. \tag{4.61}$$

Hence from (4.60)

$$\Phi_{\dot\phi}(x,y,\omega) = \frac{16A\omega^2}{\mu^2a^2b^2}\sum_{\substack{m=1\\n=1}}^{\infty}\sum_{\substack{q=1\\s=1}}^{\infty}\frac{\sin\frac{m\pi x}{a}\sin\frac{n\pi y}{b}\sin\frac{q\pi x}{a}\sin\frac{s\pi y}{b}}{T_{mn}T_{qs}P_nP_sR_mR_q}G_{ns}V_{mnqs}$$

$$\omega \leq 1.256\frac{U_o}{\delta^*},$$

$$\Phi_{\dot\phi}(x,y,\omega) = \frac{32A\omega^2}{\mu^2a^2b^2}\left(\frac{\omega\delta^*}{U_o}\right)^{-1}\sum_{\substack{m=1\\n=1}}^{\infty}\sum_{\substack{q=1\\s=1}}^{\infty}\frac{\sin\frac{m\pi x}{a}\sin\frac{n\pi y}{b}\sin\frac{q\pi x}{a}\sin\frac{s\pi y}{b}}{T_{mn}T_{qs}P_nP_sR_mR_q}G_{ns}V_{mnqs}$$

$$\omega > 1.256\frac{U_o}{\delta^*}.$$

(4.62)

The plate velocity power spectral density should be a real, even function. Hence, upon summation equation (4.62) must be real in order that it be a valid solution for the plate velocity spectral density. Substituting for V_{mnqs} from (4.59) and rearranging, (4.62) for $\omega \leq 1.256 \frac{U_o}{\delta^*}$ may be rewritten as

$$\Phi_\phi(x,y,\omega) = \frac{16A\omega^2}{\mu^2 a^2 b^2} \left\{ \sum_{m=1}^{\infty} \sum_{n=1}^{\infty} \sum_{q=1}^{\infty} \sum_{s=1}^{\infty} \frac{\sin\frac{m\pi x}{a} \sin\frac{n\pi y}{b} \sin\frac{q\pi x}{a} \sin\frac{s\pi y}{b}}{T_{mn} T_{qs} P_n P_s R_m R_q} G_{ns} \right.$$

$$1.0066 \frac{\omega a}{U_c} \delta_{mq} R_m \cos(\nu_m - 0.463\pi)\, e^{i(\lambda_{mn} - \lambda_{qs})}$$

$$+ \sum_{m=1}^{\infty} \sum_{n=1}^{\infty} \sum_{q=1}^{\infty} \sum_{s=1}^{\infty} \frac{\sin\frac{m\pi x}{a} \sin\frac{n\pi y}{b} \sin\frac{q\pi x}{a} \sin\frac{s\pi y}{b}}{T_{mn} T_{qs} P_n P_s R_m R_q} G_{ns}$$

$$\frac{2mq\pi^2}{a^2} \cos(\nu_m + \nu_q)\, e^{i(\lambda_{mn} - \lambda_{qs})}$$

$$+ \sum_{m=1}^{\infty} \sum_{n=1}^{\infty} \sum_{q=1}^{\infty} \sum_{s=1}^{\infty} \frac{\sin\frac{m\pi x}{a} \sin\frac{n\pi y}{b} \sin\frac{q\pi x}{a} \sin\frac{s\pi y}{b}}{T_{mn} T_{qs} P_n P_s R_m R_q} G_{ns}$$

$$(1 - \delta_{mq}) \frac{mq\pi^2}{a^2} \frac{[(-1)^m (-1)^q - 1]}{\left[\left(\frac{m\pi}{a}\right)^2 - \left(\frac{q\pi}{a}\right)^2\right]} \left[R_m e^{i(\nu_q + \lambda_{mn} - \lambda_{qs})} - R_q e^{-i(\nu_m + \lambda_{qs} - \lambda_{mn})}\right]$$

$$- \sum_{m=1}^{\infty} \sum_{n=1}^{\infty} \sum_{q=1}^{\infty} \sum_{s=1}^{\infty} \frac{\sin\frac{m\pi x}{a} \sin\frac{n\pi y}{b} \sin\frac{q\pi x}{a} \sin\frac{s\pi y}{b}}{T_{mn} T_{qs} P_n P_s R_m R_q} G_{ns}$$

$$\left. \frac{mq\pi^2}{a^2} e^{-0.119(\omega a/U_c)} \left[(-1)^m e^{i(\omega a/U_c + \nu_q + \nu_m + \lambda_{mn} - \lambda_{qs})} + (-1)^q e^{-i(\omega a/U_c + \nu_q + \nu_m + \lambda_{qs} - \lambda_{mn})}\right] \right\}. \tag{4.63}$$

Since G_{ns} is a symmetrical matrix, that is,

$$G_{ns} = G_{sn}\,, \tag{4.64}$$

the first summation group may be rewritten as

$$\frac{1}{2}\sum_{m=1}^{\infty}\sum_{n=1}^{\infty}\sum_{m=1}^{\infty}\sum_{s=1}^{\infty}\frac{\sin\frac{m\pi x}{a}\sin\frac{n\pi y}{b}\sin\frac{m\pi x}{a}\sin\frac{s\pi y}{b}}{T_{mn}T_{ms}P_nP_sR_mR_m}G_{ns}$$

$$1.0066\,\frac{\omega a}{U_c}R_m\cos(\nu_m-0.463\pi)\,e^{i(\lambda_{mn}-\lambda_{ms})}$$

$$+\ \frac{1}{2}\sum_{m=1}^{\infty}\sum_{s=1}^{\infty}\sum_{m=1}^{\infty}\sum_{n=1}^{\infty}\frac{\sin\frac{m\pi x}{a}\sin\frac{s\pi y}{b}\sin\frac{m\pi x}{a}\sin\frac{n\pi y}{b}}{T_{ms}T_{mn}P_nP_sR_mR_m}G_{sn}$$

$$1.0066\,\frac{\omega a}{U_c}R_m\cos(\nu_m-0.463\pi)\,e^{i(\lambda_{ms}-\lambda_{mn})}$$

$$=\ \sum_{m=1}^{\infty}\sum_{n=1}^{\infty}\sum_{m=1}^{\infty}\sum_{s=1}^{\infty}\frac{\sin\frac{m\pi x}{a}\sin\frac{n\pi y}{b}\sin\frac{m\pi x}{a}\sin\frac{s\pi y}{b}}{T_{mn}T_{ms}P_nP_sR_mR_m}G_{ns}$$

$$1.0066\,\frac{\omega a}{U_c}R_m\cos(\nu_m-0.463\pi)\,\frac{1}{2}\left[e^{i(\lambda_{mn}-\lambda_{ms})}+e^{-i(\lambda_{mn}-\lambda_{ms})}\right]$$

$$=\ \sum_{m=1}^{\infty}\sum_{n=1}^{\infty}\sum_{q=1}^{\infty}\sum_{s=1}^{\infty}\frac{\sin\frac{m\pi x}{a}\sin\frac{n\pi y}{b}\sin\frac{q\pi x}{a}\sin\frac{s\pi y}{b}}{T_{mn}T_{qs}P_nP_sR_mR_q}G_{ns}$$

$$1.0066\,\frac{\omega a}{U_c}\delta_{mq}R_m\cos(\nu_m-0.463\pi)\cos(\lambda_{mn}-\lambda_{qs})\,. \tag{4.65}$$

By applying similar arguments to the last three summation groups, one can show that (4.62) becomes

$$\Phi_\phi(x,y,\omega)=\frac{16A\omega^2}{\mu^2a^2b^2}\sum_{m=1}^{\infty}\sum_{n=1}^{\infty}\sum_{q=1}^{\infty}\sum_{s=1}^{\infty}\frac{\sin\frac{m\pi x}{a}\sin\frac{n\pi y}{b}\sin\frac{q\pi x}{a}\sin\frac{s\pi y}{b}}{T_{mn}T_{qs}P_nP_sR_mR_q}G_{ns}$$

$$\Bigg\{1.0066\,\frac{\omega a}{U_c}\delta_{mq}R_m\cos(\nu_m-0.463\pi)\cos(\lambda_{mn}-\lambda_{qs})$$

$$+\frac{2mq\pi^2}{a^2}\cos(\nu_m+\nu_q)\cos(\lambda_{mn}-\lambda_{qs})+(1-\delta_{mq})\frac{mq\pi^2}{a^2}\,\frac{[(-1)^m(-1)^q-1]}{\left[\left(\frac{m\pi}{a}\right)^2-\left(\frac{q\pi}{a}\right)^2\right]}$$

$$[R_m\cos(\nu_q+\lambda_{mn}-\lambda_{qs})-R_q\cos(\nu_m+\lambda_{qs}-\lambda_{mn})]$$

$$-\frac{mq\pi^2}{a^2}e^{-0.115(\omega a/U_c)}\left[(-1)^m\cos\left(\frac{\omega a}{U_c}+\nu_q+\nu_m+\lambda_{mn}-\lambda_{qs}\right)\right.$$

$$\left.\left.+(-1)^q\cos\left(\frac{\omega a}{U_c}+\nu_q+\nu_m+\lambda_{qs}-\lambda_{mn}\right)\right]\right\}\,. \tag{4.66}$$

for $\omega \leq 1.256 \frac{U_o}{\delta^*}$.

By defining

$$W_{mnqs} = 1.0066 \frac{\omega a}{U_c} \delta_{mq} R_m \cos(\nu_m - 0.463\pi) \cos(\lambda_{mn} - \lambda_{qs})$$

$$+ \frac{2mq\pi^2}{a^2} \cos(\nu_m + \nu_q) \cos(\lambda_{mn} - \lambda_{qs}) + (1 - \delta_{mq}) \frac{mq\pi^2}{a^2} \frac{[(-1)^m(-1)^q - 1]}{\left[\left(\frac{m\pi}{a}\right)^2 - \left(\frac{q\pi}{a}\right)^2\right]}$$

$$[R_m \cos(\nu_q + \lambda_{mn} - \lambda_{qs}) - R_q \cos(\nu_m + \lambda_{qs} - \lambda_{mn})]$$

$$- \frac{mq\pi^2}{a^2} e^{-0.115(\omega a/U_c)} \left[(-1)^m \cos\left(\frac{\omega a}{U_c} + \nu_q + \nu_m + \lambda_{mn} - \lambda_{qs}\right)\right.$$

$$\left. + (-1)^q \cos\left(\frac{\omega a}{U_c} + \nu_q + \nu_m + \lambda_{qs} - \lambda_{mn}\right)\right] \tag{4.67}$$

and noting that arguments applied to equation (4.65) for $\omega \leq 1.256 \frac{U_o}{\delta^*}$ are also valid for the frequency range $\omega > 1.256 \frac{U_o}{\delta^*}$, one may write the plate velocity power spectral density as

$$\Phi_\phi(x,y,\omega) = \frac{16A\omega^2}{\mu^2 a^2 b^2} \sum_{\substack{m=1\\n=1}}^{\infty} \sum_{\substack{q=1\\s=1}}^{\infty} \frac{\sin\frac{m\pi x}{a} \sin\frac{n\pi y}{b} \sin\frac{q\pi x}{a} \sin\frac{s\pi y}{b}}{T_{mn} T_{qs} P_n P_s R_m R_q} G_{ns} W_{mnqs} \qquad \omega \leq 1.256 \frac{U_o}{\delta^*},$$

$$\Phi_\phi(x,y,\omega) = \frac{32A\omega^2}{\mu^2 a^2 b^2} \left(\frac{\omega\delta^*}{U_o}\right)^{-1} \sum_{\substack{m=1\\n=1}}^{\infty} \sum_{\substack{q=1\\s=1}}^{\infty} \frac{\sin\frac{m\pi x}{a} \sin\frac{n\pi y}{b} \sin\frac{q\pi x}{a} \sin\frac{s\pi y}{b}}{T_{mn} T_{qs} P_n P_s R_m R_q} G_{ns} W_{mnqs} \qquad \omega > 1.256 \frac{U_o}{\delta^*}.$$

(4.68)

4.3 Development of the Cavity Acoustic Pressure Cross Spectral Density

4.3.1 Cavity Acoustic Pressure due to an Arbitrary Plate Velocity Distribution

The equations governing acoustic phenomena are the momentum equation,

$$\rho_{a_o} \frac{\partial \vec{u}}{\partial t} + \nabla p_a = 0, \tag{4.69}$$

the continuity equation,

$$\frac{\partial \rho_a}{\partial t} + \rho_{a_o} \nabla \cdot \vec{u} = 0, \tag{4.70}$$

and the equation of state,

$$p_a = c^2 \rho_a. \tag{4.71}$$

It should be noted that the subscript "zero" in the above equations refer to time average quantities, whereas non-subscripted quantites are the instantaneous or fluctuating components.

Reference to Figure 1, for an arbitrary plate velocity $\phi(x, y, t)$, indicates that equations (4.69), (4.70), and (4.71) must be solved subject to the following boundary conditions:

$$\begin{aligned}
&u_x(0, y, z, t) = 0 && \text{(a)}\\
&u_x(a, y, z, t) = 0 && \text{(b)}\\
&u_y(x, 0, z, t) = 0 && \text{(c)}\\
&u_y(x, b, z, t) = 0 && \text{(d)}\\
&u_z(x, y, 0, t) = 0 && \text{(e)}\\
&u_z(x, y, -d, t) = \phi(x, y, t) && \text{(f)}.
\end{aligned} \tag{4.72}$$

Equation (4.69) was derived on the basis of an inviscid fluid. Hence, the acoustic field may be assumed irrotational, and the acoustic phase velocity may be defined in terms of a velocity potential (ψ) as follows.

$$\vec{u}(x, y, z, t) = \nabla \psi(x, y, z, t). \tag{4.73}$$

Equation (4.73) only specifies ψ to within an arbitrary function of time. Hence, in order that ψ be uniquely specified, it is necessary to further define

$$p_a(x, y, z, t) = -\rho_{a_0} \frac{\partial \psi(x, y, z, t)}{\partial t}. \tag{4.74}$$

Substitution of (4.73) and (4.74) into (4.69) identically satisfies (4.69). It remains only to satisfy (4.70) and (4.71). Substituting (4.71) into (4.70), one finds that

$$\frac{1}{c^2} \frac{\partial p_a}{\partial t} + \rho_{a_0} \nabla \cdot \vec{u} = 0. \tag{4.75}$$

Substitution of (4.74) and (4.73) into (4.75) results in the scalar wave equation in ψ: that is,

$$\nabla^2 \psi - \frac{1}{c^2} \frac{\partial^2 \psi}{\partial t^2} = 0. \tag{4.76}$$

Separation of variables techniques yields a solution to (4.76):

$$\begin{aligned} \psi(x, y, z, t) = [C_1 \sin k_x x + C_2 \cos k_x x] [C_3 \sin k_y y + C_4 \cos k_y y] \\ [C_5 \sin k_z z + C_6 \cos k_z z] C_7 e^{ikct}, \end{aligned} \tag{4.77}$$

where

$$k_x^2 + k_y^2 + k_z^2 = k^2. \tag{4.78}$$

Application of the boundary conditions (4.72a) through (4.72e) to equation (4.77), by means of (4.73), yields

$$C_1 = C_3 = C_5 = 0, \tag{4.79}$$

$$k_x = \frac{j\pi}{a}, \tag{4.80}$$

$$k_y = \frac{\ell \pi}{b}, \tag{4.81}$$

where j and ℓ are integers. Further, by defining

$$\omega = kc \tag{4.82}$$

and by utilizing (4.79), (4.80), and (4.81), it is seen that

$$\psi(x,y,z,t) = \sum_{\substack{j=0\\ \ell=0}}^{\infty\infty} C_{2_j} \cos\frac{j\pi x}{a} C_{4_\ell} \cos\frac{\ell\pi y}{b} C_6 \cos(k_{z_{j\ell}} z) C_7 e^{i\omega t}. \tag{4.83}$$

Combining all the constants, one may assume that the solution for $\psi(x,y,z,t)$ takes the form

$$\psi(x,y,z,t) = \sum_{\substack{j=0\\ \ell=0}}^{\infty\infty} \cos\frac{j\pi x}{a} \cos\frac{\ell\pi y}{b} \int_{-\infty}^{\infty} Y_{j\ell}(\omega) \cos(k_{z_{j\ell}} z) e^{i\omega t} \frac{d\omega}{\sqrt{2\pi}}. \tag{4.83a}$$

Substitution of (4.83a) into (4.76) readily shows that (4.83a) satisfies the wave equation, and by applying the above arguments, boundary conditions (4.72a) through (4.72e) are satisfied. It therefore remains only to satisfy the final boundary condition (4.72f): that is,

$$\phi(x,y,t) = \sum_{\substack{j=0\\ \ell=0}}^{\infty\infty} \cos\frac{j\pi x}{a} \cos\frac{\ell\pi y}{b} \int_{-\infty}^{\infty} Y_{j\ell}(\omega) \left\{-k_{z_{j\ell}} \sin\left[k_{z_{j\ell}}(-d)\right]\right\} e^{i\omega t} \frac{d\omega}{\sqrt{2\pi}}. \tag{4.84}$$

Let

$$X_{j\ell}(\omega) = k_{z_{j\ell}}(\omega)\, Y_{j\ell}(\omega) \sin(k_{z_{j\ell}} d) \tag{4.85}$$

Equation (4.84) may be rewritten as

$$\phi(x,y,t) = \sum_{\substack{j=0\\ \ell=0}}^{\infty\infty} \cos\frac{j\pi x}{a} \cos\frac{\ell\pi y}{b} \int_{-\infty}^{\infty} X_{j\ell}(\omega)\, e^{i\omega t} \frac{d\omega}{\sqrt{2\pi}}. \tag{4.86}$$

Equation (4.86) is essentially a two-dimensional Fourier cosine series in x and y; hence $X(\omega)$ may be evaluated by determination of the Fourier coefficients of (4.86). By utilization of the orthogonality principle, it may be shown that

$$\int_{-\infty}^{\infty} X_{j\ell}(\omega)\, e^{i\omega t} \frac{d\omega}{\sqrt{2\pi}} = \frac{4}{ab(1+\delta_{0j})(1+\delta_{0\ell})} \int_0^b\!\!\int_0^a \phi(x,y,t) \cos\frac{j\pi x}{a} \cos\frac{\ell\pi y}{b}\, dx\, dy\,. \tag{4.87}$$

Transformation of (4.87) yields

$$X_{j\ell}(\omega) = \frac{4}{ab(1+\delta_{0j})(1+\delta_{0\ell})} \int_{-\infty}^{\infty}\int_0^b\int_0^a \phi(x,y,t) \cos\frac{j\pi x}{a} \cos\frac{\ell\pi y}{b} e^{-i\omega t}\, dx\, dy \frac{dt}{\sqrt{2\pi}}. \qquad (4.88)$$

Thus, from (4.85)

$$Y_{j\ell}(\omega) = \frac{4}{ab(1+\delta_{0j})(1+\delta_{0\ell})k_{z_{j\ell}} \sin k_{z_{j\ell}} d} \int_{-\infty}^{\infty}\int_0^b\int_0^a \phi(x,y,t) \cos\frac{j\pi x}{a} \cos\frac{\ell\pi y}{b} e^{-i\omega t}\, dx\, dy \frac{dt}{\sqrt{2\pi}}$$

(4.89)

and using this result in (4.83a) yields

$$\psi(x,y,z,t) = \frac{2}{\pi ab} \sum_{\substack{j=0\\ \ell=0}}^{\infty} \cos\frac{j\pi x}{a} \cos\frac{\ell\pi y}{b} \int_{-\infty}^{\infty} \frac{\cos k_{z_{j\ell}} z}{(1+\delta_{0j})(1+\delta_{0\ell})k_{z_{j\ell}} \sin k_{z_{j\ell}} d}$$

$$\left\{\int_{-\infty}^{\infty}\int_0^b\int_0^a \phi(x,y,t)\cos\frac{j\pi x}{a} \cos\frac{\ell\pi y}{b} e^{-i\omega t}\, dxdydt\right\} e^{i\omega t}\, d\omega .$$

(4.90)

The cavity acoustic pressure for an arbitrary, deterministic plate velocity is, from (4.74) and (4.90),

$$p_a(x,y,z,t) = \frac{-2i\rho_{a_0}}{\pi ab} \sum_{\substack{j=0\\ \ell=0}}^{\infty} \cos\frac{j\pi x}{a} \cos\frac{\ell\pi y}{b} \int_{-\infty}^{\infty} \frac{\omega \cos k_{z_{j\ell}} z}{(1+\delta_{0j})(1+\delta_{0\ell})k_{z_{j\ell}} \sin k_{z_{j\ell}} d}$$

$$\left\{\int_{-\infty}^{\infty}\int_0^b\int_0^a \phi(x,y,t) \cos\frac{j\pi x}{a} \cos\frac{\ell\pi y}{b} e^{-i\omega t}\, dxdydt\right\} e^{i\omega t}\, d\omega .$$

(4.91)

4.3.2 Cavity Acoustic Pressure Cross Correlation

The cavity acoustic pressure cross correlation is defined as

$$Q_{aa}(x_1,x_2,y_1,y_2,z_1,z_2,t_1,t_2) = E\left[p_a(x_1,y_1,z_1,t_1)\, p_a(x_2,y_2,z_2,t_2)\right] . \qquad (4.92)$$

From (4.91) and (4.92), by utilizing the knowledge that the only random quantity in the expression for $p_a(x,y,z,t)$ is the plate velocity, one may write the acoustic pressure cross correlation as

$$Q_{aa}(x_1,x_2,y_1,y_2,z_1,z_2,t_1,t_2) = \frac{-4\rho_o^2}{\pi^2 a^2 b^2} \sum_{\substack{j=0\\ \ell=0}}^{\infty} \sum_{\substack{r=0\\ t=0}}^{\infty} \cos\frac{j\pi x_1}{a} \cos\frac{\ell\pi y_1}{b} \cos\frac{r\pi x_2}{a} \cos\frac{t\pi y_2}{b}$$

$$\left\{\int_{-\infty}^{\infty}\int_{-\infty}^{\infty} \frac{\omega\Omega \cos k_{z_{j\ell}} z_1 \cos k_{z_{rt}} z_2}{(1+\delta_{0j})(1+\delta_{0\ell})(1+\delta_{0r})(1+\delta_{0t}) k_{z_{j\ell}}(\omega) k_{z_{rt}}(\Omega) \sin k_{z_{j\ell}} d \sin k_{z_{rt}} d}\right.$$

$$\left[\int_{-\infty}^{\infty}\int_{-\infty}^{\infty}\int_0^b\int_0^a\int_0^b\int_0^a E\left[\phi(x_1,y_1,t_1)\,\phi(x_2,y_2,t_2)\right] \cos\frac{j\pi x_1}{a} \cos\frac{\ell\pi y_1}{b}\right.$$

$$\left.\left.\cos\frac{r\pi x_2}{a} \cos\frac{t\pi y_2}{b} e^{-i\omega t_1} e^{-i\Omega t_2}\, dx_1 dy_1 dx_2 dy_2 dt_1 dt_2\right] e^{i\omega t_1} e^{i\Omega t_2}\, d\omega\, d\Omega\right\} . \tag{4.93}$$

From (4.28) and (4.32), however,

$$E\left[\phi(x_1,y_1,t_1)\,\phi(x_2,y_2,t_2)\right] = Q_{\phi\phi}(x_1,x_2,y_1,y_2,\tau) \tag{4.94}$$

Therefore, (4.93) becomes

$$Q_{aa}(x_1,x_2,y_1,y_2,z_1,z_2,t_1,t_2) = \frac{-4\rho_o^2}{\pi^2 a^2 b^2} \sum_{\substack{j=0\\ \ell=0}}^{\infty} \sum_{\substack{r=0\\ t=0}}^{\infty} \cos\frac{j\pi x_1}{a} \cos\frac{\ell\pi y_1}{b} \cos\frac{r\pi x_2}{a} \cos\frac{t\pi y_2}{b}$$

$$\left\{\int_{-\infty}^{\infty}\int_{-\infty}^{\infty} \frac{\omega\Omega \cos k_{z_{j\ell}} z_1 \cos k_{z_{rt}} z_2}{(1+\delta_{0j})(1+\delta_{0\ell})(1+\delta_{0r})(1+\delta_{0t}) k_{z_{j\ell}}(\omega) k_{z_{rt}}(\Omega) \sin k_{z_{j\ell}} d \sin k_{z_{rt}} d}\right.$$

$$\left[\int_{-\infty}^{\infty}\int_{-\infty}^{\infty}\int_0^b\int_0^a\int_0^b\int_0^a Q_{\phi\phi}(x_1,x_2,y_1,y_2,\tau) \cos\frac{j\pi x_1}{a} \cos\frac{\ell\pi y_1}{b}\right.$$

$$\left.\left.\cos\frac{r\pi x_2}{a} \cos\frac{t\pi y_2}{b} e^{-i\omega t_1} e^{-i\Omega t_2}\, dx_1 dy_1 dx_2 dy_2 dt_1 dt_2\right] e^{i\omega t_1} e^{i\Omega t_2}\, d\omega\, d\Omega\right\} . \tag{4.95}$$

It is now of interest to examine the following portion of (4.95):

$$\int_{-\infty}^{\infty}\int_{-\infty}^{\infty} Q_{\phi\phi}(x_1,x_2,y_1,y_2,\tau)\, e^{-i\omega t_1} e^{-i\Omega t_2}\, dt_1\, dt_2 . \tag{4.96}$$

By recalling that $\tau = t_2 - t_1$, one may rewrite (4.96):

$$\int_{-\infty}^{\infty} Q_{\phi\phi}(x_1,x_2,y_1,y_2,\tau)\, e^{-i\Omega\tau} \int_{-\infty}^{\infty} e^{-i(\omega+\Omega)t_1}\, dt_1 . \tag{4.97}$$

However, from (4.33)

$$S_{\phi\phi}(x_1,x_2,y_1,y_2,\omega) = \frac{1}{\sqrt{2\pi}} \int_{-\infty}^{\infty} Q_{\dot{\zeta}\dot{\zeta}}(x_1,x_2,y_1,y_2,\tau)\, e^{-i\omega\tau}\, d\tau \tag{4.33}$$

Therefore, (4.97) becomes

$$\sqrt{2\pi}\; S_{\phi\phi}(x_1,x_2,y_1,y_2,\omega) \int_{-\infty}^{\infty} e^{-i(\omega+\Omega)t_1}\, dt_1 . \tag{4.98}$$

Finally, since

$$\int_{-\infty}^{\infty} e^{-i(\omega+\Omega)t_1}\, dt_1 = 2\pi\delta(\omega+\Omega) \tag{4.99}$$

equation (4.98) becomes

$$(2\pi)^{3/2}\, S_{\phi\phi}(x_1,x_2,y_1,y_2,\Omega)\, \delta(\omega+\Omega). \tag{4.100}$$

Hence, (4.93) becomes

$$Q_{aa}(x_1,x_2,y_1,y_2,z_1,z_2,t_1,t_2) = \frac{-(2\pi)^{3/2}\, 4\rho_{a_o}^2}{\pi^2 a^2 b^2} \sum_{\substack{j=0\\ \ell=0}}^{\infty} \sum_{\substack{r=0\\ t=0}}^{\infty} \cos\frac{j\pi x_1}{a} \cos\frac{\ell\pi y_1}{b} \cos\frac{r\pi x_2}{a} \cos\frac{t\pi y_2}{b}$$

$$\int_{-\infty}^{\infty}\int_{-\infty}^{\infty} \frac{\omega\Omega \cos k_{z_{j\ell}} z_1 \cos k_{z_{rt}} z_2}{(1+\delta_{0j})(1+\delta_{0\ell})(1+\delta_{0r})(1+\delta_{0t}) k_{z_{j\ell}}(\omega) k_{z_{rt}}(\Omega) \sin k_{z_{j\ell}} d \sin k_{z_{rt}} d}$$

$$\left\{ \int_0^b\int_0^a\int_0^b\int_0^a S_{\phi\phi}(x_1,x_2,y_1,y_2,\Omega) \cos\frac{j\pi x_1}{a} \cos\frac{\ell\pi y_1}{b} \cos\frac{r\pi x_2}{a} \cos\frac{t\pi y_2}{b}\, dx_1 dy_1 dx_2 dy_2 \right\}$$

$$\delta(\omega+\Omega)\, e^{i\omega t_1} e^{i\Omega t_2}\, d\omega\, d\Omega . \tag{4.101}$$

Integration over ω, and use of the identity

$$\tau = t_2 - t_1$$

lead to the conclusion that equation (4.101) may be written:

$$Q_{aa}(x_1,x_2,y_1,y_2,z_1,z_2,\tau) = \frac{-8\sqrt{2}\,\rho_{a_0}^2}{\sqrt{\pi}\,a^2 b^2} \sum_{\substack{j=0\\ \ell=0}}^{\infty} \sum_{\substack{r=0\\ t=0}}^{\infty} \cos\frac{j\pi x_1}{a} \cos\frac{\ell\pi y_1}{b} \cos\frac{r\pi x_2}{a} \cos\frac{t\pi y_2}{b}$$

$$\int_{-\infty}^{\infty} \frac{-\Omega^2 \cos k_{j\ell} z_1 \cos k_{rt} z_2}{(1+\delta_{0j})(1+\delta_{0\ell})(1+\delta_{0r})(1+\delta_{0t})\,k_{j\ell}(-\Omega)\,k_{rt}(\Omega) \sin k_{j\ell} d \,\sin k_{rt} d}$$

$$\left\{\int_0^b\!\!\int_0^a\!\!\int_0^b\!\!\int_0^a S_{\dot{p}\dot{p}}(x_1,x_2,y_1,y_2,\Omega) \cos\frac{j\pi x_1}{a} \cos\frac{\ell\pi y_1}{b} \cos\frac{r\pi x_2}{a} \cos\frac{t\pi y_2}{b}\, dx_1 dy_1 dx_2 dy_2\right\}$$

$$e^{i\Omega\tau}\, d\Omega\,. \qquad (4.102)$$

It should be noted that, from (4.78), (4.80), (4.81), and (4.82),

$$k_{j\ell}(\omega) = \left[\frac{\omega^2}{c^2} - \left(\frac{j\pi}{a}\right)^2 - \left(\frac{\ell\pi}{b}\right)^2\right]^{1/2} \qquad (4.103)$$

Thus,

$$k_{j\ell}(\omega) = k_{j\ell}(-\omega)\,, \qquad (4.104)$$

and the cavity acoustic pressure cross correlation may be written:

$$Q_{aa}(x_1,x_2,y_1,y_2,z_1,z_2,\tau) = \frac{-8\sqrt{2}\,\rho_{a_0}^2}{\sqrt{\pi}\,a^2 b^2} \sum_{\substack{j=0\\ \ell=0}}^{\infty} \sum_{\substack{r=0\\ t=0}}^{\infty} \cos\frac{j\pi x_1}{a} \cos\frac{\ell\pi y_1}{b} \cos\frac{r\pi x_2}{a} \cos\frac{t\pi y_2}{b}$$

$$\int_{-\infty}^{\infty} \frac{\Omega^2 \cos k_{j\ell} z_1 \cos k_{rt} z_2}{(1+\delta_{0j})(1+\delta_{0\ell})(1+\delta_{0r})(1+\delta_{0t})\,k_{j\ell}(\Omega)\,k_{rt}(\Omega) \sin k_{j\ell} d \,\sin k_{rt} d}$$

$$\left\{\int_0^b\!\!\int_0^a\!\!\int_0^b\!\!\int_0^a S_{\dot{p}\dot{p}}(x_1,x_2,y_1,y_2,\Omega) \cos\frac{j\pi x_1}{a} \cos\frac{\ell\pi y_1}{b} \cos\frac{r\pi x_2}{a} \cos\frac{t\pi y_2}{b}\, dx_1 dy_1 dx_2 dy_2\right\}$$

$$e^{i\Omega\tau}\, d\Omega\,. \qquad (4.105)$$

4.3.3 Cavity Acoustic Pressure Cross Spectral Density

The cavity acoustic pressure cross spectral density is defined as the Fourier transform of the cross correlation: that is,

$$S_{aa}(x_1,x_2,y_1,y_2,z_1,z_2,\omega) = \frac{1}{\sqrt{2\pi}}\int_{-\infty}^{\infty} Q_{aa}(x_1,x_2,y_1,y_2,z_1,z_2,\tau)\, e^{-i\omega\tau}\, d\tau. \qquad (4.106)$$

Thus, from (4.105)

$$S_{aa}(x_1,x_2,y_1,y_2,z_1,z_2,\omega) = \frac{8\rho_o^2}{\pi a^2 b^2} \sum_{\substack{j=0\\ \ell=0}}^{\infty} \sum_{\substack{r=0\\ t=0}}^{\infty} \cos\frac{j\pi x_1}{a}\cos\frac{\ell\pi y_1}{b}\cos\frac{r\pi x_2}{a}\cos\frac{t\pi y_2}{b}$$

$$\Bigg\{ \int_{-\infty}^{\infty}\int_{-\infty}^{\infty} \frac{\Omega^2 \cos k_{z_{j\ell}} z_1 \cos k_{z_{rt}} z_2}{(1+\delta_{0j})(1+\delta_{0\ell})(1+\delta_{0r})(1+\delta_{0t}) k_{z_{j\ell}}(\Omega) k_{z_{rt}}(\Omega) \sin k_{z_{j\ell}} d \sin k_{z_{rt}} d}$$

$$\left[\int_0^b\int_0^a\int_0^b\int_0^a S_{\phi\phi}(x_1,x_2,y_1,y_2,\Omega) \cos\frac{j\pi x_1}{a}\cos\frac{\ell\pi y_1}{b}\cos\frac{r\pi x_2}{a}\cos\frac{t\pi y_2}{b}\, dx_1 dy_1 dx_2 dy_2\right]$$

$$e^{i\Omega\tau} d\Omega\, e^{-i\omega\tau}\, d\tau\Bigg\}. \qquad (4.107)$$

If the expression for the plate velocity cross spectral density from (4.60) is now substituted into (4.107) and subscripts are reassigned such that j, k, m, and n apply to the acoustics problem and q, r, s, and t apply to the plate,

$$S_{aa}(x_1,x_2,y_1,y_2,z_1,z_2,\omega) = \frac{8\rho_o^2}{\pi a^2 b^2} \sum_{\substack{j=0\\ k=0}}^{\infty} \sum_{\substack{m=0\\ n=0}}^{\infty} \cos\frac{j\pi x_1}{a}\cos\frac{k\pi y_1}{b}\cos\frac{m\pi x_2}{a}\cos\frac{n\pi y_2}{b}$$

$$\int_{-\infty}^{\infty}\int_{-\infty}^{\infty} \frac{\Omega^2 \cos k_{z_{jk}} z_1 \cos k_{z_{mn}} z_2}{(1+\delta_{0j})(1+\delta_{0k})(1+\delta_{0m})(1+\delta_{0n}) k_{z_{jk}}(\Omega) k_{z_{mn}}(\Omega) \sin k_{z_{jk}} d \sin k_{z_{mn}} d}$$

$$\Bigg\{\frac{16A\Omega^2}{\mu^2 a^2 b^2} \sum_{\substack{q=1\\ r=1}}^{\infty} \sum_{\substack{s=1\\ t=1}}^{\infty} \int_0^b\int_0^a\int_0^b\int_0^a \frac{\sin\frac{q\pi x_1}{a}\sin\frac{r\pi y_1}{b}\sin\frac{s\pi x_2}{a}\sin\frac{t\pi y_2}{b}}{T_{qr}(\Omega) T_{st}(\Omega) P_r(\Omega) P_t(\Omega) R_q(\Omega) R_s(\Omega)} V_{qrst}(\Omega)\, G_{rt}(\Omega)$$

$$\cos\frac{j\pi x_1}{a}\cos\frac{k\pi y_1}{b}\cos\frac{m\pi x_2}{a}\cos\frac{n\pi y_2}{b}\, dx_1 dy_1 dx_2 dy_2\Bigg\} e^{i\Omega\tau} d\Omega\, e^{-i\omega\tau}\, d\tau$$

$$\Omega \le 1.256\,\frac{U_o}{\delta^*},$$

$$S_{aa}(x_1,x_2,y_1,y_2,z_1,z_2,\omega) = \frac{8\rho_{a_0}^2}{\pi a^2 b^2} \sum_{\substack{j=0\\k=0}}^{\infty} \sum_{\substack{m=0\\n=0}}^{\infty} \cos\frac{j\pi x_1}{a} \cos\frac{k\pi y_1}{b} \cos\frac{m\pi x_2}{a} \cos\frac{n\pi y_2}{b}$$

$$\int_{-\infty}^{\infty}\int_{-\infty}^{\infty} \frac{\Omega^2 \cos k_{z_{jk}} z_1 \cos k_{z_{mn}} z_2}{(1+\delta_{0j})(1+\delta_{0k})(1+\delta_{0m})(1+\delta_{0n}) k_{z_{jk}}(\Omega) k_{z_{mn}}(\Omega) \sin k_{z_{jk}} d \sin k_{z_{mn}} d}$$

$$\left\{ \frac{32 A\Omega^2}{\mu^2 a^2 b^2} \left(\frac{\Omega\delta}{U_o}\right)^{-3} \sum_{\substack{q=1\\r=1}}^{\infty} \sum_{\substack{s=1\\t=1}}^{\infty} \int_0^b\int_0^a\int_0^b\int_0^a \frac{\sin\frac{q\pi x_1}{a} \sin\frac{r\pi y_1}{b} \sin\frac{s\pi x_2}{a} \sin\frac{t\pi y_2}{b}}{T_{qr}(\Omega) T_{st}(\Omega) P_r(\Omega) P_t(\Omega) R_q(\Omega) R_s(\Omega)} V_{qrst}(\Omega) G_{rt}(\Omega)\right.$$

$$\left. \cos\frac{j\pi x_1}{a} \cos\frac{k\pi y_1}{b} \cos\frac{m\pi x_2}{a} \cos\frac{n\pi y_2}{b}\, dx_1 dy_1 dx_2 dy_2 \right\} e^{i\Omega\tau} d\Omega\, e^{-i\omega\tau} d\tau$$

$$\Omega > 1.256 \frac{U_o}{\delta^*} . \tag{4.108}$$

Let

$$F_{qrst}(x_1,x_2,y_1,y_2) = \sin\frac{q\pi x_1}{a} \sin\frac{r\pi y_1}{b} \sin\frac{s\pi x_2}{a} \sin\frac{t\pi y_2}{b} , \tag{4.109}$$

$$f_{qrst}(\Omega) = \frac{G_{rt}(\Omega) V_{qrst}(\Omega)}{T_{qr}(\Omega) T_{st}(\Omega) P_r(\Omega) P_t(\Omega) R_q(\Omega) R_s(\Omega)} , \tag{4.110}$$

$$X(\Omega) = \begin{cases} \dfrac{16 A\Omega^2}{\mu^2 a^2 b^2} & \Omega \leq 1.256 \dfrac{U_o}{\delta^*} \\[2ex] \dfrac{32 A\Omega^2}{\mu^2 a^2 b^2} \left(\dfrac{\Omega\delta}{U_o}\right)^{-3} & \Omega > 1.256 \dfrac{U_o}{\delta^*} , \end{cases} \tag{4.111}$$

$$G_{jkmn}(x_1,x_2,y_1,y_2) = \cos\frac{j\pi x_1}{a} \cos\frac{k\pi y_1}{b} \cos\frac{m\pi x_2}{a} \cos\frac{n\pi y_2}{b} , \tag{4.112}$$

$$g_{jkmn}(z_1,z_2,\Omega) = \frac{\Omega^2 \cos k_{z_{jk}} z_1 \cos k_{z_{mn}} z_2}{k_{z_{jk}}(\Omega) k_{z_{mn}}(\Omega) \sin k_{z_{jk}} d \sin k_{z_{mn}} d} . \tag{4.113}$$

From the above definitions, (4.108) may be rewritten as

$$S_{aa}(x_1,x_2,y_1,y_2,z_1,z_2,\omega) = \frac{8\rho_{a_0}^2}{\pi a^2 b^2} \sum_{\substack{j=0\\k=0}}^{\infty} \sum_{\substack{m=0\\n=0}}^{\infty} G_{jkmn}(x_1,x_2,y_1,y_2)$$

$$\int_{-\infty}^{\infty}\left\{\int_{-\infty}^{\infty} \frac{g_{jkmn}(z_1,z_2,\Omega)}{(1+\delta_{0j})(1+\delta_{0k})(1+\delta_{0m})(1+\delta_{0n})} X(\Omega)\right.$$

$$\sum_{\substack{q=1\\r=1}}^{\infty} \sum_{\substack{s=1\\t=1}}^{\infty} \left[\int_0^b\int_0^a\int_0^b\int_0^a F_{qrst}(x_1,x_2,y_1,y_2) f_{qrst}(\Omega)\, G_{jkmn}(x_1,x_2,y_1,y_2)\, dx_1 dy_1 dx_2 dy_2\right]$$

$$\left. e^{i\Omega\tau} d\Omega\right\} e^{-i\omega\tau} d\tau$$

(4.114)

The form of (4.114) indicates that the integration over Ω and the space variables x_1, x_2, y_1, and y_2 may be performed separately. This is easily seen by rearranging (4.114) as follows:

$$S_{aa}(x_1,x_2,y_1,y_2,z_1,z_2,\omega) = \frac{8\rho_{a_0}^2}{\pi a^2 b^2} \sum_{\substack{j=0\\k=0}}^{\infty} \sum_{\substack{m=0\\n=0}}^{\infty} \sum_{\substack{q=1\\r=1}}^{\infty} \sum_{\substack{s=1\\t=1}}^{\infty} \frac{G_{jkmn}(x_1,x_2,y_1,y_2)}{(1+\delta_{0j})(1+\delta_{0k})(1+\delta_{0m})(1+\delta_{0n})}$$

$$\left[\int_0^b\int_0^a\int_0^b\int_0^a F_{qrst}(x_1,x_2,y_1,y_2)\, G_{jkmn}(x_1,x_2,y_1,y_2)\, dx_1 dy_1 dx_2 dy_2\right]$$

$$\int_{-\infty}^{\infty}\left\{\int_{-\infty}^{\infty} g_{jkmn}(z_1,z_2,\Omega)\, X(\Omega)\, f_{qrst}(\Omega)\, e^{i\Omega\tau} d\Omega\right\} e^{-i\omega\tau} d\tau.$$

(4.115)

Since the inverse Fourier transform is defined as

$$f(\tau) = \frac{1}{\sqrt{2\pi}} \int_{-\infty}^{\infty} F(\omega)\, e^{i\omega\tau} d\omega ,$$

the integration over frequency of the bracketed terms in (4.115) results in

$$\sqrt{2\pi}\, g_{jkmn}(z_1,z_2,\tau)\, X(\tau)\, f_{qrst}(\tau) . \qquad (4.116)$$

When (4.116) is inserted into (4.115) and the integration over τ is performed, (4.115) becomes

$$S_{aa}(x_1,x_2,y_1,y_2,z_1,z_2,\omega) = \frac{16\rho_{a_0}^2}{a^2b^2} \sum_{\substack{j=0\\k=0}}^{\infty} \sum_{\substack{m=0\\n=0}}^{\infty} \sum_{\substack{q=1\\r=1}}^{\infty} \sum_{\substack{s=1\\t=1}}^{\infty} G_{jkmn}(x_1,x_2,y_1,y_2)$$

$$g_{jkmn}(z_1,z_2,\omega)\, X(\omega)\, f_{qrst}(\omega) \left[\frac{1}{(1+\delta_{0j})(1+\delta_{0k})(1+\delta_{0m})(1+\delta_{0n})}\right.$$

$$\left.\int_0^b\!\!\int_0^a\!\!\int_0^b\!\!\int_0^a F_{qrst}(x_1,x_2,y_1,y_2)\; G_{jkmn}(x_1,x_2,y_1,y_2)\; dx_1dy_1dx_2dy_2\right].$$

(4.117)

It remains to perform the integration over the spacial coordinates. Using (4.109) and (4.112), by means of standard integration techniques, one finds that

$$\frac{1}{(1+\delta_{0j})(1+\delta_{0k})(1+\delta_{0m})(1+\delta_{0n})}\int_0^b\!\!\int_0^a\!\!\int_0^b\!\!\int_0^a F_{qrst}(x_1,x_2,y_1,y_2)\; G_{jkmn}(x_1,x_2,y_1,y_2)\, dx_1dy_1dx_2dy_2$$

$$= \frac{a^2b^2}{\pi^4}\,\frac{(1-\delta_{qj})(1-\delta_{rk})(1-\delta_{sm})(1-\delta_{tn})qrst\,[1-(-1)^q(-1)^j][1-(-1)^r(-1)^k][1-(-1)^s(-1)^m][1-(-1)^t(-1)^n]}{(1+\delta_{0j})\,(1+\delta_{0k})\,(1+\delta_{0m})\,(1+\delta_{0n})\,(q^2-j^2)\,(r^2-k^2)\,(s^2-m^2)(t^2-n^2)}.$$

(4.118)

Let

$$K_{jkmnqrst} = \frac{(1-\delta_{qj})(1-\delta_{rk})(1-\delta_{sm})(1-\delta_{tn})qrst\,[1-(-1)^q(-1)^j][1-(-1)^r(-1)^k][1-(-1)^s(-1)^m][1-(-1)^t(-1)^n]}{(1+\delta_{0j})\,(1+\delta_{0k})\,(1+\delta_{0m})\,(1+\delta_{0n})\,(q^2-j^2)\,(r^2-k^2)\,(s^2-m^2)(t^2-n^2)}.$$

(4.119)

From (4.117) and (4.119), the cavity acoustic pressure cross spectral density is

$$S_{aa}(x_1,x_2,y_1,y_2,z_1,z_2,\omega) = \frac{16\rho_a^2}{\pi^4} X(\omega) \sum_{\substack{j=0\\k=0}}^{\infty} \sum_{\substack{m=0\\n=0}}^{\infty} \sum_{\substack{q=1\\r=1}}^{\infty} \sum_{\substack{s=1\\t=1}}^{\infty} G_{jkmn}(x_1,x_2,y_1,y_2)$$

$$g_{jkmn}(z_1,z_2,\omega)\ f_{qrst}(\omega)\ K_{jkmnqrst} \ ,$$

(4.120)

where $G_{jkmn}(x_1,x_2,y_1,y_2)$, $g_{jkmn}(z_1,z_2,\omega)$, $f_{qrst}(\omega)$, $X(\omega)$ and $K_{jkmnqrst}$ are defined in equations (4.112), (4.113), (4.110), (4.111), and (4.119), respectively.

4.3.4 Cavity Acoustic Pressure Spectral Density

The cavity acoustic pressure spectral density is defined as

$$\Phi_a(x_1,y_1,z_1,\omega) = S_{aa}(x_1,x_1,y_1,y_1,z_1,z_1,\omega) \ . \tag{4.121}$$

Hence, from (4.120),

$$\Phi_a(x_1,y_1,z_1,\omega) = \frac{16\rho_a^2}{\pi^4} X(\omega) \sum_{\substack{j=0\\k=0}}^{\infty} \sum_{\substack{m=0\\n=0}}^{\infty} \sum_{\substack{q=1\\r=1}}^{\infty} \sum_{\substack{s=1\\t=1}}^{\infty} G_{jkmn}(x_1,x_1,y_1,y_1)$$

$$g_{jkmn}(z_1,z_1,\omega)\ f_{qrst}(\omega)\ K_{jkmnqrst} \ . \tag{4.122}$$

From (4.112), it should be noted that if $x_1 = x_2$ and $y_1 = y_2$,

$$G_{jkmn}(x_1,x_1,y_1,y_1) = G_{mnjk}(x_1,x_1,y_1,y_1) = G_{jkmn}(x_1,y_1) \ . \tag{4.123}$$

Further, from (4.113), if $z_1 = z_2$,

$$g_{jkmn}(z_1,z_1,\omega) = g_{mnjk}(z_1,z_1,\omega) = g_{jkmn}(z_1,\omega) \ . \tag{4.124}$$

Finally, note that

$$K_{jkmnqrst} = K_{mnjkstqr} \ . \tag{4.125}$$

Hence, using (4.110), (4.111), (4.123), and (4.124) in (4.122), and dropping the subscripts on the spacial coordinates, one may express the acoustic spectral density as

$$\Phi_a(x,y,z,\omega) = \frac{256 A \rho_{a_o}^2 \omega^2}{\pi^4 \mu^2 a^2 b^2} \sum_{\substack{j=0\\k=0}}^{\infty} \sum_{\substack{m=0\\n=0}}^{\infty} \sum_{\substack{q=1\\r=1}}^{\infty} \sum_{\substack{s=1\\t=1}}^{\infty} \frac{G_{jkmn}(x,y)\, g_{jkmn}(z,\omega)\, G_{rt}(\omega)}{T_{qr}(\omega) T_{st}(\omega) P_r(\omega) P_t(\omega) R_q(\omega) R_s(\omega)}$$

$$K_{jkmnqrst} \; V_{qrst}(\omega) \qquad \omega \leq 1.256 \frac{U_o}{\delta^*} ,$$

$$\Phi_a(x,y,z,\omega) = \frac{512 A \rho_{a_o}^2 \omega^2}{\pi^4 \mu^2 a^2 b^2} \left(\frac{\omega \delta^*}{U_o}\right)^{.3} \sum_{\substack{j=0\\k=0}}^{\infty} \sum_{\substack{m=0\\n=0}}^{\infty} \sum_{\substack{q=1\\r=1}}^{\infty} \sum_{\substack{s=1\\t=1}}^{\infty} \frac{G_{jkmn}(x,y)\, g_{jkmn}(z,\omega)\, G_{rt}(\omega)}{T_{qr}(\omega) T_{st}(\omega) P_r(\omega) P_t(\omega) R_q(\omega) R_s(\omega)}$$

$$K_{jkmnqrst} \; V_{qrst}(\omega) \qquad \omega > 1.256 \frac{U_o}{\delta^*} . \tag{4.126}$$

As in the case of the plate velocity spectral density, the cavity acoustic pressure spectral density must be a real, even function of frequency. Thus, by substituting V_{qrst} from (4.59) and by investigation of the summation in the frequency range $\omega \leq 1.256 \frac{U_o}{\delta^*}$, arguments similar to those applied in Section 4.2.4 along with equations (4.123), (4.124), and (4.125) show the first summation group to be

$$\frac{256 A \rho_{a_o}^2 \omega^2}{\pi^4 \mu^2 a^2 b^2} \sum_{\substack{j=0\\k=0}}^{\infty} \sum_{\substack{m=0\\n=0}}^{\infty} \sum_{\substack{q=1\\r=1}}^{\infty} \sum_{\substack{s=1\\t=1}}^{\infty} \frac{G_{jkmn}(x,y)\, g_{jkmn}(z,\omega)\, G_{rt}(\omega)\, K_{jkmnqrst}}{T_{qr}(\omega) T_{st}(\omega) P_r(\omega) P_t(\omega) R_q(\omega) R_s(\omega)}$$

$$[1.0066\, \delta_{qs} R_q \cos(\nu_q - 0.463\pi)]\, e^{i(\lambda_{qr} - \lambda_{st})}$$

$$- \frac{1}{2}\left\{\frac{256 A \rho_{a_o}^2 \omega^2}{\pi^4 \mu^2 a^2 b^2} \sum_{\substack{j=0\\k=0}}^{\infty} \sum_{\substack{m=0\\n=0}}^{\infty} \sum_{\substack{q=1\\r=1}}^{\infty} \sum_{\substack{s=1\\t=1}}^{\infty} \frac{G_{jkmn}(x,y)\, g_{jkmn}(z,\omega)\, G_{rt}(\omega)\, K_{jkmnqrst}}{T_{qr}(\omega) T_{qt}(\omega) P_r(\omega) P_t(\omega) R_q(\omega) R_s(\omega)} \right.$$

$$\left. [1.0066\, R_q \cos(\nu_q - 0.463\pi)]\, e^{i(\lambda_{qr} - \lambda_{qt})} \right\}$$

$$+ \frac{1}{2}\left\{\frac{256 A \rho_{a_o}^2 \omega^2}{\pi^4 \mu^2 a^2 b^2} \sum_{\substack{m=0\\n=0}}^{\infty} \sum_{\substack{j=0\\k=0}}^{\infty} \sum_{\substack{s=1\\t=1}}^{\infty} \sum_{\substack{q=1\\r=1}}^{\infty} \frac{G_{mnjk}(x,y)\, g_{mnjk}(z,\omega)\, G_{tr}(\omega)\, K_{mnjkstqr}}{T_{qt}(\omega) T_{qr}(\omega) P_t(\omega) P_r(\omega) R_s(\omega) R_q(\omega)} \right.$$

$$\left. [1.0066\, R_q \cos(\nu_q - 0.463\pi)]\, e^{i(\lambda_{qt} - \lambda_{qr})} \right\}$$

$$= \frac{256 A \rho_{a_o}^2 \omega^2}{\pi^4 \mu^2 a^2 b^2} \sum_{\substack{j=0\\k=0}}^{\infty} \sum_{\substack{m=0\\n=0}}^{\infty} \sum_{\substack{q=1\\r=1}}^{\infty} \sum_{\substack{s=1\\t=1}}^{\infty} \frac{G_{jkmn}(x,y)\, g_{jkmn}(z,\omega)\, G_{rt}(\omega)\, K_{jkmnqrst}}{T_{qr}(\omega) T_{st}(\omega) P_r(\omega) P_t(\omega) R_q(\omega) R_s(\omega)}$$

$$[1.0066\, \delta_{qs} R_q \cos(\nu_q - 0.463\pi)] \; \frac{1}{2}\left\{e^{i(\lambda_{qr} - \lambda_{st})} + e^{-i(\lambda_{qr} - \lambda_{st})}\right\}.$$

Hence, the first summation group is

$$\frac{256 A \rho_{a_o}^2 \omega^2}{\pi^4 \mu^2 a^2 b^2} \sum_{\substack{j=0\\k=0}}^{\infty} \sum_{\substack{m=0\\n=0}}^{\infty} \sum_{\substack{q=1\\r=1}}^{\infty} \sum_{\substack{s=1\\t=1}}^{\infty} \frac{G_{jkmn}(x,y)\, g_{jkmn}(z,\omega)\, G_{rt}(\omega)\, K_{jkmnqrst}}{T_{qr}(\omega) T_{st}(\omega) P_r(\omega) P_t(\omega) R_q(\omega) R_s(\omega)}$$

$$\left[1.0066\, \delta_{qs} R_q \cos(\nu_q - 0.463\pi) \cos(\lambda_{qr} - \lambda_{st}\right].$$

(4.127)

Similar arguments applied to the remaining summation groups lead to

$$\Phi_a(x,y,z,\omega) = \frac{256 A \rho_{a_o}^2 \omega^2}{\pi^4 \mu^2 a^2 b^2} \sum_{\substack{j=0\\k=0}}^{\infty} \sum_{\substack{m=0\\n=0}}^{\infty} \sum_{\substack{q=1\\r=1}}^{\infty} \sum_{\substack{s=1\\t=1}}^{\infty} \frac{G_{jkmn}(x,y)\, g_{jkmn}(z,\omega)\, G_{rt}(\omega)}{T_{qr}(\omega) T_{st}(\omega) P_r(\omega) P_t(\omega) R_q(\omega) R_s(\omega)}$$

$$W_{qrst}(\omega)\, K_{jkmnqrst} \qquad \omega \le 1.256 \frac{U_o}{\delta^*},$$

$$\Phi_a(x,y,z,\omega) = \frac{512 A \rho_{a_o}^2 \omega^2}{\pi^4 \mu^2 a^2 b^2} \left(\frac{\omega \delta}{U_o}\right)^{-3} \sum_{\substack{j=0\\k=0}}^{\infty} \sum_{\substack{m=0\\n=0}}^{\infty} \sum_{\substack{q=1\\r=1}}^{\infty} \sum_{\substack{s=1\\t=1}}^{\infty} \frac{G_{jkmn}(x,y)\, g_{jkmn}(z,\omega)\, G_{rt}(\omega)}{T_{qr}(\omega) T_{st}(\omega) P_r(\omega) P_t(\omega) R_q(\omega) R_s(\omega)}$$

$$W_{qrst}(\omega)\, K_{jkmnqrst} \qquad \omega > 1.256 \frac{U_o}{\delta^*}.$$

(4.128)

4.4 Non-Dimensional Spectra

The results of Sections 4.2.4 and 4.3.4 are more useful from a practical viewpoint if they are expressed in a non-dimensional form. The following sections are devoted to expressing the plate velocity and cavity acoustic pressure spectral densities in non-dimensional forms.

4.4.1 Dimensionless Plate Velocity Spectral Density

The plate velocity spectral density (equation (4.68)) is a function of the following parameters and dimensions:

μ $\left(\frac{FT^2}{L^3}\right)$

ρ_f $\left(\frac{FT^2}{L^4}\right)$

U_o $\left(\frac{L}{T}\right)$

δ^* (L)

a (L)

b (L)

U_c $\left(\frac{L}{T}\right)$

ω_{mn} $\left(\frac{1}{T}\right)$

r $\left(\frac{FT}{L}\right)$

$r_{c_{mn}}$ $\left(\frac{FT}{L}\right)$

D (FL)

Note that only three dimensions (force, length, and time) are required to specify the eleven input parameters. It is therefore necessary to select a length, force, and time scale characteristic of the system. Although there are many combinations of the eleven input parameters which result in dimensions of force, length, or time, the following were selected as characteristic dimensions because it was felt that they had the strongest effect on the plate velocity spectral density:

a	- streamwise plate dimension	(L)
$\frac{a}{U_c}$	- time for an eddy to traverse the plate in the streamwise direction	(T)
$\mu U_c^2 a$	- fictitious force based on the mass of the plate	(F)

By utilizing these characteristic dimensions, it is possible to specify dimensionless input parameters as follows:

$$
\begin{aligned}
M &= \frac{\rho_f a}{\mu} \\
U^+ &= \frac{U_o}{U_c} \\
\delta^+ &= \frac{\delta^*}{a} \\
b^+ &= \frac{b}{a} \\
\omega^+_{mn} &= \frac{\omega_{mn} a}{U_c} \\
r^+ &= \frac{ra}{\mu U_c} \\
r^+_{c_{mn}} &= \frac{r_{c_{mn}} a}{\mu U_c} = \frac{2\omega_{mn} a}{U_c} \\
D^+ &= \frac{D}{\mu U_c^2 a^2} .
\end{aligned}
\tag{4.129}
$$

Further, the spacial and frequency variables may be similarly non-dimensionalized as follows:

$$
\begin{aligned}
x^+ &= \frac{x}{a} \\
y^+ &= \frac{y}{a} \\
\omega^+ &= \frac{\omega a}{U_c} .
\end{aligned}
\tag{4.130}
$$

Based on the definition of (4.129) and (4.130), the quantities defined in equations (4.46) through (4.49), (4.52) through (4.58), and equation (4.67) may be rewritten in dimensionless terms as follows:

$$
R^+_m(\omega^+) = \{ [(m\pi)^2 - 0.987\,\omega^{+2}]^2 + 0.0529\,\omega^{+4} \}^{1/2} , \tag{4.131}
$$

$$\nu_m = \tan^{-1}\left[\frac{0.23\,\omega^{+2}}{(m\pi)^2 - 0.987\,\omega^{+2}}\right], \tag{4.132}$$

$$\lambda_{mn} = \tan^{-1}\left[\frac{r^+\omega^+}{(\omega^+_{mn})^2 - (\omega^+)^2}\right], \tag{4.133}$$

$$G^+_{mn}(\omega^+) = 0.35\,\omega^+ b^+ \delta_{mn}\left[2(0.7\,\omega^+ b^+)^2 + (m\pi)^2 + (n\pi)^2\right]$$
$$+ mn\pi^2\left[(-1)^m(-1)^n - 1\right]\left[1 - \delta_{mn}\right] + mn\pi^2\left\{2 - \left[(-1)^m + (-1)^n\right]e^{-0.7\omega^+ b^+}\right\}, \tag{4.134}$$

$$P^+_m(\omega^+) = (m\pi)^2 + (0.7\,\omega^+ b^+)^2, \tag{4.135}$$

$$T^+_{mn}(\omega^+) = \left\{\left[\left(\frac{\omega^+_{mn}}{\omega^+}\right)^2 - 1\right]^2 + \left[2\frac{r^+}{r^+_{c_{mn}}}\frac{\omega^+_{mn}}{\omega^+}\right]^2\right\}^{1/2}, \tag{4.136}$$

$$W^+_{jkmn}(\omega^+) = 1.0066\,\omega^+\delta_{jm}\cos(\nu_j - 0.463\,\pi)\cos(\lambda_{jk} - \lambda_{mn})$$
$$+ 2jm\pi^2\cos(\nu_j + \nu_m)\cos(\lambda_{jk} - \lambda_{mn})$$
$$+ (1 - \delta_{jm})\frac{jm\pi^2\left[(-1)^j(-1)^m - 1\right]}{\left[(j\pi)^2 - (m\pi)^2\right]}\left[R^+_j\cos(\nu_m + \lambda_{jk} - \lambda_{mn}) - R^+_m\cos(\nu_j + \lambda_{mn} - \lambda_{jk})\right]$$
$$- jm\pi^2 e^{-0.115\omega^+}\left[(-1)^j\cos(\omega^+ + \nu_j + \nu_m + \lambda_{jk} - \lambda_{mn}) + (-1)^m\cos(\omega^+ + \nu_j + \nu_m + \lambda_{mn} - \lambda_{jk})\right]. \tag{4.137}$$

Further, by defining

$$\Phi^+_\phi(x^+, y^+, \omega^+) = \frac{\Phi_\phi(x^+, y^+, \omega^+)}{\alpha^2 U_c a}, \tag{4.138}$$

and utilizing the above definitions and equation (4.68), the non-dimensional form of the plate velocity spectral density can easily be shown to be

$$\Phi_{\phi}^{+}(x^{+}, y^{+}, \omega^{+}) = 4.38 \times 10^{-4} M^{2} \delta^{+} \omega^{+^{-2}}$$

$$\sum_{\substack{m=1 \\ n=1}}^{\infty} \sum_{\substack{q=1 \\ s=1}}^{\infty} \frac{\sin m\pi x^{+} \sin q\pi x^{+} \sin \frac{n\pi y^{+}}{b^{+}} \sin \frac{s\pi y^{+}}{b^{+}} G_{ns}^{+}(\omega^{+}) \Psi_{mnqs}^{+}(\omega^{+})}{T_{mn}^{+}(\omega^{+}) T_{qs}^{+}(\omega^{+}) P_{n}^{+}(\omega^{+}) P_{s}^{+}(\omega^{+}) R_{m}^{+}(\omega^{+}) R_{q}^{+}(\omega^{+})}$$

$$\omega^{+} \delta^{+} \leq 1.932 ,$$

$$\Phi_{\phi}^{+}(x^{+}, y^{+}, \omega^{+}) = 3.2 \times 10^{-3} M^{2} \delta^{+^{-2}} \omega^{+^{-5}}$$

$$\sum_{\substack{m=1 \\ n=1}}^{\infty} \sum_{\substack{q=1 \\ s=1}}^{\infty} \frac{\sin m\pi x^{+} \sin q\pi x^{+} \sin \frac{n\pi y^{+}}{b^{+}} \sin \frac{s\pi y^{+}}{b^{+}} G_{ns}^{+}(\omega^{+}) \Psi_{mnqs}^{+}(\omega^{+})}{T_{mn}^{+}(\omega^{+}) T_{qs}^{+}(\omega^{+}) P_{n}^{+}(\omega^{+}) P_{s}^{+}(\omega^{+}) R_{m}^{+}(\omega^{+}) R_{q}^{+}(\omega^{+})}$$

$$\omega^{+} \delta^{+} > 1.932 . \tag{4.139}$$

4.4.2 Dimensionless Cavity Acoustic Pressure Spectral Density

The cavity acoustic pressure spectral density is a function of all of the parameters affecting the plate velocity spectral density (see Section 4.4.1) plus the following additions:

$$c \left(\frac{L}{T}\right)$$

$$d \ (L)$$

$$\rho_{a_0} \left(\frac{FT^2}{L^4}\right)$$

In addition, there is one more variable in the case of the acoustic spectral density, namely, the length dimension (z) perpendicular to the plane of the plate.

Since the plate vibration provides the excitation for the acoustic pressure in the cavity, it would seem reasonable to select the same characteristic dimensions for non-dimensionalization of the cavity acoustic pressure spectral density as were used for the plate velocity spectral density. The dimensionless input parameters for the cavity acoustic pressure spectral density are, therefore, those presented in equation (4.129) plus the following additions:

$$c^+ = \frac{c}{U_c}$$
$$d^+ = \frac{d}{a} \qquad (4.140)$$
$$\rho^+ = \frac{\rho_a a_o}{\mu} .$$

Likewise, the variables are those presented in equation (4.130) plus

$$z^+ = \frac{z}{a} . \qquad (4.141)$$

Since the non-dimensionalization has been performed with the same characteristic dimensions as in the case of the plate velocity spectral density, the dimensionless quantities defined in equations (4.131) to (4.137) are also applicable to the cavity acoustic pressure spectral density. Noting that $K_{jkmnqrst}$ is already dimensionless, one needs only to define

$$k^+_{z_{jk}}(\omega^+) = \left[\left(\frac{\omega^+}{c^+}\right)^2 - (j\pi)^2 - \left(\frac{k\pi}{b^+}\right)^2\right]^{1/2} , \qquad (4.142)$$

$$U^+_{jkmn}(\omega^+) = k^+_{z_{jk}}(\omega^+) k^+_{z_{mn}}(\omega^+) \sin k^+_{z_{jk}} d^+ \sin k^+_{z_{mn}} d^+ , \qquad (4.143)$$

and

$$\Phi^+_a(x^+, y^+, z^+, \omega^+) = \frac{\Phi_a(x^+, y^+, z^+, \omega^+) a}{a^2 \mu^2 U_c^3} , \qquad (4.144)$$

in order to specify the dimensionless form of the cavity acoustic pressure spectral density. By use of equations (4.128), (4.131) through (4.137), and

(4.142) through (4.144), the dimensionless form of the cavity acoustic spectral density can easily be shown from (4.128) to be

$$\Phi_a^+(x^+, y^+, z^+, \omega^+) = \frac{7.008 \times 10^{-3}}{\pi^4} \rho^{+2} M^2 \delta^+ \sum_{\substack{j=0\\k=0}}^{\infty} \sum_{\substack{m=0\\n=0}}^{\infty} \sum_{\substack{q=1\\r=1}}^{\infty} \sum_{\substack{s=1\\t=1}}^{\infty} \left\{ \frac{G_{rt}^+(\omega^+) W_{qrst}^+(\omega^+) K_{jkmnqrst}}{U_{jkmn}^+(\omega^+)} \right.$$

$$\left. \frac{\cos j\pi x^+ \cos m\pi x^+ \cos \frac{k\pi y^+}{b^+} \cos \frac{n\pi y^+}{b^+} \cos k_{z_{jk}}^+ z^+ \cos k_{z_{mn}}^+ z^+}{T_{qr}^+(\omega^+) T_{st}^+(\omega^+) P_r^+(\omega^+) P_t^+(\omega^+) R_q^+(\omega^+) R_s^+(\omega^+)} \right\}$$

$$\omega^+ \delta^+ \leq 1.932 ,$$

$$\Phi_a^+(x^+, y^+, z^+, \omega^+) = \frac{5.112 \times 10^{-2}}{\pi^4} \rho^{+2} M^2 \delta^{+-2} \omega^{+-3} \sum_{\substack{j=0\\k=0}}^{\infty} \sum_{\substack{m=0\\n=0}}^{\infty} \sum_{\substack{q=1\\r=1}}^{\infty} \sum_{\substack{s=1\\t=1}}^{\infty} \left\{ \frac{G_{rt}^+(\omega^+) W_{qrst}^+(\omega^+) K_{jkmnqrst}}{U_{jkmn}^+(\omega^+)} \right.$$

$$\left. \frac{\cos j\pi x^+ \cos m\pi x^+ \cos \frac{k\pi y^+}{b^+} \cos \frac{n\pi y^+}{b^+} \cos k_{z_{jk}}^+ z^+ \cos k_{z_{mn}}^+ z^+}{T_{qr}^+(\omega^+) T_{st}^+(\omega^+) P_r^+(\omega^+) P_t^+(\omega^+) R_q^+(\omega^+) R_s^+(\omega^+)} \right\}$$

$$\omega^+ \delta^+ > 1.932 .$$

(4.145)

V

RESULTS

The following section presents plate velocity spectra and cavity acoustic spectra calculated from equations (4.139) and (4.145) by means of a digital computer for selected data cases. The purpose of these calculations was threefold. First, the calculated plate velocity spectral density may be compared with existing measurements of plate response to turbulent excitation, thereby providing a check on the validity of the analytic solution for the plate velocity statistics. Secondly, the effects of all major parameters are not readily discernible from equations (4.139) and (4.145), and it was felt that calculated spectra for selected cases would better define these effects. Finally, it was necessary to check the range of validity of the assumption that the cavity acoustic pressure had negligible effect in the excitation of the plate.

The spectral densities were selected for computation over the cross spectral densities because they were most easily computed and gave the desired results: namely, the effect of major parameters on the cavity acoustic pressure statistics, and the range of validity of the above stated assumption.

The computations were performed partially on the IBM 704 digital computer at the U. S. Navy Underwater Sound Laboratory, and the remainder on the IBM 7090 digital computer at the David Taylor Model Basin.

5.1 Results of Plate Velocity Spectral Density Computations

The plate velocity spectral density was computed from the dimensionless equation (4.139). Computations were performed on the IBM 704 digital computer by an iterative process. In all cases, the summation terms in equation (4.139) appeared to converge monotonically, and the solution was accepted if two successive iterations agreed within three percent. This tolerance was selected as a compromise between desired accuracy and reasonable computation time.

The dimensionless plate velocity spectrum was generated by computing the spectral density at a dimensionless frequency one cycle above each dimensionless plate natural frequency, and at three points, equally spaced in frequency, between each pair of adjacent natural frequencies. Peculiarities of the particular computer program used for the generation of the frequencies at which the spectral density was to be computed were responsible for the spectral density being computed at a dimensionless frequency one cycle higher than the plate natural frequency. The resulting error in the computed plate velocity spectrum at plate resonances should be very small, except at very low frequencies or for very small values of damping.

5.1.1 Comparison with Existing Experimental Data

In order to check the validity of the analytically derived plate spectral density, it was desirable to compare the computed plate velocity spectral density from equation (4.139) to available experimental data. Unfortunately, all existing experimental information deals with fixed edge plates whereas equation

(4.139) pertains only to a simply supported plate. However, the spectral levels for a simply supported plate should be of the same order of magnitude as those for a plate with clamped edges, even though the plate natural frequencies will be different in the two cases. It was therefore decided to compare the general level of the spectrum predicted by equation (4.139) with available data for a clamped edge plate.

Some of the most reliable experimental data on the turbulent flow excitation of flat plates are those of Bull *et al.* [15]. Bull measured the displacement spectral density of 3.5 × 3.5 inch steel plates of varying thicknesses to turbulent boundary layer excitation in a wind tunnel. Since no acoustic cavity was placed behind the plate, the effects of acoustic back pressure are negligible. Figure 8 presents Bull's measurements of the response of a 3.5 × 3.5 × 0.010 inch plate to air flowing at a free stream velocity of 539 ft/sec. The measured displacement thickness was 0.172 inch. The measurement was taken at a position 0.95 inch upstream from the trailing edge of the plate and centered in the lateral direction. Bull measured the modal damping for the first two plate modes and found them to be 3.8 percent critical and 0.5 percent critical, respectively. He states, however, that the measurements were accurate only to ± 23 percent.

Figure 9 presents the computer solution to equation (4.139), converted to the ratio of displacement spectral density to turbulent pressure spectral density, for input data corresponding to Bull's experiment. The dimensionless input parameters were

$$M = 0.099$$
$$U^+ = 1.54 \text{ (assumed)}$$
$$\delta^+ = 0.0491$$
$$b^+ = 1.0$$
$$D^+ = 0.001745$$
$$\frac{r^+}{r^+_{mn}} = 0.005 \text{ (assumed)} .$$

Since ω^+_{mn} and $r^+_{c_{mn}}$ are functions of D^+ and b^+ they need not be independently specified. It should also be noted that U^+, which specifies the ratio of the free stream velocity to the convection velocity, is assumed to be constant. This assumption is not true in fact, since the value of U^+ is a function of $\omega\delta^*/U_o$ as shown in Figure 4. However, computations are greatly simplified by assuming U^+ to be constant. Finally, note that the modal damping is assumed to be constant with frequency and equal to the value measured by Bull for the 2-1 mode. In general, the modal damping is not constant, but this assumption eased computational difficulties. In the computation of the spectrum of Figure 9, the spectral densities were computed at radial frequencies 0.005 cycle (that is, equal to the damping - critical damping ratio) above the plate natural frequencies, and at three points equally spaced in frequency between each adjacent pair of natural frequencies. This procedure resulted in more accurate spectral levels for the low values of damping being used.

Figure 10 compares the theoretically derived spectrum for the simply supported edge condition (Figure 9) with Bull's measurements for the fixed edge condition (Figure 8). Note that, as expected, the natural frequencies are not in agreement because of the different edge conditions imposed on the two cases. Hence, the spectra for the two cases are not in exact agreement.

However, the envelopes of both spectra are in substantial agreement, especially at the higher frequencies. This fact lends credence to this analysis and to the ability of equation (4.139) to predict correctly the velocity spectral density of simply supported plates.

For the higher plate modes, it seems reasonable that the modal stiffness and mass become less and less affected by the plate edge conditions. Hence, for this linear system, it would further seem reasonable that a line connecting the major spectral peaks in the clamped edge case should be very similar in shape and amplitude to one connecting the major spectral peaks in the simply supported case, especially at the higher frequencies. For purposes of discussion here, such a line will be defined as a "peak spectrum." Figure 11 presents the "peak spectra" derived from Figures 8 and 9. The agreement in shape is excellent above 700 cps, and the amplitudes agree within 5 db. This discrepancy in amplitude may easily be due to discrepancies between the assumed value of the damping used in the computed spectrum and the damping present at higher modes in Bull's experiment.

From the above, it appears that the plate velocity spectral density predicted by equation (4.139) is valid for the simply supported plate excited by turbulent boundary layer pressure fluctuations for cases in which the acoustic environment has negligible effect. It may further be concluded that the "peak spectrum" of a flow excited plate is essentially independent of the plate boundary conditions at frequencies above the first few plate natural modes. From an engineering standpoint, this conclusion allows an estimation of the maximum flow excited plate vibration level above a certain frequency from equation (4.139) without regard to boundary conditions. Determination of this lower frequency limit will be treated in the next section.

5.1.2 Effect of Major Parameters on Plate Velocity Spectrum

As stated in Section II, the objective of this study is to provide the submarine sonar systems designer with information concerning the acoustic environment of sonar transducers and the major parameters which may affect this environment. Therefore, the data cases used to show the effects of the major parameters on the plate velocity spectrum were selected with the submarine application in mind. It must be stressed that in all cases the effects of any plate-generated acoustic pressure have been neglected.

The major input parameters for the dimensionless plate spectral density are presented in equation (4.129). For the purposes of this discussion, the variables stated in equation (4.130) may also be considered major parameters. From the definitions of ω^+_{mn} and $r^+_{c_{mn}}$, it can be shown that these parameters are functions only of D^+ and b^+. Further, U^+ is assumed to be equal to 1.54 throughout this analysis. Hence, the only parameters which need be specified in order to obtain a solution to (4.139) are $M, \delta^+, b^+, r^+, D^+, x^+, y^+$, and the range of interest of ω^+.

By inspection of equation (4.139) and equations (4.131) through (4.137), it is evident that effects of b^+, r^+, D^+, x^+, y^+, and ω^+ are obscured by the summation term in (4.139). However, the parameters M and δ^+ occur only outside of the summation, so that the effect of these parameters on the dimensionless plate velocity spectral density are immediately obvious. For most submarine applications, b^+ will vary between 0.5 and 1.0, and it was felt that variations in b^+ over this range would change the plate natural frequencies but would not significantly alter the general level of the spectrum. Hence, the effect of plate shape (b^+) was not investigated in this study. This omission leaves only the damping (r^+), the plate rigidity (D^+), plate point of interest (x^+, y^+), and frequency (ω^+) as parameters to be investigated. The effects of each of these parameters will be discussed below.

5.1.2.1 Effect of Plate Coordinates

Dimensionless input parameters which fall in the range of interest for submarine applications are as follows:

$$
\begin{aligned}
M &= 18.9 \\
D^+ &= 10.3 \\
\delta^+ &= 2.31 \times 10^{-2} \\
b^+ &= 0.6667 \\
r^+ &= 0.1\, r^+_{c_{mn}} \quad \text{(assumed)}.
\end{aligned}
$$

The position of maximum plate vibration is usually of greatest interest as far as plate coordinates are concerned. It seems reasonable that the maximum level would occur at the center of the plate. Hence, the effect of plate coordinates was investigated over the range of plate coordinates $0.2 \leq x^+ \leq 0.5$, $y^+ \leq 0.5$. The frequency range of interest was selected to be $10 \leq \omega^+ \leq 3000$.

Figures 12, 13, and 14 present dimensionless plate velocity spectra for the above stated case with plate coordinates (x^+, y^+) of (1/5, 1/3), (1/3, 1/3), and (1/2, 1/3), respectively. These three spectra show significant differences in shape below a dimensionless frequency of 1000 because of the points of measurement falling on different plate modal nodes or antinodes. A table of the plate dimensionless natural frequencies below 1000 dimensionless cycles is presented in Table 1. Note, for example, that $x^+ = 1/2,\ y^+ = 1/3$

TABLE 1

PLATE DIMENSIONLESS NATURAL FREQUENCIES BELOW $\omega^+ = 1000$

Input Parameters

$M = 18.9$ $\delta^+ = 0.0231$

$D^+ = 10.3$ $b^+ = 0.6667$

$r^+ = 0.1\, r^+_{c_{mn}}$

	ω_{mn}		
m \ n	1	2	3
1	102.9	316.8	673.1
2	198.0	411.8	768.1
3	356.3	570.2	926.5
4	578.1	791.9	
5	863.1		

places the point of interest at the plate center; hence one would not expect to observe $\omega^+_{12}, \omega^+_{21}, \omega^+_{41}, \omega^+_{42}$, etc. However, this position is antinode for $\omega^+_{11}, \omega^+_{13}, \omega^+_{31}$, etc. Figure 14 clearly shows resonances at the frequencies (from Table 1) associated with the 1-1, 1-3, 3-1, and 5-1 modes, whereas the 1-2, 2-1, 4-1, and 4-2 modes are not discernible. Similar effects may be noted in Figures 12 and 13. This fact further supports the validity of equation (4.139).

Consider now the "peak spectra" derived from Figures 12, 13, and 14 above the first plate natural frequency. A comparison of these "peak spectra" is presented in Figure 15. Inspection of Figure 15 shows negligible effect of plate coordinates on the dimensionless plate velocity "peak spectra density" above the first plate mode. It is concluded, therefore, that plate coordinates in the range $0.2 \leq x^+ \leq 0.5, y^+ = 0.333$ have no effect on the dimensionless plate velocity "peak spectral density." This conclusion, in addition to the observations made above concerning Figures 12, 13, and 14, supports the further conclusion that, above the first natural frequency, the effect of changing the point of observation on the plate (plate coordinates) is a change in shape of the dimensionless plate velocity spectrum without changing the general level of the spectrum.

5.1.2.2 Effect of Plate Damping

By utilizing the same input parameters listed in Section 5.1.2.1, the dimensionless plate velocity spectrum was computed for two additional values of damping at the midpoint of the plate $(x^+ = 1/2, y^+ = 1/3)$ over the frequency range $10 \leq \omega^+ \leq 3000$. These additional values of damping were 0.01 $r^+_{c_{mn}}$ and 0.05 $r^+_{c_{mn}}$ The resulting dimensionless plate velocity spectra for these cases are presented in Figures 16 and 17, respectively. Thus, Figures 14, 16, and 17 show the effect of damping alone on the dimensionless plate velocity spectral density. Comparison of these figures shows that an increase in damping decreases the spectral density in the region of the natural frequencies present in the spectra, as would be expected. The amount of this reduction in spectral level is most easily investigated by inspection of the dimensionless "peak spectra" constructed from Figures 14, 16, and 17. A comparison of the "peak spectra" for the three damping cases is presented in Figure 18. It should be noted here that the first plate dimensionless natural frequency (ω^+_{11})

falls above $\omega^+ = \frac{1.932}{\delta^+}$, and that the "peak spectra" presented in Figures 15 and 18 only apply above ω^+_{11}. Hence, any conclusion drawn from the dimensionless "peak spectra" apply only to dimensionless frequencies above $1.932/\delta^+$. Figure 18 shows the effect of damping on the dimensionless plate velocity spectral density at the plate natural frequencies. Note that the slope on the "peak spectrum" is also slightly changed as the damping is varied. This effect may be a result of the computational procedure of computing the dimensionless spectral density at a dimensionless frequency one cycle higher than the plate natural dimensionless frequency. Since the slope change, as noted above, was slight, it was not felt that this effect warranted a complete investigation. The effect of damping on the slope of the "peak spectrum" will be discussed as it appears in Figure 18. However, it should be kept in mind that this effect may have no physical basis.

Figure 19 presents the effect of damping on the "peak spectrum" over the range of damping $0.01 \leq \frac{r^+}{r^+_{c_{mn}}} \leq 0.1$ for the dimensionless frequency of 200, which is equivalent to $\omega^+\delta^+ = 4.62$. This effect may be expressed as

$$10 \log_{10} \Phi^+_{\dot{\varphi}_p}\left(\frac{1}{2}, \frac{1}{3}, \frac{4.62}{\delta^+}\right) = -101.5 - 20 \log_{10}\left(\frac{100 r^+}{r^+_{c_{mn}}}\right). \tag{5.1}$$

It is obvious from (5.1) that the "peak spectrum," and hence, the dimensionless plate velocity spectral density at the plate natural frequencies, varies inversely as the second power of plate damping at the dimensionless frequency of $4.62/\delta^+$.

Figure 20 presents the variation in slope of the dimensionless "peak spectrum" with damping over the same range of damping. This effect may be described by

$$10 \log_{10} \frac{\Phi^{+}_{\dot{\phi}_p}\left(\frac{1}{2}, \frac{1}{3}, \omega^{+}\right)}{\Phi^{+}_{\dot{\phi}_p}\left(\frac{1}{2}, \frac{1}{3}, 10\,\omega^{+}\right)} = -68.5 + 5 \log_{10}\left(\frac{100\, r^{+}}{r^{+}_{c_{mn}}}\right) \qquad \begin{array}{l} \omega^{+} > \omega^{+}_{11}, \\ \omega^{+} > \dfrac{1.932}{\delta^{+}}. \end{array} \tag{5.2}$$

From (5.2), it is seen that, for dimensionless frequencies above the first plate dimensionless natural frequency and above $1.932/\delta^{+}$, the slope of the dimensionless "peak velocity spectrum" increases with the one-half power of damping.

From the above, it may be concluded that the plate damping has a pronounced effect on the dimensionless plate spectral density at dimensionless frequencies corresponding to the plate natural frequencies present in the spectrum. The major effect of damping is to decrease the dimensionless spectral density at these frequencies according to approximately the inverse second power of the damping. This conclusion was also reached by Bull <u>et al.</u> [15] in their investigation on the flow excited vibrations of plates. This lends further support to the validity of this analysis.

5.1.2.3 Effect of Plate Rigidity

By use of the values of M, δ^{+}, b^{+}, and r^{+} prescribed in Section 5.1.2.1, the dimensionless plate velocity spectral density was computed at the plate center $(x^{+} = 1/2, y^{+} = 1/3)$ over the dimensionless frequency range of 11 to 3000 for the additional values of D^{+} of 5.15 and 15.45. The results of these computations are presented in Figures 21 and 22, respectively. The effect of a change in D^{+} alone over the range 5.15 to 15.45 can be seen from Figures

14, 21, and 22. Comparison of these figures shows that the prime effect of D^+ is to change both the dimensionless natural frequencies and the dimensionless velocity spectral density at those natural frequencies present in the spectrum. From consideration of basic vibration theory, this result is not unexpected.

It is again instructive to examine the dimensionless "peak velocity spectra" derived from Figures 19, 21, and 22. Figure 23 presents this comparison. It is seen that the prime effect of the plate rigidity is to change the lower limits of applicability of the "peak velocity spectrum" without significantly changing the spectral level. This becomes obvious when it is recalled that the "peak spectrum" for the application described here is only valid above the first dimensionless plate natural frequency, and it can be shown that the first plate dimensionless natural frequency varies as the one-half power of D^+. Comparison of the lower limiting frequencies in Figure 23 bear out this relation.

5.1.3 Dimensionless Plate Velocity "Peak Spectral Density"

As previously stated, the dimensionless plate velocity "peak spectral density" is a useful engineering result in that it allows prediction of the maximum plate velocity spectral levels. Often this knowledge is sufficient to enable the engineer to make a decision concerning a design problem or an equipment specification. It would therefore be desirable to derive an expression by which the dimensionless "peak plate velocity spectrum" could be predicted. Such an expression would have the further advantage that it would show the effect of the major parameters on the dimensionless plate velocity spectrum at the dimensionless plate natural frequencies. The results of the above sections provide sufficient data for such a derivation over the range of parameters pertinent to the submarine application.

From equation (4.139) and the discussion in Section 5.1.2, it is obvious that the dimensionless plate velocity "peak spectral density" $[\Phi^+_{\phi_p}(x^+, y^+, \omega^+)]$ is proportioned to $M^2 \delta^{+^{-2}}$ for dimensionless frequencies above $1.932/\delta^+$. Section 5.1.2.1 further concludes that, in the range $1/5 \leq x^+ \leq 1/2,\ y^+ = 1/3$, the dimensionless peak spectral density is independent of the plate coordinates x^+ and y^+. Hence,

$$\Phi^+_{\phi_p}(x^+, y^+, \omega^+) = \Phi^+_{\phi_p}(\omega^+) \qquad \frac{1}{5} \leq x^+ \leq \frac{1}{2},\ y^+ = \frac{1}{3}. \tag{5.3}$$

Further, in Section 5.1.2.2, the effect of damping on the amplitude and slope of the dimensionless plate "peak velocity spectrum" was presented in equations (5.1) and (5.2). Finally, Section 5.1.2.3 showed that the effect of D^+ was essentially that of shifting the lower dimensionless frequency limit of application of the "peak spectrum" concept.

By noting from Figures 15, 18, and 23, that the slope of the dimensionless "peak spectral density" is constant with dimensionless frequency on a semi-logarithmic scale, and by recalling that for the submarine application $\omega^+_{11} > \frac{1.932}{\delta^+}$, it would seem reasonable from (5.3) and the above discussion to assume the following form for the plate velocity "peak spectral density":

$$\Phi^+_{\phi_p}(\omega^+) = C_1 M^2 \delta^{+^{-2}} \left(\frac{r^+}{r^+_{c_{mn}}}\right)^n \omega^{+^{s(r^+/r^+_{c_{mn}})}} \qquad \frac{1}{5} \leq x^+ \leq \frac{1}{2},\ y^+ = \frac{1}{3}, \tag{5.4}$$

$$\omega^+ > \omega^+_{11}\ ,\ \omega^+ > \frac{1.932}{\delta^*}\ ;$$

or, in logarithmic form:

$$10 \log_{10} \Phi^{+}_{\phi_p}(\omega^{+}) = C_2 + 20 \log_{10} M - 20 \log_{10} \delta^{+} + 10\, n \log_{10}\left(\frac{r^{+}}{r^{+}_{c_{mn}}}\right) + 10\, g\left(\frac{r^{+}}{r^{+}_{c_{mn}}}\right) \log_{10} \omega^{+}$$

$$\frac{1}{5} \leq x^{+} \leq \frac{1}{2},\ y^{+} = \frac{1}{3},$$

$$\omega^{+} > \omega^{+}_{11},\ \omega^{+} > \frac{1.932}{\delta^{+}}. \tag{5.4a}$$

where C_2, n, and $g(r^{+})$ are to be determined from (5.1) and (5.2).

Using the values of M and δ^{+} given in Section 5.1.2.1, comparison of (5.1) and (5.4a) yields

$$-101.5 - 20 \log_{10}\left(\frac{100\, r^{+}}{r^{+}_{c_{mn}}}\right) = C_2 + 10\, g\left(\frac{r^{+}}{r^{+}_{c_{mn}}}\right) \log_{10} \frac{4.62}{\delta^{+}} + 58.4 + 10\, n \log_{10}\left(\frac{r^{+}}{r^{+}_{c_{mn}}}\right), \tag{5.5}$$

from which

$$n = -2 \tag{5.6}$$

and

$$C_2 = -199.9 - 10\, g\left(\frac{r^{+}}{r^{+}_{c_{mn}}}\right) \log_{10} \frac{4.62}{\delta^{+}}. \tag{5.7}$$

Substituting (5.6) and (5.7) into (5.4a) results in

$$10 \log_{10} \Phi^{+}_{\phi_p}(\omega^{+}) = -199.9 + 20 \log_{10} M - 20 \log_{10} \delta^{+} - 20 \log_{10}\left(\frac{r^{+}}{r^{+}_{c_{mn}}}\right) + 10\, g\left(\frac{r^{+}}{r^{+}_{c_{mn}}}\right) \log_{10} \frac{\omega^{+}\delta^{+}}{4.62}$$

$$\frac{1}{5} \leq x^{+} \leq \frac{1}{2},\ y^{+} = \frac{1}{2},$$

$$\omega^{+} > \omega^{+}_{11},\ \omega^{+} > \frac{1.932}{\delta^{+}}. \tag{5.4b}$$

Comparison of (5.4b) and (5.2) yields

$$-68.5 + 5 \log_{10}\left(\frac{100\, r^{+}}{r^{+}_{c_{mn}}}\right) = 10\, g\left(\frac{r^{+}}{r^{+}_{c_{mn}}}\right)$$

or

$$g\left(\frac{r^+}{r^+_{c_{mn}}}\right) = -6.85 + 0.5\log_{10}\left(\frac{100\,r^+}{r^+_{c_{mn}}}\right). \tag{5.8}$$

Substituting (5.8) into (5.4b) yields

$$10\log_{10}\Phi^+_{\phi_p}(\omega^+) = -199.9 + 20\log_{10}M - 20\log_{10}\delta^+ - 20\log_{10}\left(\frac{r^+}{r^+_{c_{mn}}}\right)$$

$$-\left[68.5 + 5\log_{10}\left(\frac{100\,r^+}{r^+_{c_{mn}}}\right)\right]\log_{10}\left(\frac{\omega^+\delta^+}{4.62}\right)$$

$$\frac{1}{5} \leq x^+ \leq \frac{1}{2}\,,\; y^+ = \frac{1}{3}\,,$$

$$\omega^+ > \omega^+_{11}\,,\; \omega^+ > \frac{1.932}{\delta^+} \tag{5.9}$$

or, by a slight rearrangement,

$$10\log_{10}\Phi^+_{\phi_p}(\omega^+) = -159.9 - 20\log_{10}\left(\frac{100\,r^+}{r^+_{c_{mn}}}\,\frac{\delta^+}{M}\right) - \left[68.5 + 5\log_{10}\left(\frac{100\,r^+}{r^+_{c_{mn}}}\right)\right]\log_{10}\left(\frac{\omega^+\delta^+}{4.62}\right)$$

$$\frac{1}{5} \leq x^+ \leq \frac{1}{2}\,,\; y^+ = \frac{1}{3}\,,$$

$$\omega^+ > \omega^+_{11}\,,\; \omega^+ > \frac{1.932}{\delta^+}\,, \tag{5.9a}$$

where

$$\omega^+_{11} = \pi^2\sqrt{D^+}\left(\frac{b^{+2}+1}{b^{+2}}\right) \tag{5.10}$$

and

$$r^+_{c_{mn}} = 2\,\omega^+_{mn} \tag{5.11}$$

Figure 24 compares the dimensionless plate velocity "peak spectrum" calculated from equation (5.9a) to the computed spectrum of Figure 16. Agreement between the dimensionless plate velocity spectral density at the plate natural frequencies and the dimensionless "peak spectrum" are seen to be excellent. It may therefore be concluded that equation (5.9a) accurately represents the effect of major parameters on the dimensionless plate velocity spectral density at the plate natural frequencies and further predicts a plate velocity "peak spectrum" in agreement with results computed from equation (4.139).

5.2 Results of Cavity Acoustic Pressure Spectral Density Computations

The dimensionless cavity acoustic pressure spectral density was computed from equation (4.145). Computations were performed on the IBM 704 and the IBM 7090 digital computers by iterative processes. Again, the summation terms in equation (4.145) appeared to converge monotonically in all cases. However, because of the octuple summation in (4.145), the computational time required for a spectral point was large, especially at the higher plate modes. Therefore, the solution was accepted if two successive iterations agreed within 20 percent. This gave a computational accuracy to within ± 1 decibel, which compares well with experimental accuracy. Even with this fairly large tolerance, the computation of the dimensionless cavity acoustic pressure spectral density for a frequency corresponding to the 5-1 plate mode required more than 20 hours on the IBM 704 computer. The IBM 7090 computer proved to be approximately eight times faster.

Because of the large computer time required per spectrum, the dimensionless cavity acoustic spectrum was generated by computing the spectral density at a dimensionless frequency equal to each dimensionless plate natural frequency plus the ratio of damping to critical damping, and at two points, equally spaced in frequency, between each pair of adjacent plate natural frequencies. It will be recalled that the plate velocity spectrum was generated similarly, except that the spectral density was computed at three points, equally spaced in frequency, between each pair of adjacent natural frequencies. This change results in a cavity acoustic pressure spectrum less precise than the plate velocity spectrum, but the computer time requirement dictated some time economies.

It will be recalled that acoustic damping effects have been neglected in the derivation of equation (4.145), and that the only damping effects are associated with the plate. It was thus felt that solutions of (4.145) at or above the first cavity acoustic natural frequency would not be physically valid. Hence, computations of the dimensionless cavity acoustic pressure spectrums were confined, with two exceptions, below the first cavity acoustic natural frequency.

To the author's knowledge, no experimental information exists for a case corresponding to the theoretical model treated here.

The purpose of computing the dimensionless cavity acoustic pressure spectra from equation (4.145) was to show the effects of major parameters and to establish the range of validity of the assumption that the acoustic back pressure may be neglected.

5.2.1 Effect of Major Parameters on the Cavity Acoustic Pressure Spectrum

The data cases used to study the effects of major parameters were selected with the submarine application in mind. Since the plate natural frequencies and critical modal damping (ω^+_{mn} and $r^+_{c_{mn}}$) are functions of D^+ and b^+, and $U^+ = 1.54$ throughout this analysis, the independent major parameters affecting the dimensionless cavity acoustic pressure spectral density are $M, \delta^+, b^+, r^+, D^+, c^+, d^+, \rho^+, x^+, y^+, z^+, \omega^+$.

Inspection of equation (4.145) and equations (4.131) through (4.137), (4.142) and (4.143) shows that the effects of $b^+, r^+, D^+, c^+, d^+, x^+, y^+, z^+$, and ω^+ are obscured by the summation, whereas the effects of M, δ^+, and ρ^+ are explicit in (4.145). The effect of the cavity dimensions, b^+ and d^+, will be primarily that of redistributing the cavity acoustic natural frequencies, and since these computations were confined, for the most part, below the first cavity acoustic natural frequency, the effects of b^+ and d^+ were not investigated.

As previously stated, the damping (r^+) present in this analysis is associated with the plate. Note that the terms in equation (4.145) containing r^+ (namely, $\lambda_{mn}, T_{mn}, W_{jkmn}$) occur in exactly the same combinations and are summed over the same range of indices as the same terms containing r^+ in equation (4.139). If the concept of a "peak spectrum" is again introduced for the cavity acoustic pressure, it would seem reasonable from the above to suspect that the effect of damping on the cavity acoustic "peak spectrum" should be the same as that on the plate velocity "peak spectrum." Hence, from equations (5.1) and (5.2), it is assumed that

$$10 \log_{10} \Phi^+_{a_p}\left(x^+, y^+, z^+, \frac{4.62}{\delta^+}\right) = C_1 - 20 \log_{10}\left(\frac{100\, r^+}{r^+_{c_{mn}}}\right) \tag{5.12}$$

and

$$10 \log_{10} \frac{\Phi^+_{a_p}(x^+, y^+, z^+, \omega^+)}{\Phi^+_{a_p}(x^+, y^+, z^+, 10\,\omega^+)} = C_2 + 5 \log_{10}\left(\frac{100 r^+}{r^+_{c_{mn}}}\right) \qquad \begin{array}{l} \omega^+ > \omega^+_{11}\ , \\ \omega^+ > \dfrac{1.932}{\delta^+}\ , \end{array} \tag{5.13}$$

where C_1 is the acoustic pressure "peak spectral density" at a dimensionless frequency of $\frac{4.62}{\delta^+}$, and C_2 is the slope of the "peak spectrum" with frequency. These constants will be evaluated in a later section.

From the above, it remains to investigate the effects of D^+, c^+, x^+, y^+, z^+, and ω^+.

5.2.1.1 Effect of Cavity Coordinates

Dimensionless input parameters which fall in the range of interest for submarine sonar applications are

$$\begin{aligned} M &= 18.9 \\ D^+ &= 10.3 \\ \delta^+ &= 2.31 \times 10^{-2} \\ b^+ &= 0.6667 \\ r^+ &= 0.1\, r^+_{c_{mn}} \\ c^+ &= 454 \\ d^+ &= 0.3333 \\ \rho^+ &= 18.9\ . \end{aligned}$$

Note that the first five parameters are the same as those listed in Section 5.1.2.1 for the plate. This set of parameters will hereafter be referred to as Case 1.

The effect of plate coordinates w^s investigated for the following sets of cavity coordinates (x^+, y^+, z^+):

$$\left(\frac{1}{2}, \frac{1}{3}, 0\right)$$

$$\left(\frac{1}{2}, \frac{1}{3}, -\frac{1}{6}\right)$$

$$\left(\frac{1}{2}, \frac{1}{3}, -\frac{1}{3}\right)$$

$$\left(\frac{1}{3}, \frac{1}{3}, -\frac{1}{6}\right).$$

Because of computer time limitations, the frequency range of interest was $10 < \omega^+ < 1000$. The first cavity acoustic dimensionless natural frequency is 1426. The computed dimensionless cavity acoustic pressure spectral densities for the Case 1 parameters and the above listed coordinates are presented in Figures 25 through 28, respectively. Close inspection of these figures reveals very small differences between these spectra throughout the entire frequency range. At the higher frequencies, it may be seen that the dimensionless cavity acoustic pressure spectral density is slightly greater at the bottom of the cavity $(z^+ = 0)$ than at the plate $(z^+ = -1/3)$. Also note (from Table 1) that the 1-1, 3-1, and 1-3 plate modes appear in the cavity acoustic pressure spectra of Figures 25 through 28, regardless of cavity coordinates. The above observations suggest that the dimensionless cavity acoustic pressure spectral density is nearly uniform with position (over the range of coordinates investigated) throughout the cavity at dimensionless frequencies below the first cavity acoustic natural frequency. This is further borne out by Figure 29, which compres the dimensionless cavity acoustic pressure "peak spectra" derived from Figures 25 through 28 above the first plate natural frequency. It is seen that the effect of cavity position on the "peak spectra" is very small in the range investigated; hence, it will be assumed

$$\Phi^{+}_{a_p}(x^{+}, y^{+}, z^{+}, \omega^{+}) = \Phi^{+}_{a_p}(\omega^{+}) \qquad \frac{1}{3} \leq x^{+} \leq \frac{1}{2}\,,\ y^{+} = \frac{1}{3}\,,\ -\frac{1}{3} \leq z^{+} \leq 0\,,$$

$$\omega^{+} < \omega^{+}_{11}\,,\ \omega^{+} > \frac{1.932}{\delta^{+}}\,. \tag{5.14}$$

From the above, it is concluded that, in the range of space variables $1/3 \leq x^{+} \leq 1/2$, $y^{+} = 1/3$, $-1/3 \leq z^{+} \leq 0$, the dimensionless cavity acoustic pressure spectral density is essentially uniform for dimensionless frequencies less than 2/3 of first cavity acoustic natural frequency. It is therefore assumed that the dimensionless cavity acoustic pressure "peak spectral density" is independent of space coordinates.

5.2.1.2 Effect of Speed of Sound of Cavity Fluid

A change of the cavity fluid involves a change in the values of c^{+} and ρ^{+}. The effect of ρ^{+}, as previously stated, is explicitly stated in equation (4.145). Hence, changing the cavity fluid provides a simple method of determining the effect of c^{+} on the dimensionless cavity acoustic pressure spectral density. To this end, the following parameters were selected:

$$\begin{aligned}
M &= 18.9 \\
\delta^{+} &= 0.0231 \\
b^{+} &= 0.6667 \\
r^{+} &= 0.1\, r^{+}_{c_{mn}} \\
D^{+} &= 18.9 \\
d^{+} &= 0.3333 \\
c^{+} &= 100 \\
\rho^{+} &= 0.0221\,.
\end{aligned}$$

This set of parameters will hereafter be referred to as Case 4. A summary of all parameter cases is presented in Table 2.

TABLE 2
PARAMETERS USED FOR COMPUTATION OF ACOUSTIC PRESSURE SPECTRA

PARAMETER	CASE 1	CASE 2	CASE 3	CASE 4
M	18.9	0.51	0.0221	18.9
δ^+	0.0231	0.0202	0.0202	0.0231
b^+	0.6667	0.6667	0.6667	0.6667
d^+	0.3333	0.3333	0.3333	0.3333
$r^+/r^+_{c_{mn}}$	0.1	0.1	0.1	0.1
D^+	10.3	0.0004	0.0259	10.3
c^+	454	5	5	100
ρ^+	18.9	0.51	0.0221	0.0221
ω^+_{11}	102.9	0.641	5.16	102.9
first acoustic natural frequency	1426	15.71	15.71	314.2
$\dfrac{1.932}{\delta^+}$	83.7	95.7	95.7	83.7

The dimensionless cavity acoustic pressure spectral density was computed for the following dimensionless spacial coordinates (x^+, y^+, z^+):

$$\left(\frac{1}{2}, \frac{1}{3}, 0, \omega^+\right)$$

$$\left(\frac{1}{2}, \frac{1}{3}, -\frac{1}{6}, \omega^+\right)$$

$$\left(\frac{1}{2}, \frac{1}{3}, -\frac{1}{3}, \omega^+\right).$$

The frequency range of interest was $10 < \omega^+ < 500$. From Table 2, it is seen that this range includes the first acoustic natural frequency of the cavity. The computed spectra for Case 4 are presented in Figures 30, 31, and 32.

Comparison of Figures 30 through 32 again shows no effect due to cavity coordinates below a dimensionless frequency equal to 2/3 of the first cavity acoustic natural frequency. Above this point, the acoustic pressure spectrum at the plate becomes higher than the spectrum at the bottom and middle of the cavity. This result is not in agreement with the results of Case 1, which showed the cavity acoustic pressure spectrum to be slightly larger at the bottom of the cavity than at the plate. This discrepancy is not understood, although it seems to be due to the change in cavity fluids.

Note further that the cavity acoustic natural frequency appears as a singularity in the spectra of Figures 30, 31, and 32. This is due to the absence of acoustic damping.

Comparisons of Figures 25 and 30, 26 and 31, and 27 and 32 show a constant difference in the dimensionless cavity acoustic pressure spectral density (independent of frequency) out to a dimensionless frequency equal to approximately 2/3 of the Case 4 cavity acoustic natural frequency. From previous discussion and equation (4.145), it was shown that $\Phi_a^+(x^+, y^+, z^+, \omega^+)$ was proportional to ρ^{+2}. The above discussion indicates that the combined effect of ρ^+ and c^+ is a constant difference in the spectra and is independent of frequency. It appears reasonable, therefore, to assume

$$\Phi_a^+(x^+, y^+, z^+, \omega^+) \sim c^{+n} ,$$

where n is an exponent to be determined. The difference between the dimensionless spectra of Case 1 and Case 4 is 84.9 db. Therefore, from the above

$$10 \log_{10} \frac{\Phi_a'(x', y', z', \omega')_1}{\Phi_a'(x', y', z', \omega')_4} = 84.9 = 20 \log_{10}\left(\frac{\rho_1'}{\rho_4'}\right) + 10\, n \log_{10}\left(\frac{c_1'}{c_4'}\right) , \tag{5.15}$$

where the subscripts refer to the case number. From equation (5.15) and the values of Table 2,

$$n = 4 \tag{5.16}$$

and thus

$$\Phi_a'(x', y', z', \omega') \propto c'^4 . \tag{5.17}$$

5.2.1.3 Effects of Damping and Frequency

As stated in Section 5.2.1, the only damping present is that of the plate, and the damping terms in equation (4.145) occur in exactly the same form as in the equation for the dimensionless plate velocity spectral density (equation (4.139)). Therefore, it is reasonable to assume that the variation of the dimensionless cavity acoustic pressure spectral density with damping is the same as that of the dimensionless plate velocity spectral density.

It will be recalled that the effect of damping was shown by means of the dimensionless plate velocity "peak spectra." The "peak spectrum" concept is also useful from an engineering standpoint in examining the dimensionless cavity acoustic pressure spectra. Because of the intended application of this work, the "peak spectra" are only derived for dimensionless frequencies above $1.932\, \delta'$. Further, as the plate boundary conditions affect the spectral density at the lower modes, and as the intent of the "peak spectrum" is to generalize the results into a useful engineering tool, independent of plate boundary conditions, the "peak spectra" only apply above the first dimensionless plate natural frequency. It was upon the above arguments that the assumed forms for the damping and frequency effects on the dimensionless cavity acoustic pressure "peak spectrum" (equations (5.12) and (5.13)) were based.

From equation (5.12) and Figure 29, it can be shown that

$$C_1 = -20.5 \,. \tag{5.18}$$

From equation (5.13) and Figure 29, it can further be shown that

$$C_2 = -93.5 \,. \tag{5.19}$$

Hence, the effects of damping and frequency on the dimensionless cavity acoustic pressure "peak spectrum" at dimensionless frequencies above $1.932/\delta'$ and ω'_{11} may be written, taking account of equation (5.14):

$$10 \log_{10} \Phi'_{a_p}(\omega') = -20.5 - 20 \log_{10}\left(\frac{100\, r'}{r'_{c_{mn}}}\right) \tag{5.20}$$

and

$$10 \log_{10} \frac{\Phi'_{a_p}(\omega')}{\Phi'_{a_p}(10\,\omega')} = -93.5 + 5 \log_{10}\left(\frac{100\, r'}{r'_{c_{mn}}}\right). \tag{5.21}$$

5.2.1.4 Effect of Plate Rigidity

The plate rigidity (D') originates from the plate equations and, like the damping, occurs in exactly the same form in equation (4.145) as it does in equation (4.139). Therefore, by the same arguments used above, the effect of the dimensionless plate rigidity on the cavity acoustic pressure spectral density should be the same as its effect on the plate velocity spectral density. In Section 5.1.2.3, it was shown that the plate rigidity redistributed the plate natural frequencies and altered the dimensionless plate velocity spectrum at these frequencies. Its effect on the "peak velocity spectrum" was to alter the lower limit of applicability because of the changes in ω^+_{11} (since the "peak spectrum" is only applicable above ω^+_{11}).

The dimensionless cavity acoustic pressure "peak spectrum" derived herein will have the same limitations as the dimensionless plate velocity "peak spectrum." For the submarine sonar application, these limitations are not severe, but for aircraft and missile applications, the cavity acoustic pressure "peak spectra" lower limit will probably fall above the frequency range of interest; that is, the lowest frequency limit of application of the "peak spectrum" $(1.932/\delta^+)$ will probably be near the upper frequency limit of interest in these applications. In an effort to provide some data in the range of interest of these applications, and to better define the effect of D^+ at frequencies below $1.932/\delta^+$, dimensionless cavity acoustic pressure spectra were computed for two additional data cases. These were Cases 2 and 3, and the parameters used are presented in Table 2.

Figures 33 and 34 present the Case 2 results in the dimensionless frequency range $0.1 < \omega^+ \leq 6$ for the dimensionless coordinates (1/2, 1/3, -1/6) and (1/2, 1/3, -1/3), respectively. Note, from Table 2, that the above frequency range lies below $1.932/\delta^+$ and also below the first acoustic natural frequency of the cavity. Again, these spectra show no effect of cavity coordinates as the highest frequency falls below 2/3 of the first cavity acoustic natural frequency.

Figures 35 and 36 present the Case 3 dimensionless cavity acoustic pressure spectra in the dimensionless frequency range $1.0 < \omega^+ < 30$ for cavity dimensionless coordinates (1/2, 1/3, -1/6) and (1/2, 1/3, -1/3), respectively. Again, this frequency range falls below $1.932/\delta^+$ but includes, in the case of Figure 35, the first two acoustic natural frequencies of the cavity. Comparison of Figures 35 and 36 again shows no effects of cavity coordinates out to a dimensionless frequency equal to 2/3 of the first cavity acoustic natural frequency.

Table 2 shows that M, D^+, and ρ^+ are the only parameters varied from Case 2 to Case 3. The effects of M and ρ^+ are known. Hence, Cases 2 and 3 may be used to show the effect of D^+ below the dimensionless frequency $1.932/\delta^+$. Comparison of Figures 33 and 34 with Figures 35 and 36 again shows the shift in the plate natural frequencies with a change in D^+ as previously observed. Hence, in order to show any frequency dependent effects of D^+, it would seem prudent to show these effects relative to the first plate natural frequency. Knowing the effects of M and ρ^+, and recognizing that the cavity acoustic pressure spectrum is independent of position for frequencies less than 2/3 of the first cavity natural frequency, one can show that, below this frequency,

$$10 \log_{10} \frac{\Phi_a^+(x^+, y^+, z^+, \omega^+/\omega_{11}^+)_3}{\Phi_a^+(x^+, y^+, z^+, \omega^+/\omega_{11}^+)_2} = 20 \log_{10}\left(\frac{M_3 \rho_3^+}{M_2 \rho_2^+}\right) + f\left(D_2^+, D_3^+, \frac{\omega^+}{\omega_{11}^+}\right), \tag{5.22}$$

where the subscripts 2 and 3 refer to the Case numbers. Figure 37 presents a construction of $f(D_2^+, D_3^+, \omega^+/\omega_{11}^+)$ from Figures 34 through 37 for dimensionless frequencies below 2/3 of the first acoustic natural frequency. As can be seen from Figure 37, the effect of D^+ is a rather pronounced function of frequency. A precise description of this effect is difficult from the above data, and the large amount of computer time required to produce a spectrum prevented a more detailed study. An approximation of the effect of D' at frequencies below $1.932/\delta'$ can be found by considering the effect to be a constant equal to the median value of the function shown in Figure 37. In this case, one could assume

$$\Phi_a'(x', y', z', \omega') \simeq D'^{m} \qquad 0 < \omega' \leq \frac{1.932}{\delta'}, \tag{5.23}$$

where m is an exponent. The median value is shown as a dashed line in Figure 37, for which

$$m = -2.48 \simeq -2.5 . \tag{5.24}$$

Hence, as a rough approximation, the cavity acoustic pressure spectral density varies inversely with the 5/2 power of D' for dimensionless frequencies below $1.932/\delta'$. Above this frequency, the effect of D' is most easily described in terms of the dimensionless cavity acoustic pressure "peak spectrum," and this effect is to alter the lower limiting frequency via altering ω_{11}.

In conclusion, a change in D' changes all of the dimensionless natural frequencies of the plate and the associated plate velocity spectral densities. This effect is passed intact to the cavity acoustic pressure spectrum. At dimensionless frequencies above the first plate natural frequency and above $1.932/\delta'$, a change in D' merely changes the frequency range over which the dimensionless "peak spectra" concept applies; that is, the plate velocity or cavity acoustic pressure spectral densities are changed in such a way that the associated "peak spectra" are not functions of D'. However, as the "peak spectrum" concept has been shown to apply only above ω_{11}, and as ω_{11} is a function of D', the lower frequency limit of application of the "peak spectrum" is affected by D'. At frequencies below $1.932/\delta'$, the precise effect of D' has not been completely investigated. However, it has been shown to be frequency dependent, as might be suspected from the above. If the frequency dependency is neglected, the effect of D' at dimensionless frequencies below $1.932/\delta'$ can be roughly approximated by

$$\Phi_a^*(x^*, y^*, z^*, \omega^*) \sim D'^{-5/2} . \tag{5.25}$$

5.2.1.5 Dimensionless Cavity Acoustic Pressure "Peak Spectrum"

As in the case of the plate velocity spectrum, the dimensionless cavity acoustic pressure "peak spectral density" is a useful engineering result, allowing prediction of maximum cavity acoustic spectral levels at dimensionless frequencies above $1.932/\delta^*$ and above the first plate natural frequency (ω_{11}). It will also be useful to use the dimensionless cavity acoustic pressure "peak spectrum" in the next section to determine the limits of applicability of equation (4.145). The previous sections in addition to equation (4.145) provide sufficient information to derive an expression for the dimensionless cavity acoustic pressure "peak spectrum."

From Section 5.2.1.1, it was found that the "peak spectrum" was independent of cavity coordinates (in the range of coordinates examined) for the dimensionless frequency range between $1.932/\delta^*$ and 2/3 of the first cavity acoustic natural frequency. From Section 5.2.1.2, it was further determined that the "peak spectral density" was proportional to c^{*4}. Further, Section

5.2.1.4 argued that for frequencies above $1.932/\delta^+$ the effect of plate rigidity was to shift the lower limit of applicability of the "peak spectrum" in the same manner as was shown for the plate velocity "peak spectrum." By utilizing this information and equation (4.145), a general expression for the dimensionless cavity acoustic pressure "peak spectrum" may be written as follows:

$$\Phi^+_{a_p}(\omega^+) = C_1 \rho^{+2} c^{+4} M^2 \delta^{+-2} G^+(r^+, \omega^+) \qquad \frac{1}{3} \le x^+ \le \frac{1}{2},\ y^+ = \frac{1}{3},\ -\frac{1}{3} \le z^+ \le 0,\quad \omega^+ > \omega^+_{11},\ \omega^+ > \frac{1.932}{\delta^+}. \tag{5.26}$$

where C_1 is a constant, and $G^+(r^+, \omega^+)$ is a function to be determined.

Section 5.2.1.3 argued that the damping (r^+) is associated with the plate and, therefore, should enter the equation for the acoustic pressure "peak spectrum" in the same manner that it entered the plate velocity "peak spectrum." Thus, from equations (5.4) and (5.8), it is assumed that

$$G^+(r^+, \omega^+) = \left(\frac{r^+}{r^+_{c_{mn}}}\right)^n \omega^{+\left[K + 0.5 \log_{10}(100 r^+/r^+_{c_{mn}})\right]}, \tag{5.27}$$

from which

$$\Phi^+_{a_p}(\omega^+) = C_1 \rho^{+2} c^{+4} M^2 \delta^{+-2} \left(\frac{r^+}{r^+_{c_{mn}}}\right)^n \omega^{+\left[K + 0.5 \log_{10}(100 r^+/r^+_{c_{mn}})\right]} \qquad \frac{1}{3} \le x^+ \le \frac{1}{2},\ y^+ = \frac{1}{3},\ -\frac{1}{3} \le z^+ \le 0,\quad \omega^+ > \omega^+_{11},\ \omega^+ > \frac{1.932}{\delta^+}. \tag{5.28}$$

In the above, K is a constant to be determined. The constants C_1 and K can be determined from equations (5.20) and (5.21).

From equations (5.28) and (5.21),

$$-93.5 + 5 \log_{10}\left(\frac{100\, r^+}{r^+_{c_{mn}}}\right) = 10K + 5 \log_{10}\left(\frac{100\, r^+}{r^+_{c_{mn}}}\right), \tag{5.29}$$

from which

$$K = -9.35 . \tag{5.30}$$

Equation (5.20) was based on Case 1 variables. Hence, using Case 1 parameters, from equations (5.20), (5.28), and (5.30), one obtains

$$\begin{aligned} -20.5 - 20 \log_{10}\left(\frac{100\, r^+}{r^+_{c_{mn}}}\right) &= 10 \log_{10} C_1 + 10\, n \log_{10}\left(\frac{r^+}{r^+_{c_{mn}}}\right) + 190 \\ &\quad - \left[93.5 - 5 \log_{10}\left(\frac{100\, r^+}{r^+_{c_{mn}}}\right)\right] \log_{10}\left(\frac{4.62}{\delta^+}\right). \end{aligned} \tag{5.31}$$

from which

$$n = -2 \tag{5.32}$$

and

$$10 \log_{10} C_1 = -250.5 + \left[93.5 - 5 \log_{10}\left(\frac{100\, r^+}{r^+_{c_{mn}}}\right)\right] \log_{10}\left(\frac{4.62}{\delta^+}\right). \tag{5.33}$$

From equations (5.28), (5.30), (5.32), and (5.33), by a slight rearrangement, the dimensionless cavity acoustic pressure "peak spectral density" may be expressed as

$$\begin{aligned} 10 \log_{10} \Phi^+_{a_p}(\omega^+) &= -210.5 - 20 \log_{10}\left(\frac{100\, r^+}{r^+_{c_{mn}}}\right) + 20 \log_{10}\left(\frac{\rho^+ c^{+2} M}{\delta^+}\right) \\ &\quad - \left[93.5 - 5 \log_{10}\left(\frac{100\, r^+}{r^+_{c_{mn}}}\right)\right] \log_{10}\left(\frac{\omega^+ \delta^+}{4.62}\right) \\ &\quad \frac{1}{3} \le x^+ \le \frac{1}{2},\ y^+ = \frac{1}{3}, \\ &\quad -\frac{1}{3} \le z^+ \le 0,\ \omega^+_{11} < \omega^+ \le \frac{2}{3}\, \omega^+_{a_1}, \end{aligned} \tag{5.34}$$

where ω'_{a_1} is the first cavity acoustic natural frequency.

Figure 38 compares the dimensionless cavity acoustic pressure "peak spectrum" computed from equation (5.34) to the dimensionless cavity acoustic pressure spectrum computed from equation (4.145) for the Case 1 parameters at the cavity coordinates (1/2, 1/3, -1/6). The agreement is very good above $\omega' = 150$. Thus, within the prescribed limits, equation (5.34) predicts a dimensionless cavity acoustic pressure "peak spectrum" that agrees well with the results of equation (4.145).

5.2.2 Limits of Applicability of Theory

At the outset of this analysis, it was assumed that the cavity acoustic pressure was much less than the turbulent pressure and thus provided negligible excitation to the plate compared to the turbulent pressure excitation. The calculated spectra and "peak spectra" of the previous sections provide the information necessary to check this assumption. Again, it should be emphasized that the calculated cavity acoustic pressure spectra are probably not physically valid above the first acoustic natural frequency.

Horton [43] shows that, if the difference between two random signals is 10 db (that is, their ratio is a factor of 10), the sum of the signals is 1/2 db greater than the larger of the two original signals (a factor of 1.12). Hence, if the turbulent pressure spectral density is 10 db larger than the cavity acoustic pressure spectral density, the error in the calculated cavity acoustic pressure spectral density would only be 1/2 db. This error is the limit of measurement accuracy. Hence, it will be assumed that this analysis is valid where the cavity acoustic spectral density is 10 db less than the turbulent pressure spectral density.

This criterion is most easily checked if the turbulent pressure spectral density (equation 3.1) is non-dimensionalized with respect to the same quantities as the cavity acoustic pressure spectral density. Let $\Phi^+(\omega^+)$ be defined by

$$\Phi^+(\omega^+) = \frac{\Phi(\omega)a}{a^2\mu^2U_c^3} = \begin{cases} 2.74 \times 10^{-5}\, M^2 \delta^+ & \omega^+ \leq \dfrac{1.932}{\delta^+} \\ 2.0 \times 10^{-4}\, M^2 {\delta^+}^{-2} {\omega^+}^{-3} & \omega^+ > \dfrac{1.932}{\delta^+} . \end{cases} \qquad (5.35)$$

From the above criterion and equations (5.34) and (5.35), the limit of applicability for dimensionless frequencies above $1.932/\delta^+$ and ω_{11} can quickly be established: that is,

$$10 \log_{10} \Phi^+(\omega^+) - 10 \log_{10} \Phi^+_{a_p}(\omega^+) \geq 10 . \qquad (5.36)$$

Substitution of equations (5.34) and (5.35) into (5.36) yields

$$10 \log_{10} \omega^+ \geq \frac{-163.5 - 20 \log_{10}\left(\dfrac{100 r^+}{r^+_{c_{mn}}} \dfrac{1}{\rho^+ {c^+}^2}\right) + \left[93.5 - 5 \log_{10}\left(\dfrac{100 r^+}{r^+_{c_{mn}}}\right)\right] \log_{10}\left(\dfrac{4.62}{\delta^+}\right)}{63.5 - 5 \log_{10}\left(\dfrac{100 r^+}{r^+_{c_{mn}}}\right)}$$

$$\frac{1}{3} \geq x^+ \geq \frac{1}{2} , y^+ = \frac{1}{3} , -\frac{1}{3} \geq z^+ \geq 0 ,$$

$$\omega^+ > \omega^+_{11} , \omega^+ > \frac{1.932}{\delta^+} . \qquad (5.37)$$

It is seen from equation (5.37) that within the limits cited the limit of applicability turns out to be a lower frequency limit of application of the cavity acoustic pressure spectrum. Use of the Case 1 parameters in equation (5.37) results in a lower limiting dimensionless frequency of 403. Figure 39 presents a comparison of the Case 1 dimensionless cavity acoustic pressure "peak spectrum" and the dimensionless turbulent pressure spectrum for frequencies greater than $1.932/\delta'$. It can be seen that equation (5.37) predicts very closely the frequency at which the cavity acoustic pressure spectral density becomes 10 db lower than the turbulent pressure spectrum.

For dimensionless frequencies below $1.932/\delta'$, there were not sufficient computations made to understand completely the effect of plate rigidity. Therefore, an accurate applicability limitation for this analysis is not possible in the frequency range. However, if the approximation of equation (5.25) is used, an approximation of the limit of applicability may be made for frequencies below $1.932/\delta'$ as follows.

From the plate velocity spectra computations, regardless of frequency, it seems reasonable to assume (as damping only occurs in the plate)

$$\Phi_a'(x', y', z', \omega') \propto \left(\frac{100\, r'}{r_c'}\right)_{nn}^{-2} . \qquad (5.38)$$

Also, regardless of frequency, from Section 5.2.1.2,

$$\Phi_a'(x', y', z', \omega') \propto c'^4 . \qquad (5.17)$$

Further, over the range of spacial coordinates investigated, at frequencies below 2/3 of the first cavity acoustic natural frequency,

$$\Phi_a'(x', y', z', \omega') \approx \Phi_a'(\omega') . \qquad (5.39)$$

By use of equations (5.38), (5.17), (5.39), and (4.145), for frequencies below $1.932/\delta'$, it seems reasonable to assume

$$10 \log_{10} \Phi_a'(\omega') = C_1 + 10 \log_{10} (\delta' M^2) - 20 \log_{10} \left(\frac{100 r'}{r'_{mn}} \; \frac{1}{\rho' c'^2} \right) + 10 \log_{10} f(D', \omega') ,$$

(5.40)

where C_1 and $f(D', \omega')$ are to be evaluated. From the arguments of Section 5.2.1.4, $f(D', \omega')$ may be approximated by

$$f(D', \omega') \approx D'^{-5/2} \qquad \omega' > \frac{1.932}{\delta'} .$$

Therefore, equation (5.40) becomes

$$10 \log_{10} \Phi_a'(\omega') \simeq C_1 + 10 \log_{10} (\delta' M^2) - 20 \log_{10} \left(\frac{100 r'}{r'_{mn}} \; \frac{1}{\rho' c'^2} \right) - 25 \log D'$$

$$\omega' > \frac{1.932}{\delta'} .$$

(5.40a)

It remains to evaluate C_1. To provide a conservative estimate of the limit of application, it is desirable to overestimate, rather than underestimate, the value of C_1. Hence, the value of C_1 will be evaluated at a frequency for which the cavity acoustic pressure spectral density is a maximum. From Case 3 data (Figures 35 and 36) and equation (5.40a), using the value of the spectral density at ω'_{11}, one obtains

$$C_1 = -81.9 .$$

From Case 2 data (Figures 33 and 34) and equation (5.40a), following the same procedure, one obtains

$$C_1 = -89.8 .$$

In order that the estimate of the limit of applicability be as conservative as possible, the largest value of C_1 was selected. Thus, an approximation to the cavity acoustic spectrum for the frequency range $\omega' > 1.932/\delta'$ is given by

$$\Phi'_a(\omega') = -81.9 + 10 \log_{10} (\delta' M^2) - 20 \log_{10} \left(\frac{100\, r'}{r'_{c_{mn}}} \frac{1}{\rho' c'^2} \right) - 25 \log_{10} D'$$

$$\omega' < \frac{1.932}{\delta'} . \tag{5.41}$$

Again, by use of the criterion that the cavity acoustic pressure may be neglected as a driving force to the plate if

$$10 \log_{10} \frac{\Phi'(\omega')}{\Phi'_a(\omega')} > 10 ,$$

from equations (5.41) and (5.35), the following equation must be satisfied in order that equation (4.145) accurately predict the cavity acoustic pressure spectrum at dimensionless frequencies below $1.932/\delta'$:

$$20 \log_{10} \left(\frac{100\, r'}{r'_{c_{mn}}} \frac{1}{\rho' c'^2} \right) + 25 \log D' > -26.3 . \tag{5.42}$$

Using the applicability limitation of equation (5.42) with the parameters for Cases 2 and 3, it may be shown that Case 2 fails the criterion by approximately 61 db whereas Case 3 passes by approximately 12 db. Figures 40 and 41 compare the dimensionless turbulent spectrum to the computed spectrum of Cases 2 and 3, respectively, for dimensionless spacial coordinates (1/2, 1/3, -1/3). Although the exact numbers of the applicability criterion calculations are not borne out in these figures, the conclusions of the calculations are supported.

Therefore, it appears that equation (5.42) may be used as an approximate test to indicate, for a particular set of input parameters, whether or not equation (4.145) will predict an accurate dimensionless cavity acoustic pressure spectrum at frequencies below $1.932\ \delta'$. At frequencies above $1.932\ \delta'$, equation (5.37) should be used.

It should also be noted here, that the above criteria must also be satisfied for the calculation of the plate velocity spectral density by means of equation (4.139) if the back of the plate is backed by an acoustic cavity. If the back of the plate is in vacuo or in contact with an unbounded fluid medium, the above limitations do not apply.

VI
SUMMARY AND CONCLUSIONS

This study presents an exact solution for the acoustic pressure spectral density and cross spectral density in a closed space behind a simply supported plate excited by boundary layer turbulence. Unlike previous work in flow induced noise in which models of the turbulent pressure field have been approximated by simple mathematical expressions, this study utilizes an experimentally based model of the turbulent pressure field as an input. The mathematical expression for this model is presented in equation (4.4). The major assumption made in this analysis was that the acoustic pressure produced in the cavity by the random, flow excited vibrations of the plate could be neglected, with respect to the turbulent pressure, as a forcing function on the plate. This assumption greatly simplified the mathematics of the problem but necessitated an analysis to determine the range of validity of the results.

Exact mathematical solutions of the cavity acoustic pressure spectral density and cross spectral density were determined under this assumption, and the results were presented in equations (4.126) and (4.120), respectively. A useful byproduct of the mathematical analysis is a description of the plate velocity statistics, which are presented in the forms of the plate velocity cross spectral density and spectral density in equations (4.60) and (4.68), respectively. It should be noted that the equations for the plate velocity statistics are valid, without restriction, when the back of the plate is in vacuo or is in contact with a free acoustic field in which the acoustic pressure on the plate can be demonstrated to be negligible with respect to the turbulent pressure excitation. In all other cases, both the cavity acoustic pressure and plate velocity statistics given in equations (4.120), (4.126), (4.60), and (4.68) are subject to the restrictions imposed by the above assumption. These restrictions are discussed below.

A prime objective of this study was to provide the submarine sonar designer with information describing the effect of major parameters on the environment of sonar transducers. The model used in this analysis provides a fair representation of the acoustic environment of submarine sonar transducers. In order that maximum information be obtained from selected computations, the plate velocity spectral density and cavity acoustic pressure spectral density were rewritten in dimensionless form. The dimensionless form of the plate velocity spectral density is presented in equation (4.193), and the dimensionless cavity acoustic pressure spectral density in equation (4.145). Parametric studies and the range of validity of this analysis were determined from these dimensionless forms.

Computations of the plate velocity spectral density, made with a digital computer, compared well with existing experimental information. A "peak spectrum," constructed from the computed spectrum by connecting the major spectral peaks, proved to be a useful concept. From an engineering standpoint, knowledge of the "peak spectrum" is equivalent to knowledge of the maximum expected plate velocity or cavity acoustic pressure spectral densities over some range of frequencies. This information is often sufficient for making a design decision or writing specifications. Comparison of the dimensionless plate velocity "peak spectrum" with "peak spectra" constructed from experimental information further showed that, above the first plate natural frequency, the plate velocity "peak spectrum" was independent of plate boundary conditions.

From computations of the dimensionless plate velocity spectral density, with input parameters applicable to submarines, dimensionless plate velocity "peak spectra" were constructed. Analysis of these "peak spectra" enabled formulation of a mathematical expression for the dimensionless plate velocity "peak spectral density." This expression is presented in equation (5.9a), and has the advantages that it shows the effects of major parameters on the plate velocity spectrum and allows a quick estimation of the plate velocity spectrum. It should be noted that the average time required for each plate velocity spectrum, computed from equation (4.139) with the IBM 704 digital computer, was approximately 8 hours. Thus, the "peak spectrum" concept represents a substantial economic advantage.

The dimensionless cavity acoustic pressure spectral density was computed at various positions within the cavity for four data cases with a digital computer. These four cases, in addition to the aforementioned plate data, allowed determination of the effects of major parameters on the cavity acoustic pressure spectrum over the range of dimensionless frequency from approximately $1.932/\delta'$ to 2/3 of the first cavity acoustic natural frequency. Above the first cavity acoustic frequency, the cavity acoustic pressure spectrum computed from equation (4.145) is not felt to be valid since acoustic damping effects were neglected in its derivation. Again, the "peak spectrum" concept proved useful, and an equation describing the dimensionless cavity acoustic "peak spectral density" is presented in equation (5.34) over the range of dimensionless frequency between $1.932/\delta^{+}$ to 2/3 of the first acoustic natural frequency.

This equation describes the effect of major parameters on the cavity acoustic pressure spectrum. The extremely large amount of computer time required to produce each cavity acoustic pressure spectrum prevented accurate description of the "peak spectrum" over the entire range of frequency.

Since the contribution of the cavity acoustic pressure as an exciting force on the plate in this study was neglected, the results may only be used where this assumption is borne out. Comparison of the turbulent pressure spectral density and the cavity acoustic pressure spectrum was made to determine the conditions under which the results of this study are valid. For dimensionless frequencies above $1.932/\delta^{+}$, the condition was in the form of a lower frequency limit, given by equation (5.37), below which the theory is invalid. For dimensionless frequencies below $1.932/\delta^{+}$, the condition of validity could only be approximated because of an incomplete description of the effect of major parameters in this frequency range. This approximate condition is presented in equation (5.42).

In summary, the theoretical solution to this complex problem and the conditions for applicability have been obtained. From selected computed plate velocity and cavity acoustic pressure spectra, dimensionless plate velocity and cavity acoustic "peak spectra" have been derived which show the effects of major parameters on the plate velocity and cavity acoustic pressure spectra over a range of frequency of interest to the submarine sonar designer. The "peak spectra" have been shown to be useful engineering tools in that they allow a quick estimate of maximum spectral levels for a given set of input parameters. The study of major parameters, specifically the plate rigidity, at dimensionless frequencies below $1.932/\delta'$ should be completed. There is also a need for extensive experimental work in this area to verify these theoretical results and their range of application.

BIBLIOGRAPHY

1. Corcos, G. H. and Liepmann, H. W., "On the Contribution of Turbulent Boundary Layer to the Noise Inside a Fuselage," NACA TM 14 (December 1956).

2. Ribner, H. S., "Boundary Layer Induced Noise in the Interior of Aircraft," University of Toronto, U.T.I.A. Report No. 37 (April 1956).

3. Lyon, R. H., "Response of Strings to Random Noise Fields," Journal of the Acoustical Society of America, 28, 391-398 (May 1956).

4. Eringen, A. C., "Response of Beams and Plates to Random Loads," Journal of Applied Mechanics, 24, 46-52 (March 1957).

5. Kraichnan, R. H., "Noise from Boundary Layer Fluctuations," Journal of the Acoustical Society of America, 29, 65-80 (January 1957).

6. Dyer, I., "Sound Radiation Into a Closed Space from Boundary Layer Turbulence," Bolt, Beranek, and Newman Inc., Report No. 602 (December 1958).

7. Dyer, I., "Response of Plates to a Decaying and Convecting Pressure Field," Journal of the Acoustical Society of America, 31, 922-928 (July 1959).

8. Strasberg, M., "Response of Plates and Membranes to Pressure Fluctuations of a Turbulent Boundary Layer," (Abstract) Journal of the Acoustical Society of America, 30, 680 (June 1958).

9. Harrison, M., "Correlation and Spectra of Pressure Fluctuations on Wall Adjacent to a Turbulent Boundary Layer," David Taylor Model Basin Report No. 1260 (April 1958).

10. Powell, A., "On the Fatigue Failure of Structures Due to Vibration Excited by Random Pressure Fields," Journal of the Acoustical Society of America, 30, 1130-1135 (December 1958).

11. Maidanik, G. and Lyon, R. H., "Response of Strings to Moving Noise Fields," Journal of the Acoustical Society of America, 33, 1606 (November 1961).

12. Mercer, C. A., "Response of a Multi-Supported Beam to a Random Pressure Field," University of Southampton, ISAV Memorandum No. 103 (March 1964).

13. Tack, D. N. and Lambert, R. F., "Response of Bars and Plates to Boundary Layer Turbulence," Journal of the Aeronautical Society, 29, 311-322 (March 1962).

14. White, P. H., "The Transduction of Boundary Layer Noise by a Rectangular Panel," a paper delivered at Meeting of Acoustical Society of America, Austin, Texas (October 1964).

15. Bull, M. K., Wilby, J. F., and Blackman, D. R., "Wall Pressure Fluctuations in Boundary Layer Flow and Response of Simple Structures to Random Pressure Fields," University of Southampton, A.A.S.U. Report No. 243 (July 1963).

16. Collier, R. D., "The Vibration and Acoustic Radiation of a Simply Supported Plate Excited by Turbulent Boundary Layer Pressure Fluctuations," University of Connecticut, Ph.D. Dissertation (May 1966).

17. Pretlove, A. J., "Forced Vibrations of a Rectangular Panel Backed by a Closed Rectangular Cavity," Journal of Sound and Vibration, 3, 252-261 (May 1966).

18. El Baroudi, M. Y., Ludwig, G. R., and Ribner, H. S., "An Experimental Investigation of Turbulence-Excited Panel Vibration and Noise," NATO Advisory Group for Aeronautical Research and Development Report No. 465 (April 1963).

19. El Baroudi, M. Y., "Turbulence-Induced Panel Vibration," University of Toronto, UTIAS Report No. 98 (February 1964).

20. Maestrello, L., "Measurement of Noise Radiated by Boundary Layer Excited Panels," Journal of Sound and Vibration, 2, 100-115 (April 1965).

21. Maestrello, L., "Measurement and Analysis of the Response Fields of Turbulent Boundary Layer Excited Panels," Journal of Sound and Vibration, 2, 270-292 (July 1965).

22. Lighthill, M. J., "On Sound Generated Aerodynamically, I.-General Theory," Proceedings of the Royal Society (London) Series A, Vol. 211, 564-587 (March 1952).

23. Lighthill, M. J., "On Sound Generated Aerodynamically, II.-Turbulence as a Source of Sound," Proceedings of the Royal Society (London) Series A, Vol. 222, 1-32 (February 1954).

24. Heisenberg, W., "Zur Statistischen Theory der Turbulenz," Zeitschrift fur Physik, 124, 628-657 (1948).

25. Batchelor, G. K., "Pressure Fluctuations in Isotropic Turbulence," Proceedings of the Cambridge Philosophical Society, 47, 359-374 (April 1951).

26. Uberoi, M. S., "Quadruple Velocity Correlations and Pressure Fluctuations in Isotropic Turbulence," Journal of Aeronautical Sciences, 20, 197-204 (March 1953).

27. Kraichnan, R. H., "Pressure Field within Homogeneous Anisotropic Turbulence," Journal of the Acoustical Society of America, 28, 64-72 (January 1956).

28. Kraichnan, R. H., "Pressure Fluctuations in Turbulent Flow over a Flat Plate," Journal of the Acoustical Society of America, 28, 378-390 (May 1956).

29. Lilley, G. M. and Hodgson, T. H., "On the Surface Pressure Fluctuations in Turbulent Boundary Layers," NATO Advisory Group for Aeronautical Research and Development Report No. 276 (April 1960).

30. Sternberg, J., "A Theory for the Viscous Sublayer of a Turbulent Flow," Journal of Fluid Mechanics, 13, 241-272 (June 1962).

31. Gardner, S., "Surface Pressure Fluctuations Produced by Boundary Layer Turbulence," Technical Research Group, Inc., Report No. TRG-142-TN-63-5 (October 1963).

32. White, F. M., "A Unified Theory of Turbulent Wall Pressure Fluctuations," U. S. Navy Underwater Sound Laboratory Report No. 629 (December 1964).

33. Corcos, G. M., "Resolution of Pressure in Turbulence," Journal of the Acoustical Society of America, 35, 192-199 (February 1963).

34. Willmarth, W. W., "Wall Pressure Fluctuations in a Turbulent Boundary Layer," Guggenheim Aeronautical Laboratory, California Institute of Technology Report (May 1956).

35. White, P. N., "Sound Transmission of Double Flexible Walls Excited by Random Pressure Fields," University of California, Ph.D. Dissertation (January 1965).

36. Bakewell, H. P. et al., "Wall Pressure Correlations in Turbulent Pipe Flow," U. S. Navy Underwater Sound Laboratory Report No. 599 (August 1962).

37. Skudrzyk, E. J. and Haddle, G. P., "Noise Production in a Turbulent Boundary Layer by Smooth and Rough Surfaces," Journal of the Acoustical Society of America, 32, 19-34 (January 1960).

38. Willmarth, W. W. and Wooldridge, C. E., "Measurements of the Correlation Between the Fluctuating Velocities and Fluctuation Wall Pressure in a Thick Turbulent Boundary Layer," University of Michigan, College of Engineering Report 02920-2-T (April 1962).

39. Serafini, J. S., "Wall Pressure Fluctuations in a Turbulent Boundary Layer," California Institute of Technology, Ph.D. Dissertation (June 1962).

40. Corcos, G. M., "The Structure of the Turbulent Pressure Field in Boundary Layer Flows," Journal of Fluid Mechanics, 18, 353-378 (March 1964).

41. Willmarth, W. W. and Roos, F. W., "Resolution and Structure of the Wall Pressure Field Beneath a Turbulent Boundary Layer," Journal of Fluid Mechanics, 22, 81-94 (January 1965).

42. Schloemer, H. H., "Effect of Pressure Gradients on Turbulent Boundary-Layer Wall Pressure Fluctuations," U. S. Navy Underwater Sound Laboratory Report No. 747 (July 1966).

43. Horton, J. W., Fundamentals of Sonar, United States Naval Institute, Annapolis (1957).

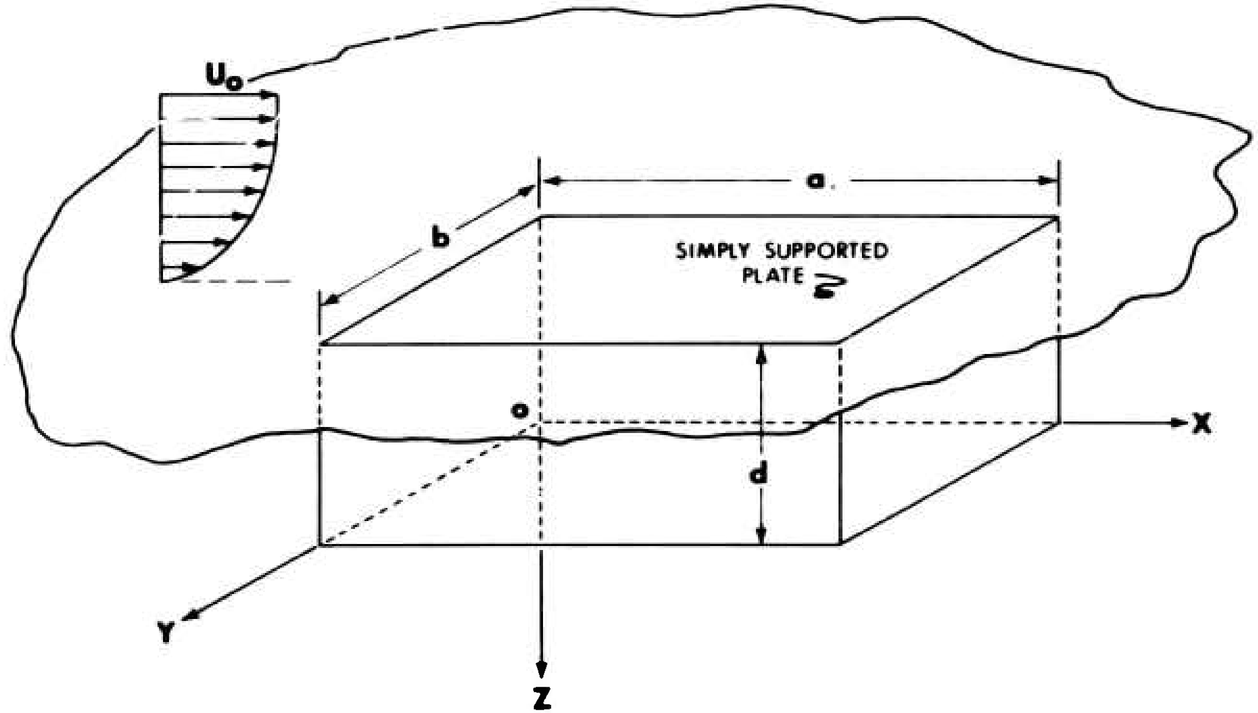

Figure 1. Illustration of the Theoretical Model

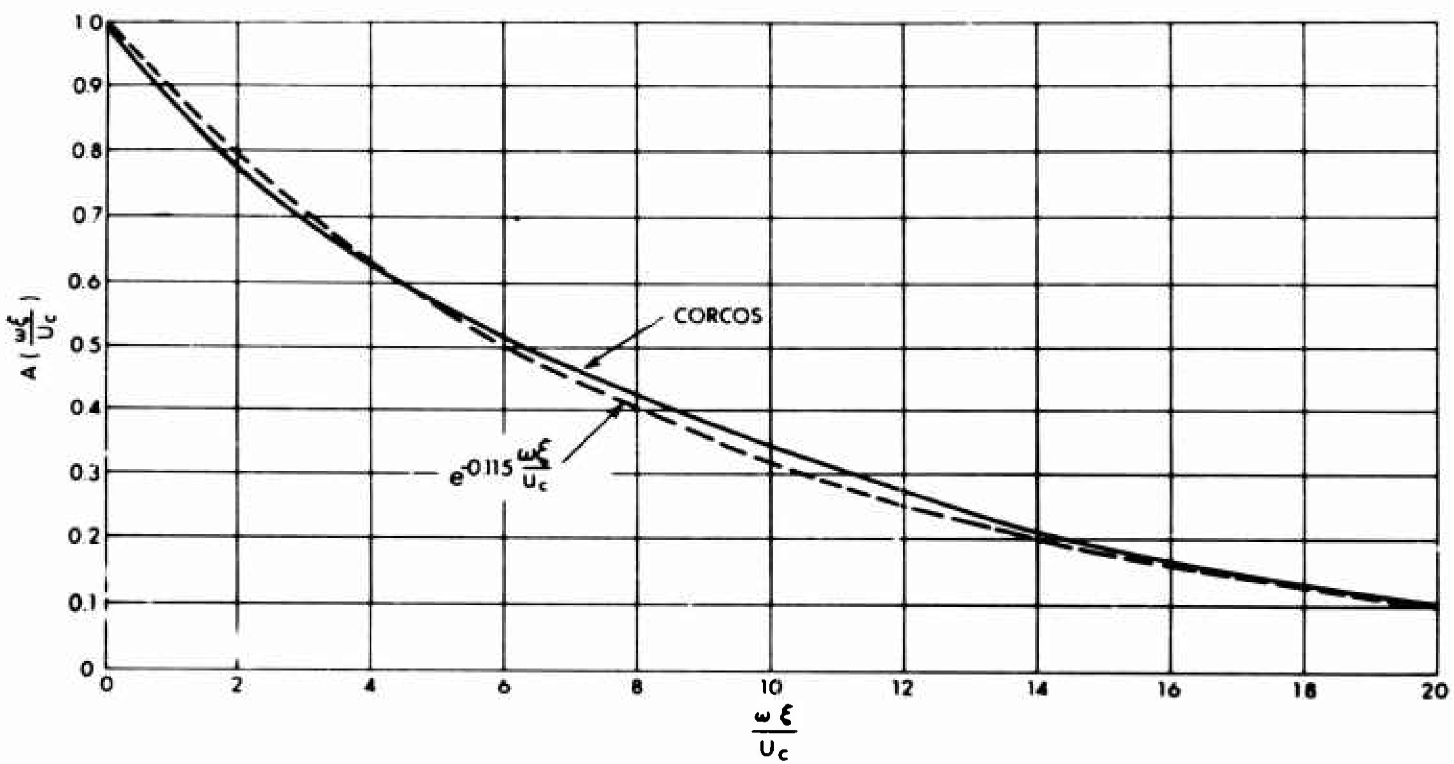

Figure 2. Longitudinal Component of the Turbulent Wall Pressure Cross Power Spectral Density [33]

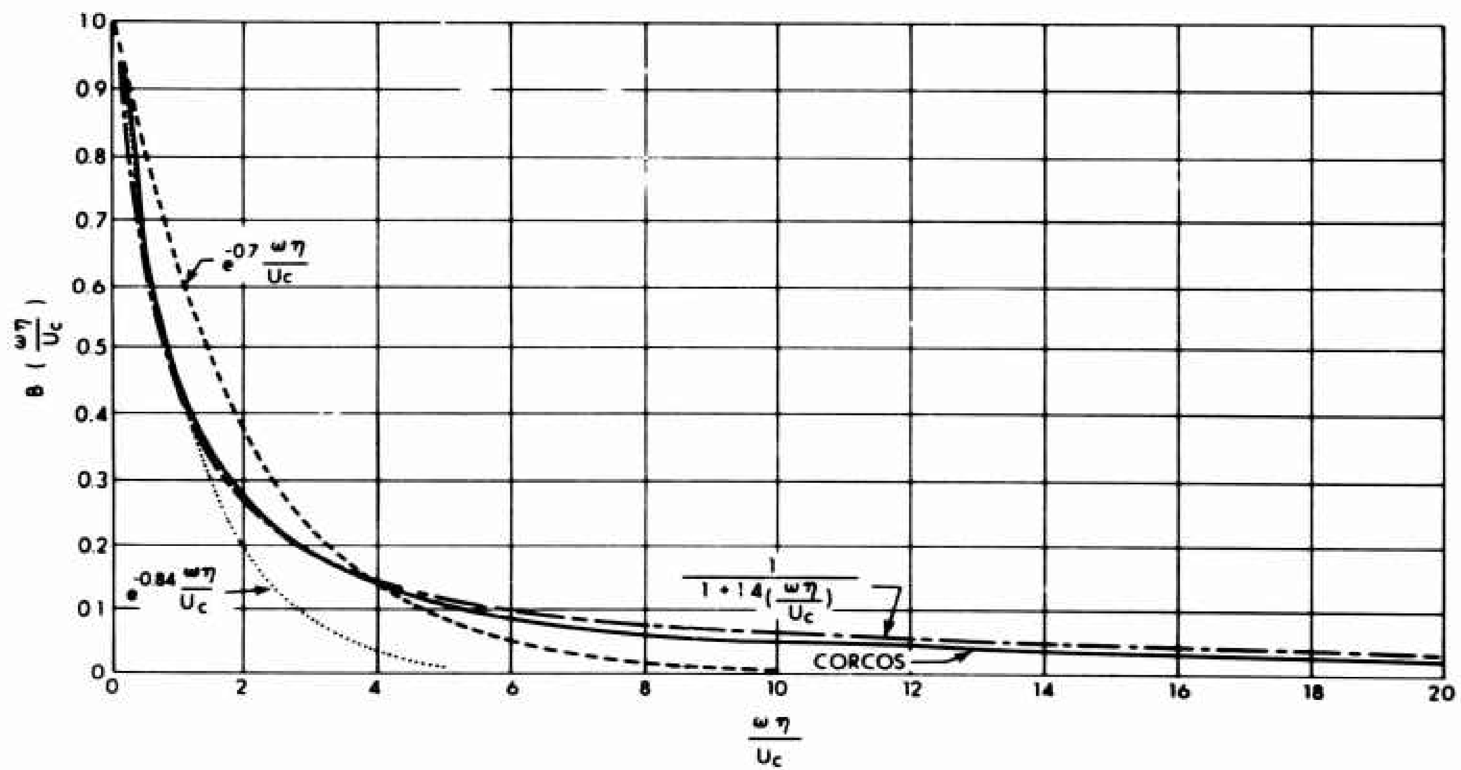

Figure 3. Lateral Component of the Turbulent Wall Pressure Cross Power Spectral Density [33]

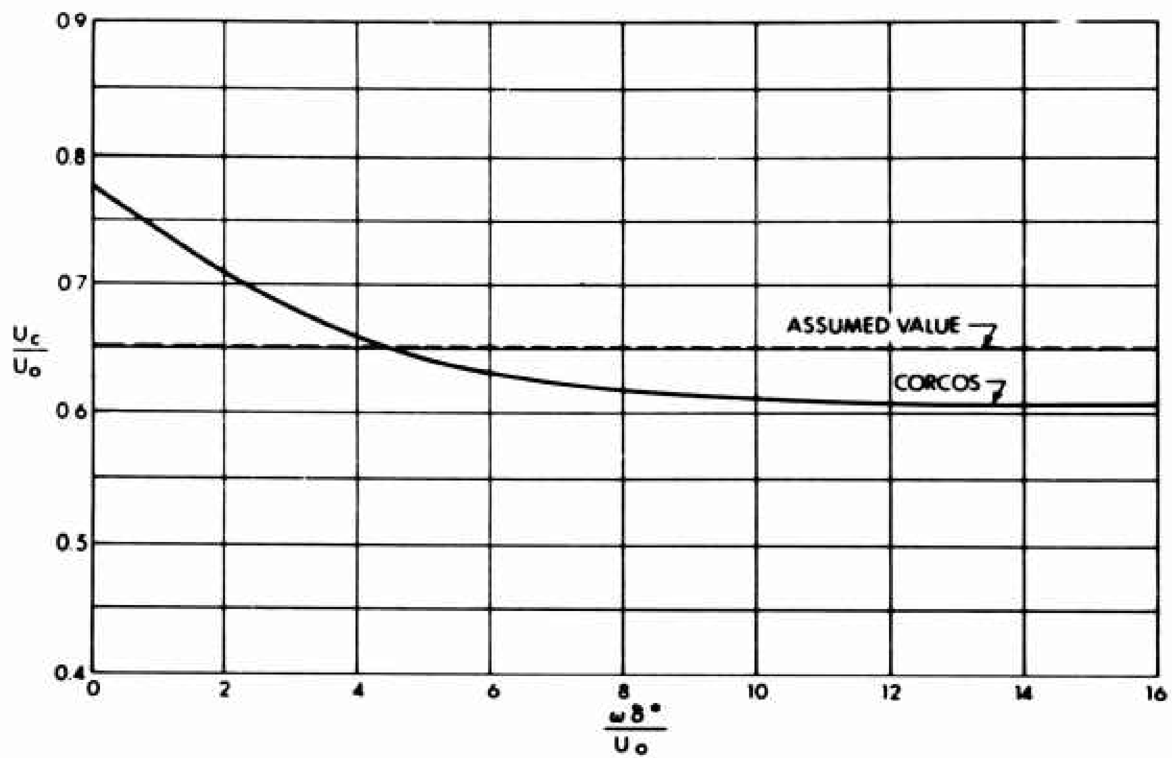

Figure 4. The Dependence of Convection Velocity on Frequency [33]

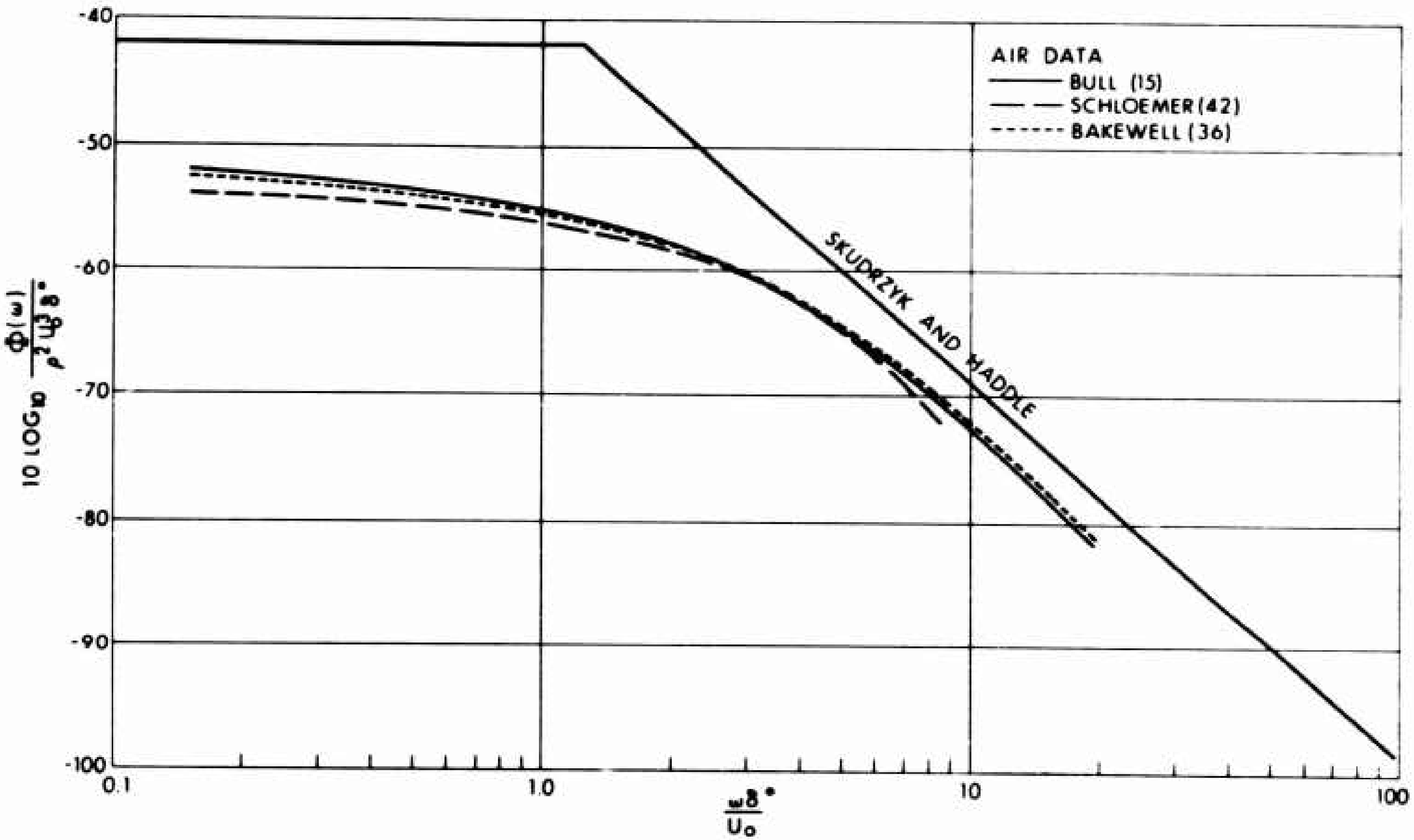

Figure 5. Turbulent Wall Pressure Power Spectra: Comparison of Theory and Experiment [15], [36], [37], [42]

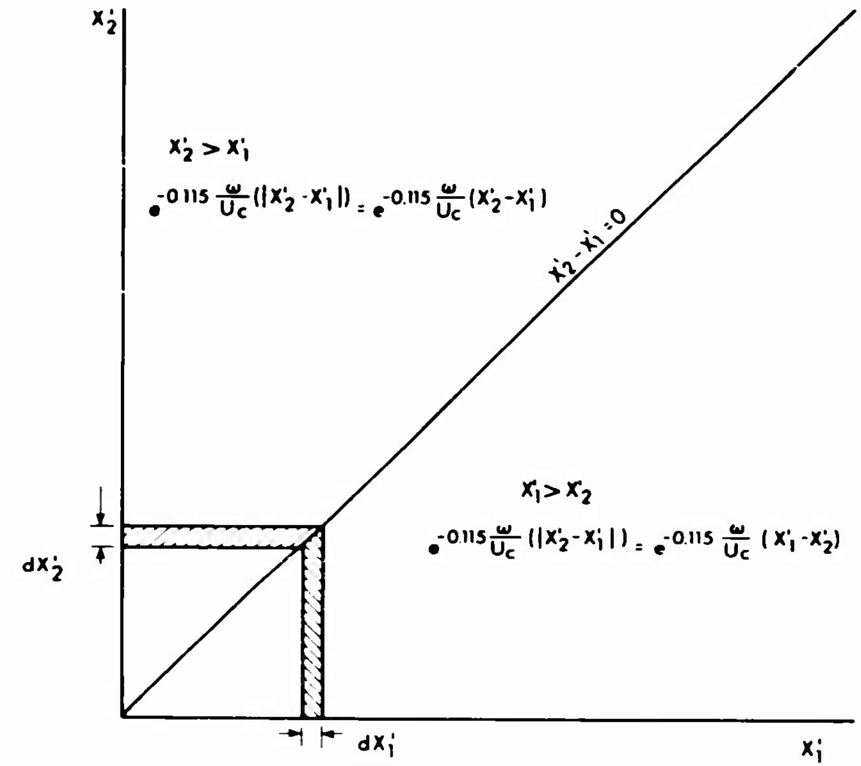

Figure 6. Limits of Integration of $I_{1_{mq}}$

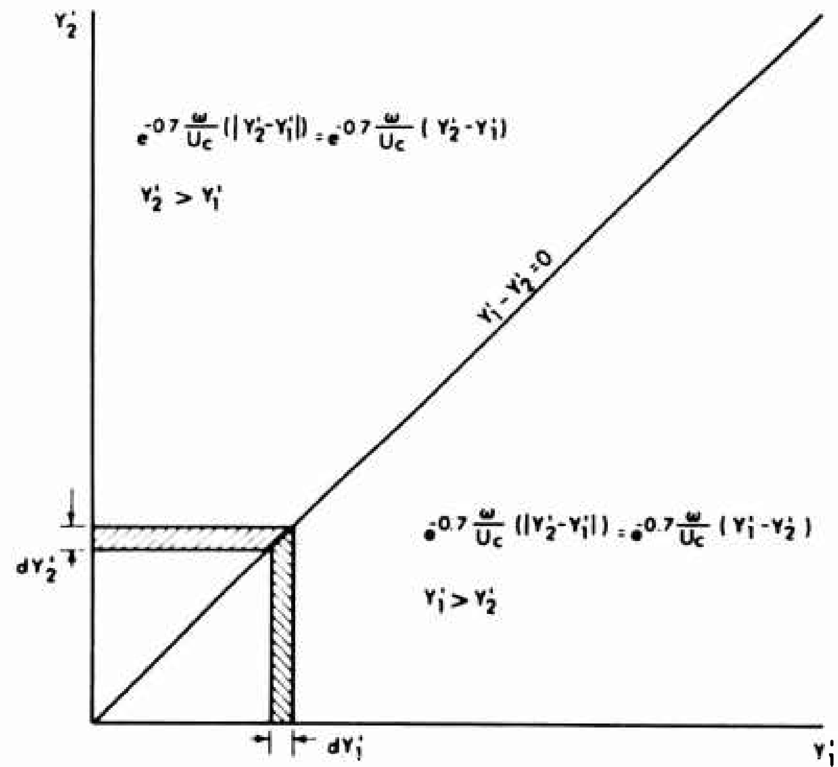

Figure 7. Limits of Integration of $I_{2_{ns}}$

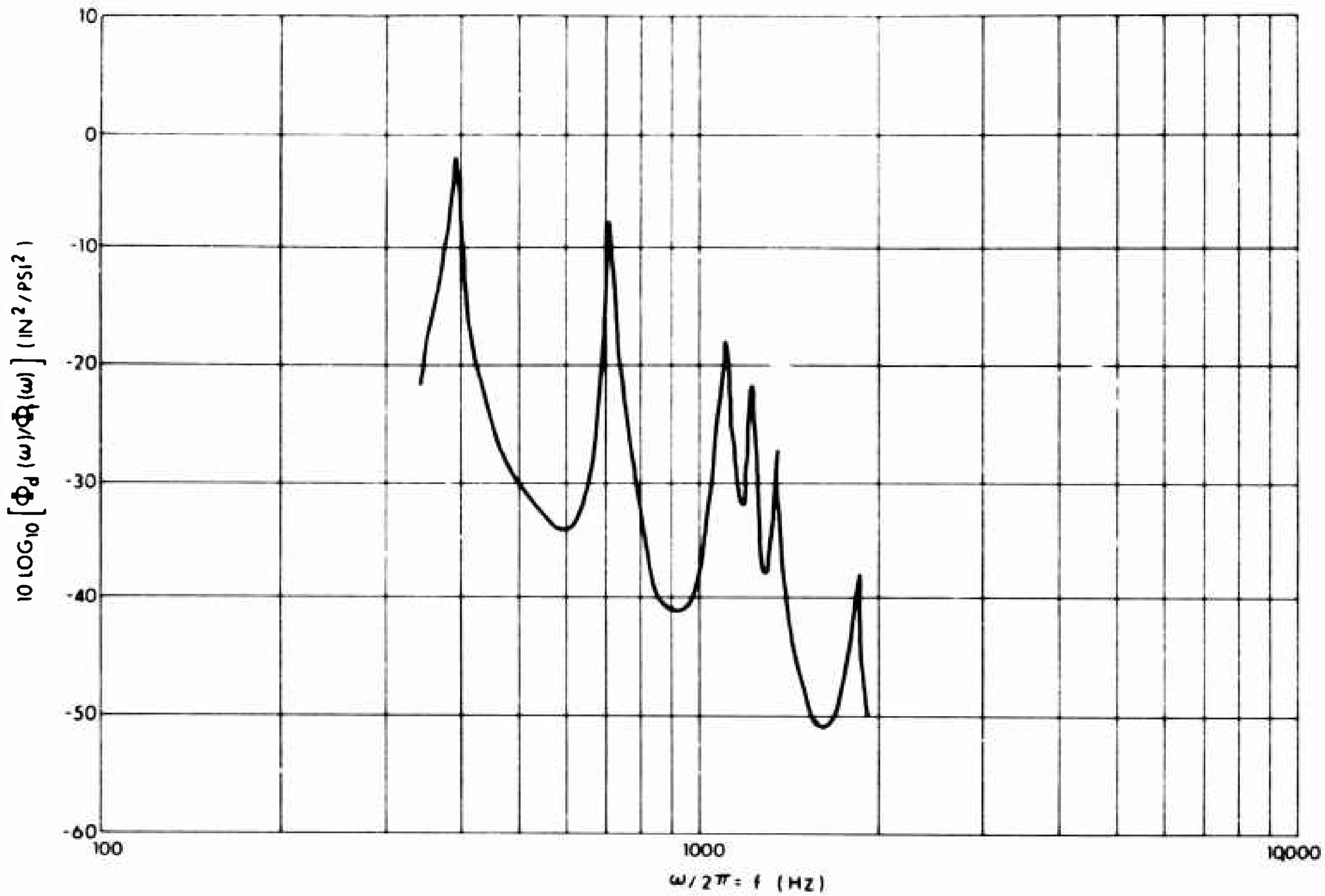

Figure 8. Measured Response of a 3.5 × 3.5 × 0.01 inch Steel Plate to Turbulent Boundary Layer Excitation [15]

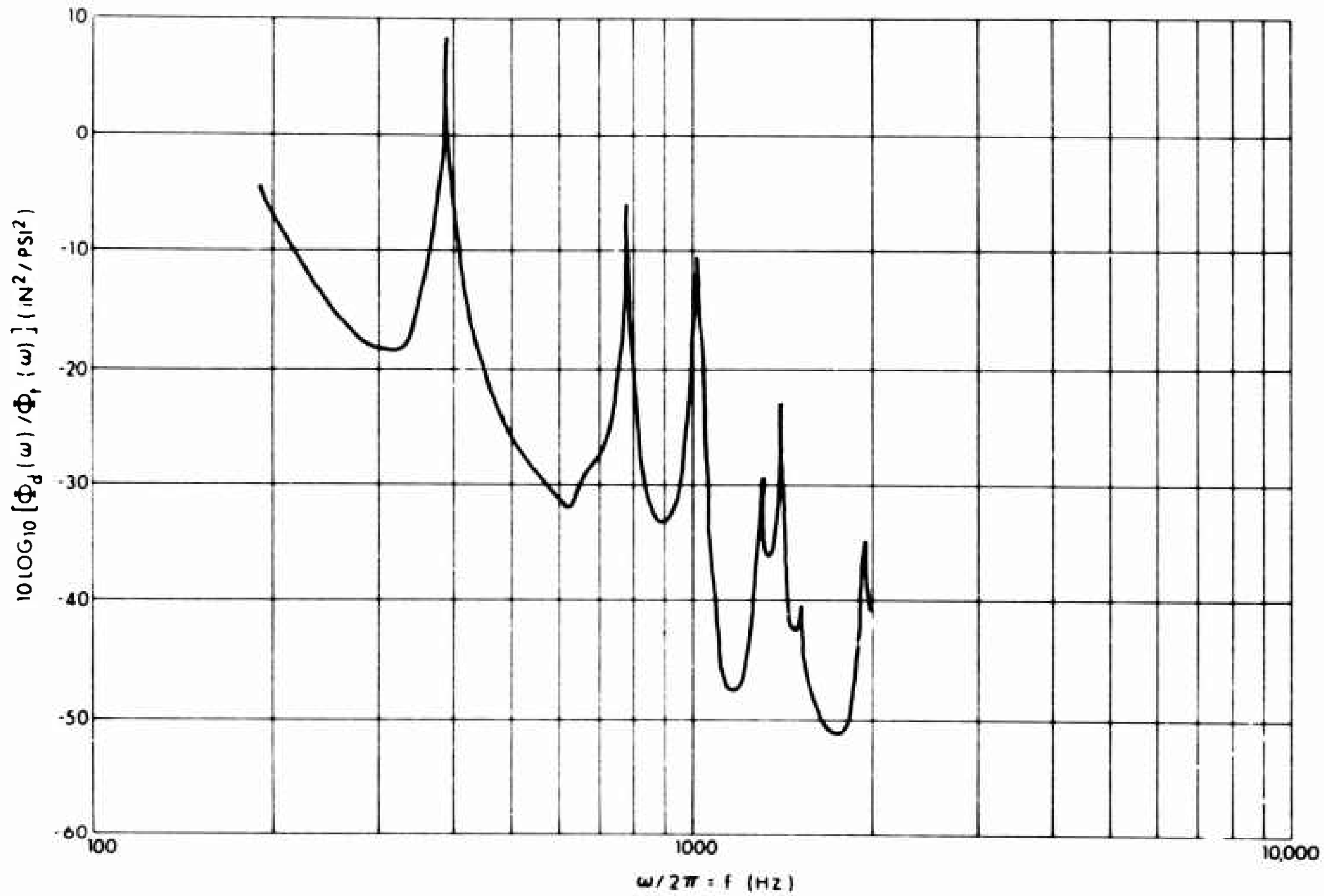

Figure 9. Computed Response of a 3.5 × 3.5 × 0.01 inch Steel Plate to Turbulent Boundary Layer Excitation

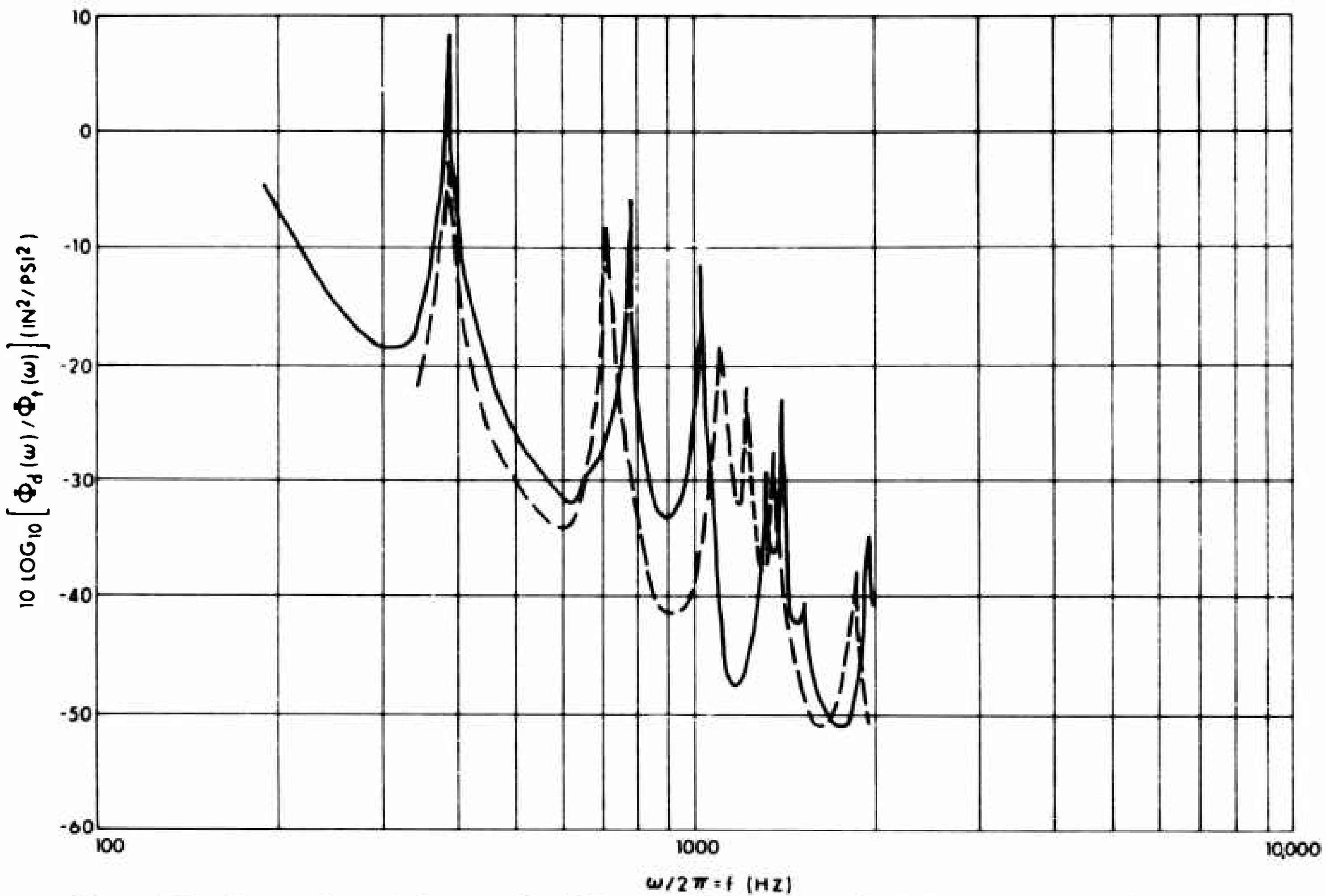

Figure 10. Comparison of Computed and Measured Response of a 3.5 × 3.5 × 0.01 inch Steel Plate Turbulent Boundary Layer Excitation

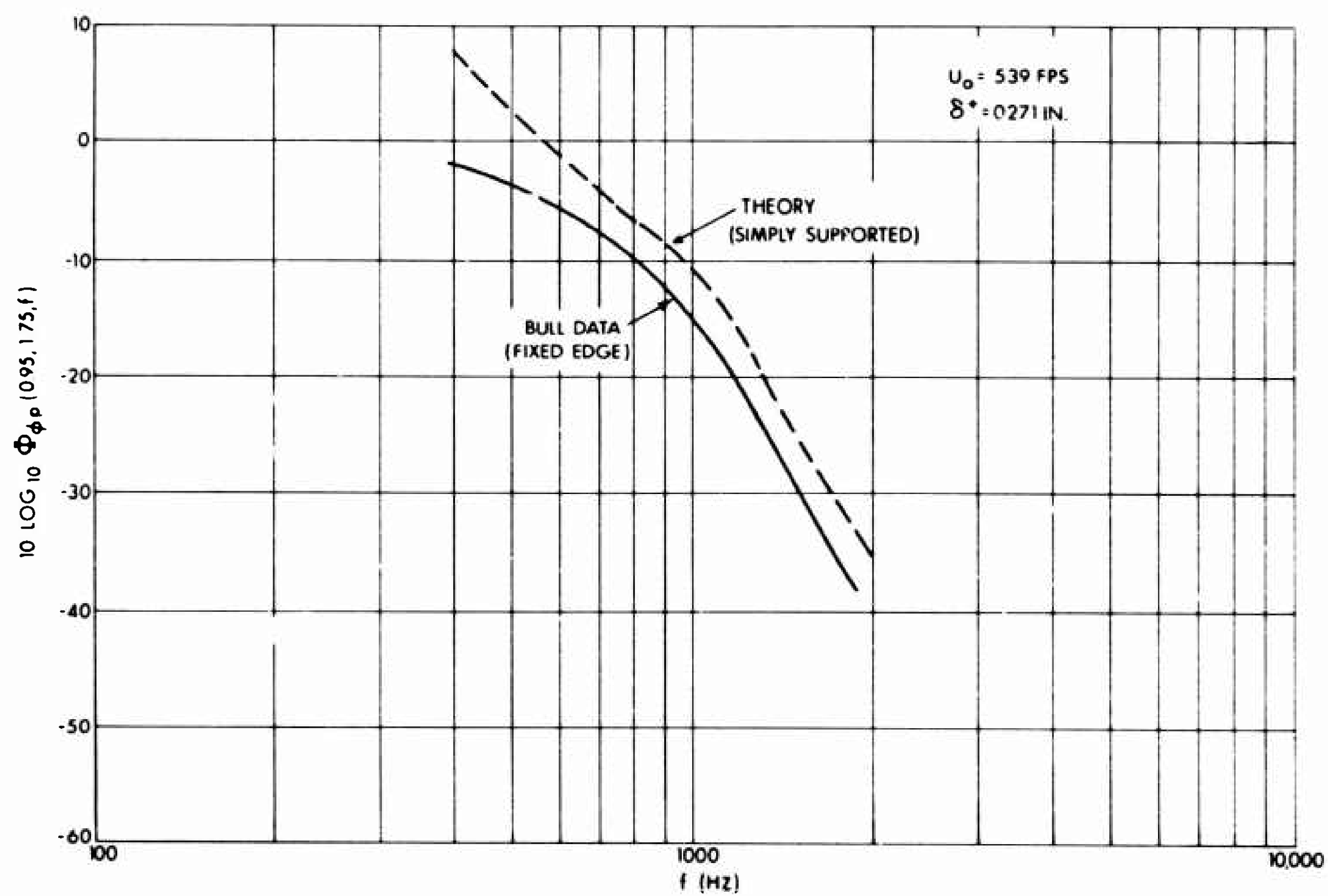

Figure 11. Comparison of Computed and Measured "Peak Spectra" for a 3.5 × 3.5 × 0.01 inch Steel Plate Excited by Boundary Layer Turbulence

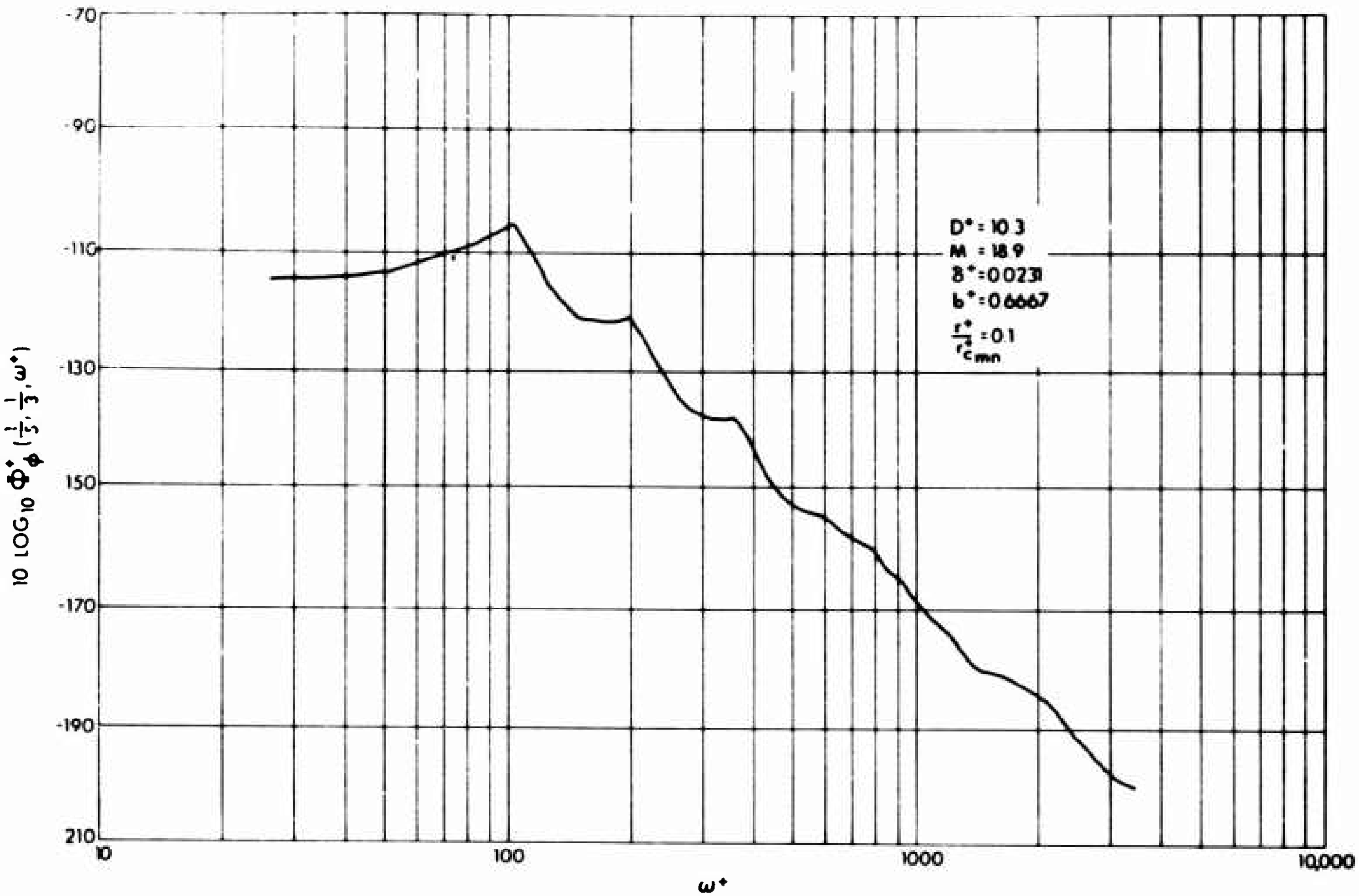

Figure 12. Computed Dimensionless Plate Velocity Power Spectrum at Dimensionless Plate Coordinates (1/5, 1/3); 10 Percent Critical Damping

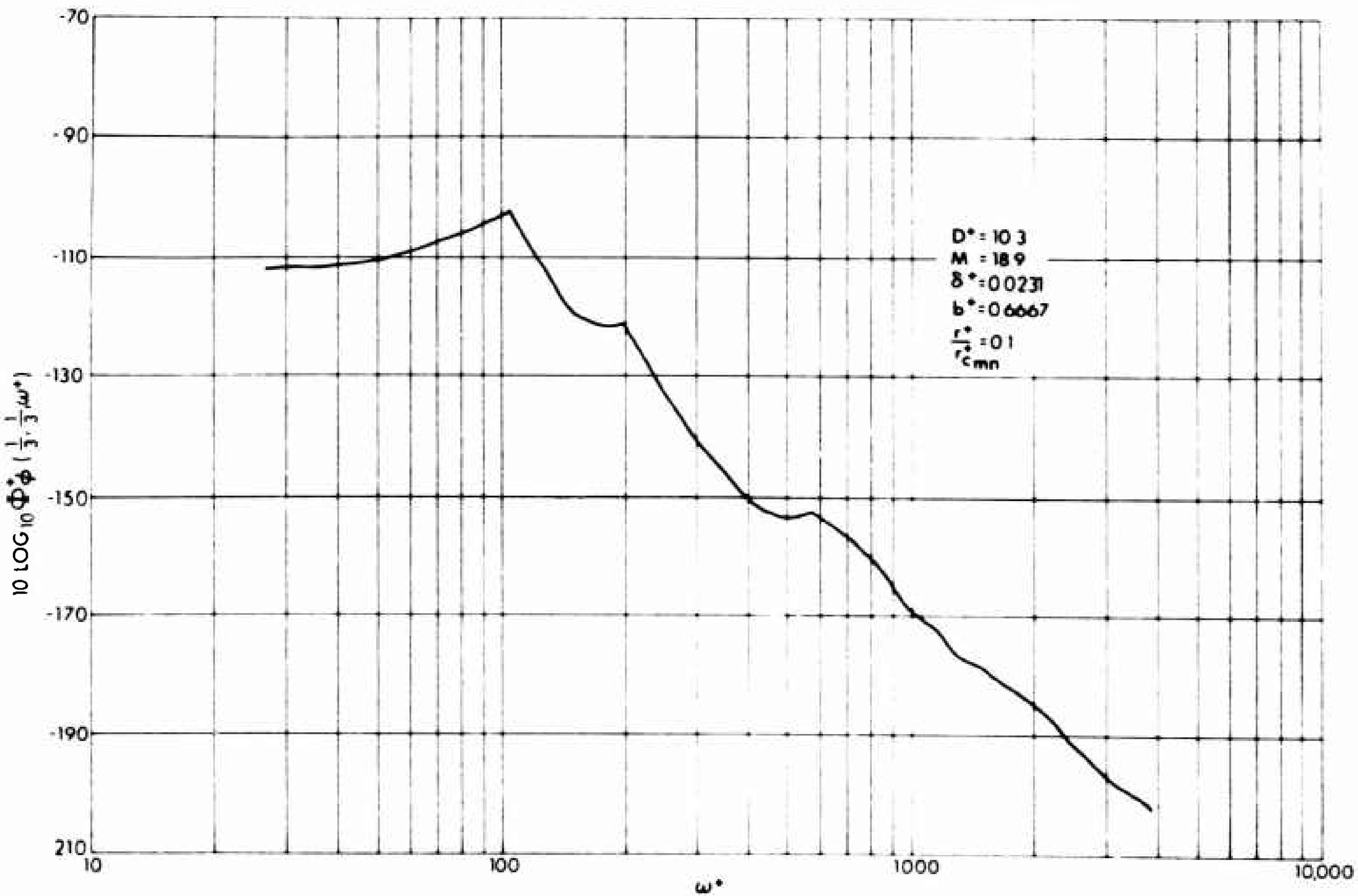

Figure 13. Computed Dimensionless Plate Velocity Power Spectrum at Dimensionless Plate Coordinates (1/3, 1/3); 10 Percent Critical Damping

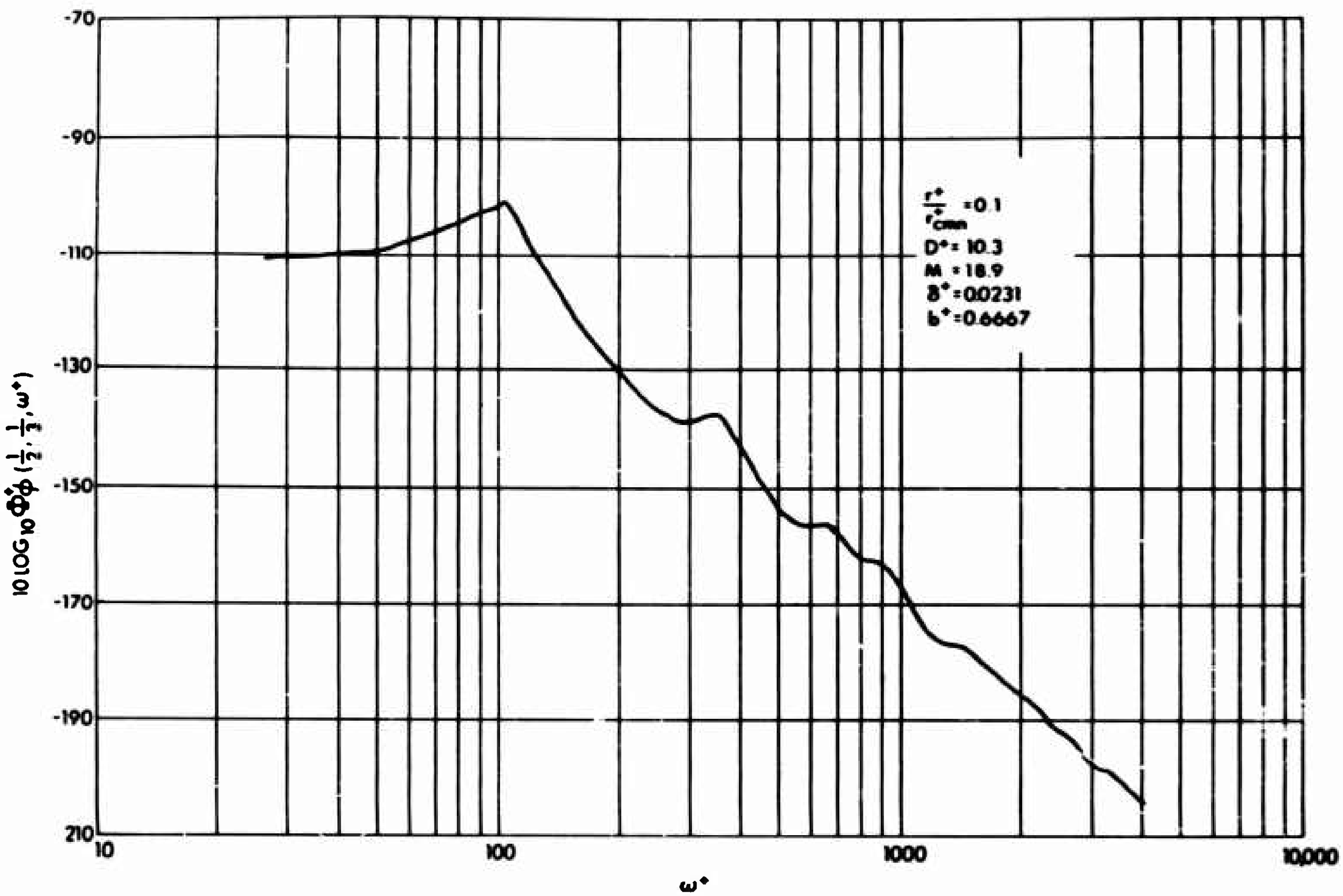

Figure 14. Computed Dimensionless Plate Velocity Power Spectrum at Dimensionless Plate Coordinates (1/2, 1/3); 10 Percent Critical Damping

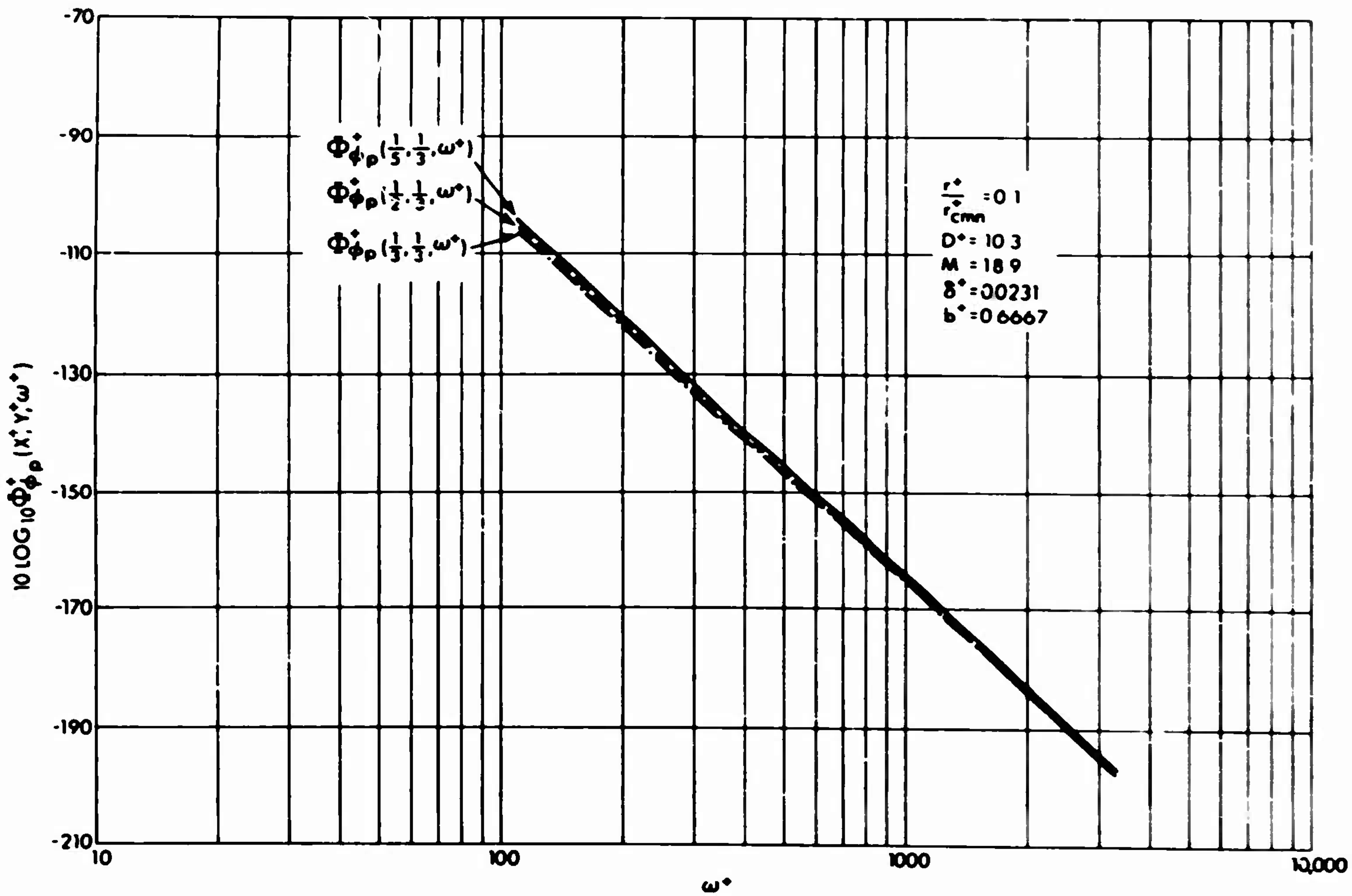

Figure 15. Effect of Plate Coordinates on the Dimensionless Plate Velocity "Peak Spectrum"

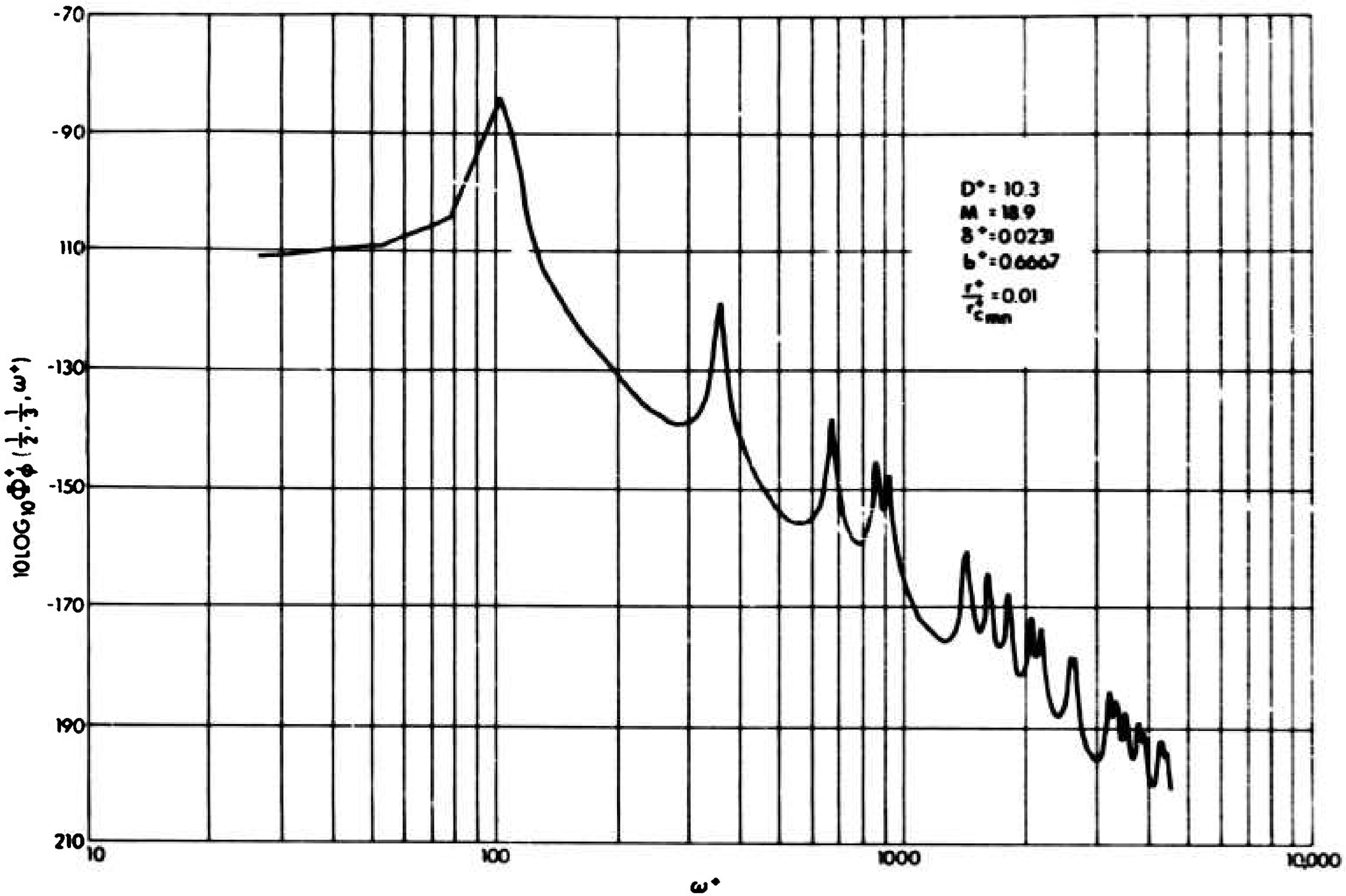

Figure 16. Computed Dimensionless Plate Velocity Power Spectrum at Dimensionless Plate Coordinates (1/2, 1/3); 1 Percent Critical Damping

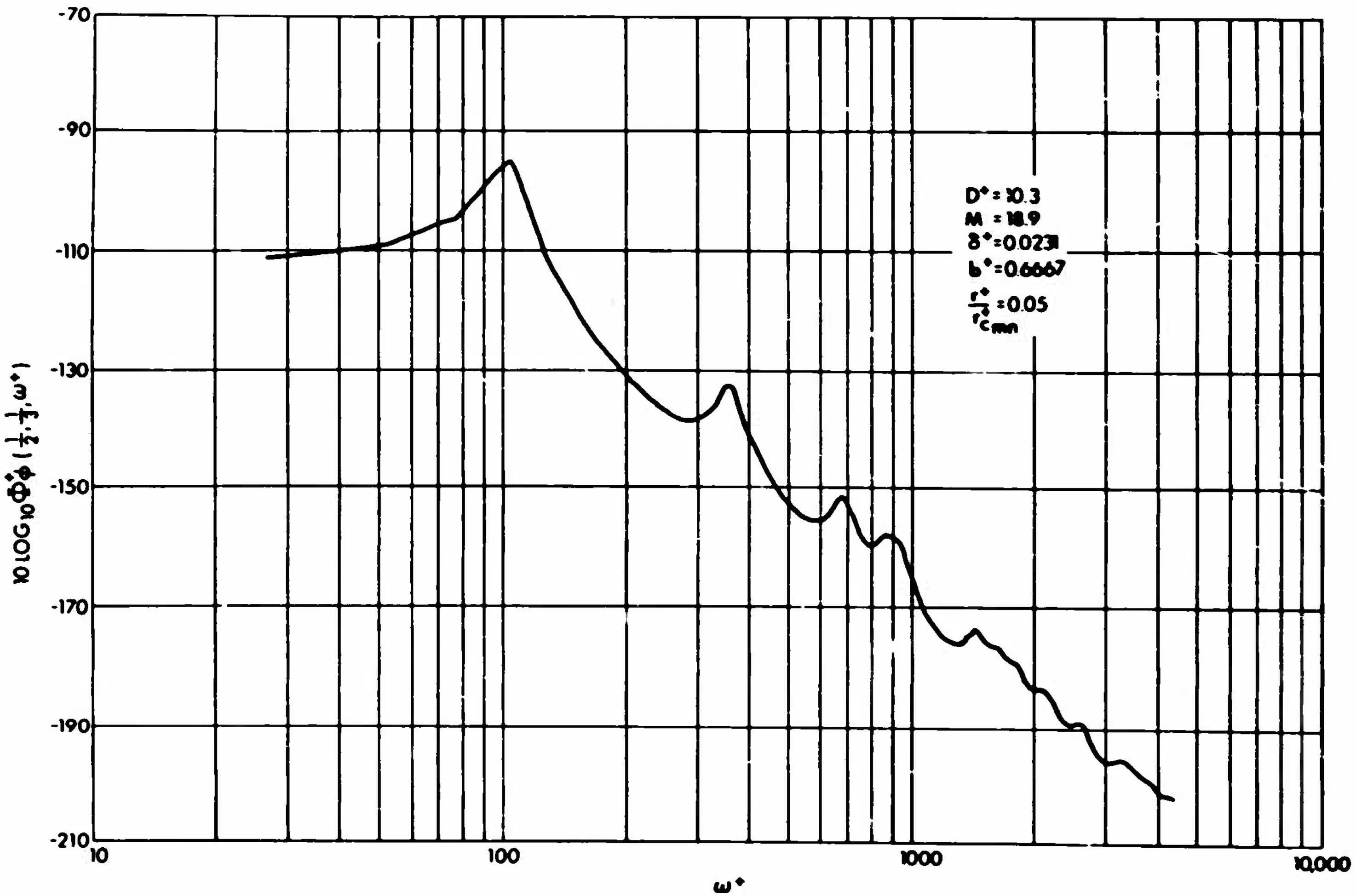

Figure 17. Computed Dimensionless Plate Velocity Power Spectrum at Dimensionless Plate Coordinates (1/2, 1/3); 5 Percent Critical Damping

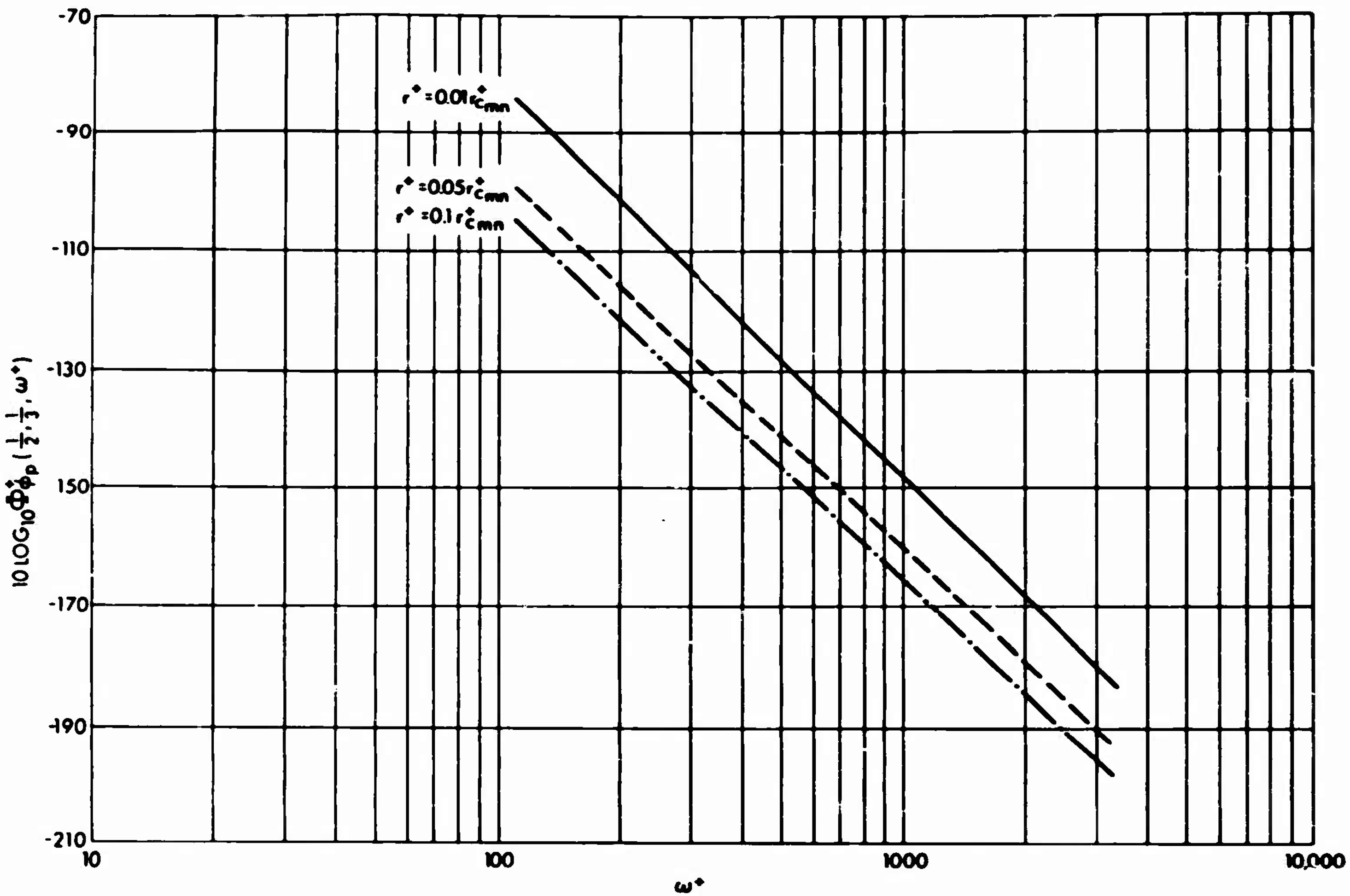

Figure 18. Effect of Plate Damping on the Dimensionless Plate Velocity "Peak Spectrum"

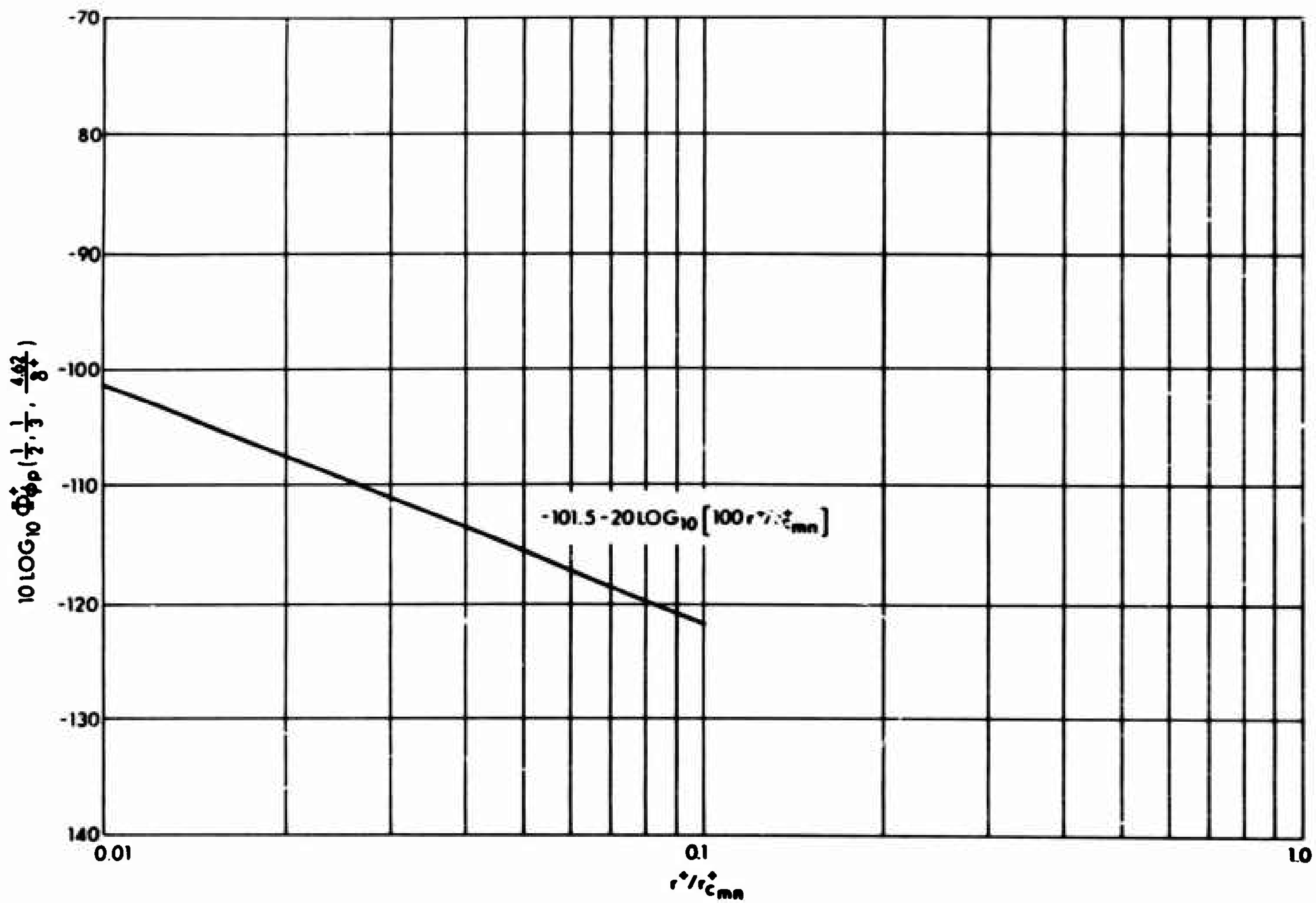

Figure 19. Effect of Plate Damping on the Dimensionless Plate Velocity "Peak Spectral Density" at $\omega^{+} = 4.62/\delta^{+}$

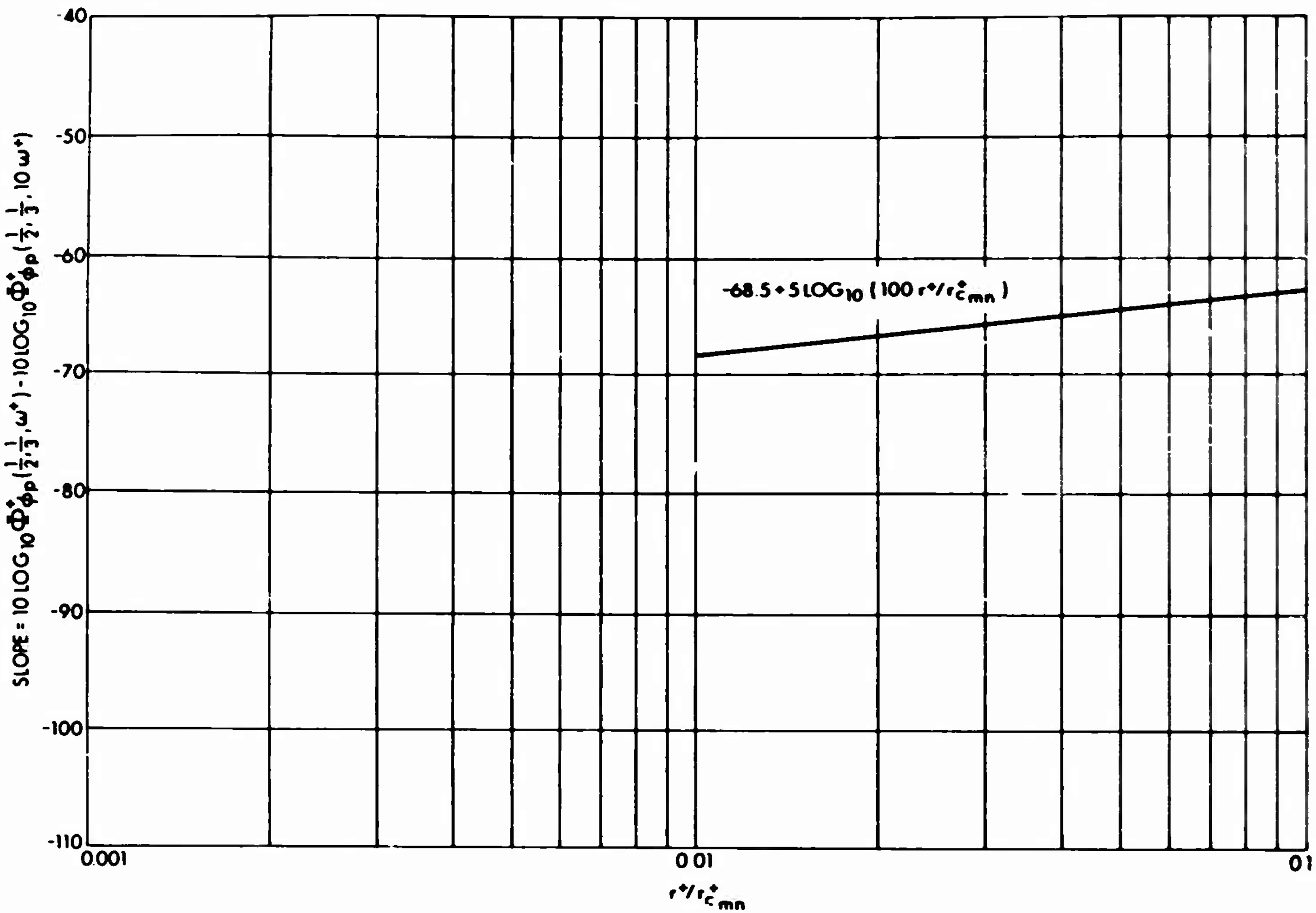

Figure 20. Effect of Plate Damping on the Slope of the Dimensionless Plate Velocity "Peak Spectrum"

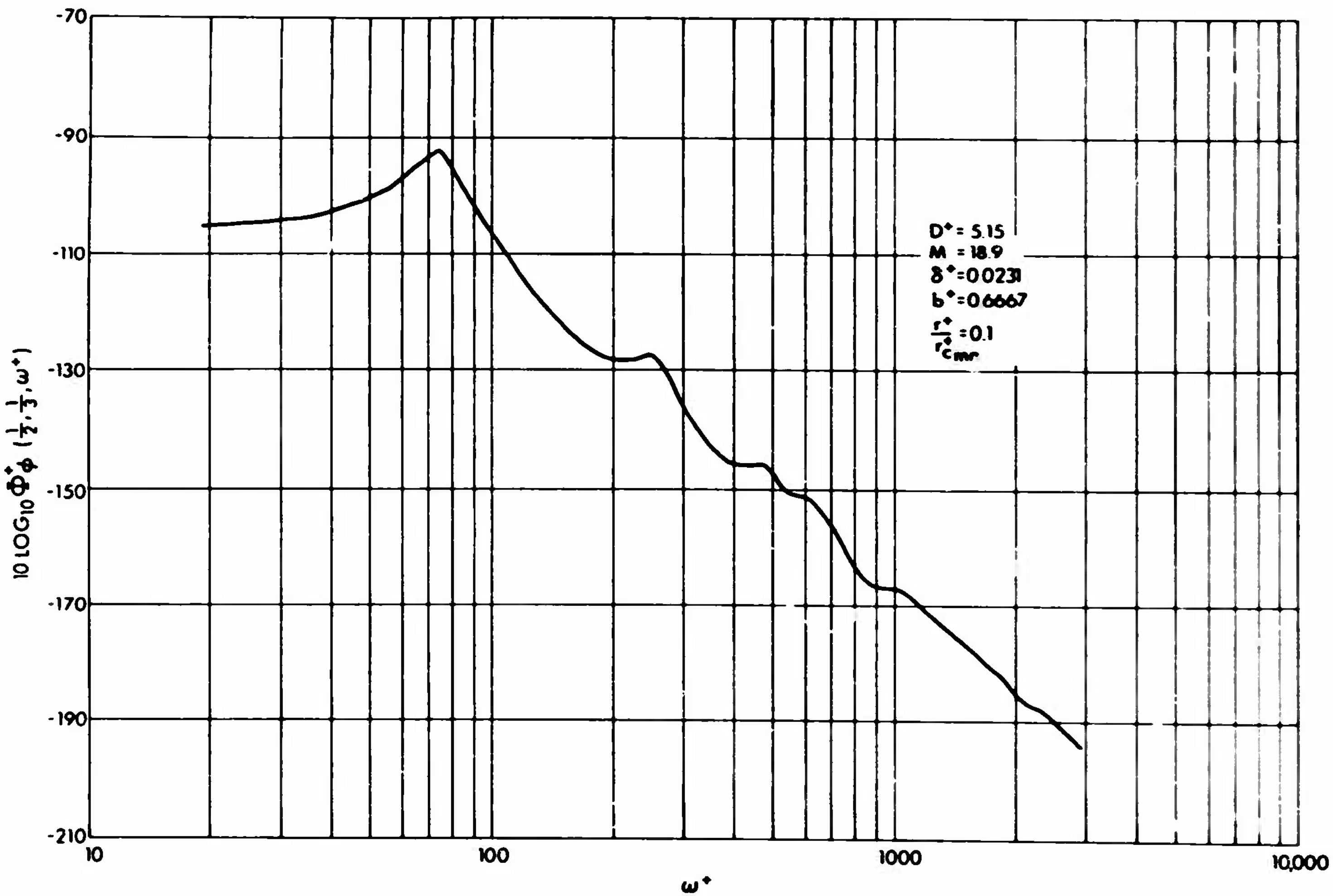

Figure 21. Computed Dimensionless Plate Velocity Power Spectrum at Dimensionless Plate Coordinates (1/2, 1/3); $D^+ = 5.15$

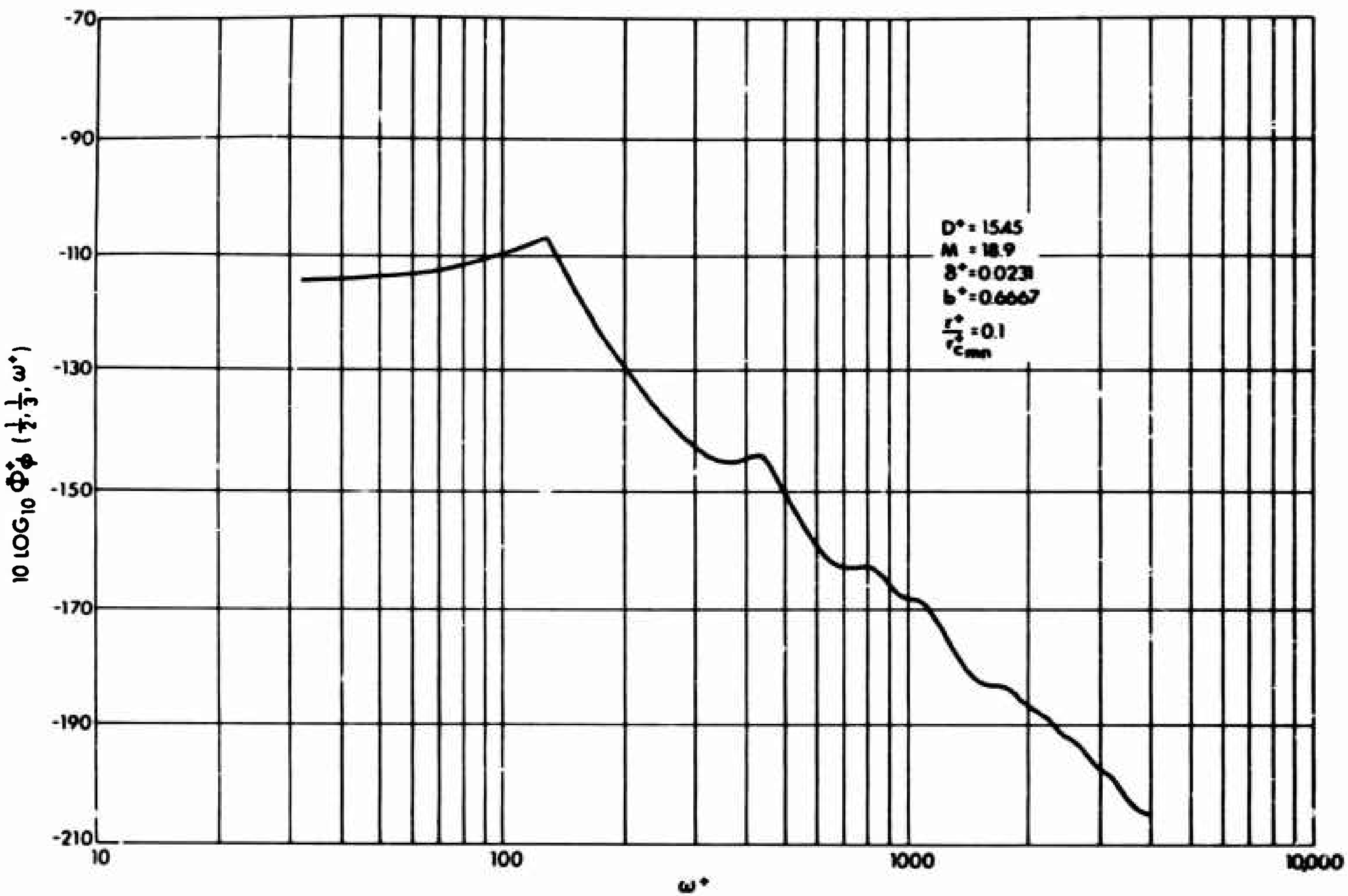

Figure 22. Computed Dimensionless Plate Velocity Power Spectrum at Dimensionless Plate Coordinates (1/2, 1/3); $D^+ = 15.45$

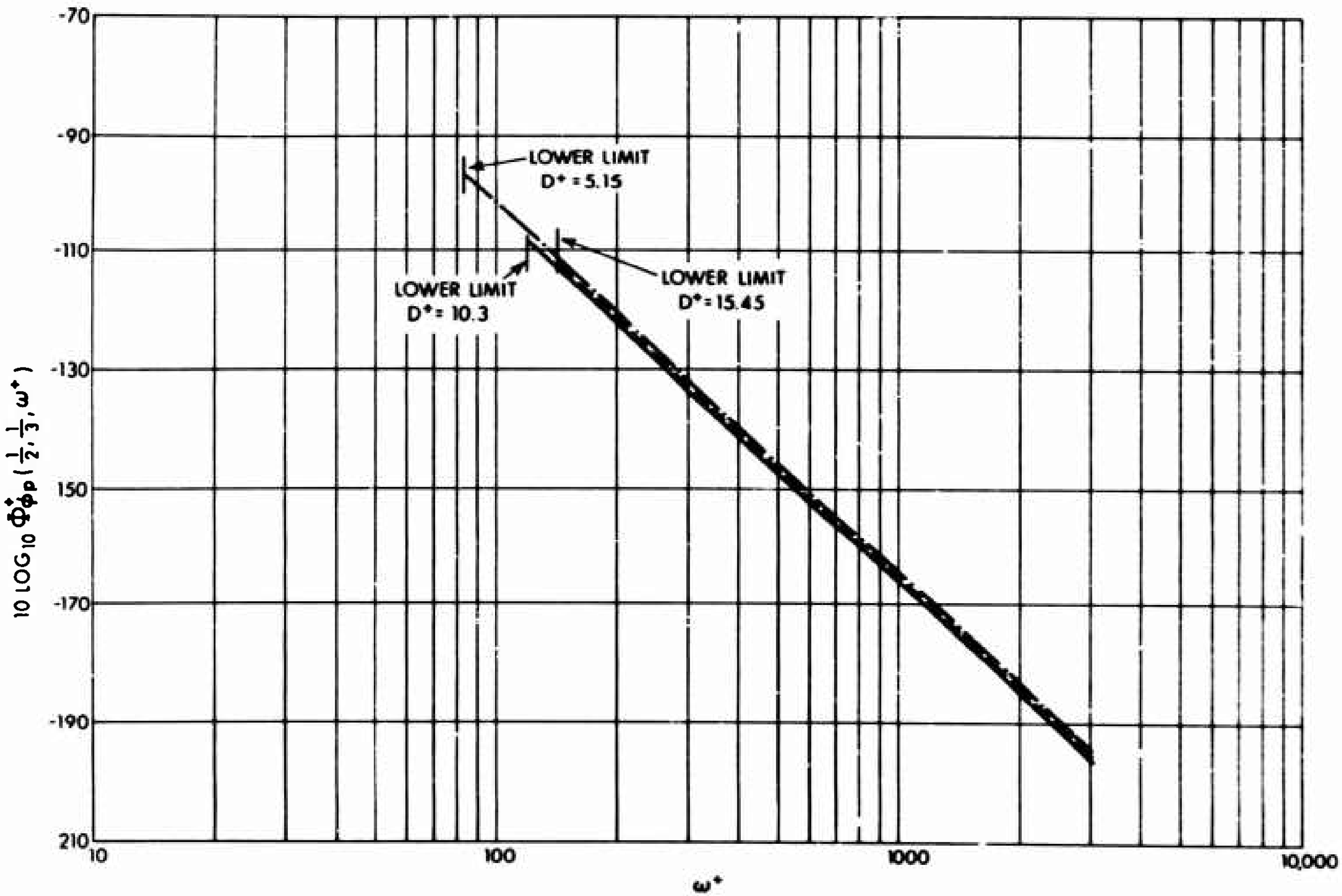

Figure 23. Effect of Plate Rigidity on the Dimensionless Plate Velocity "Peak Spectrum"

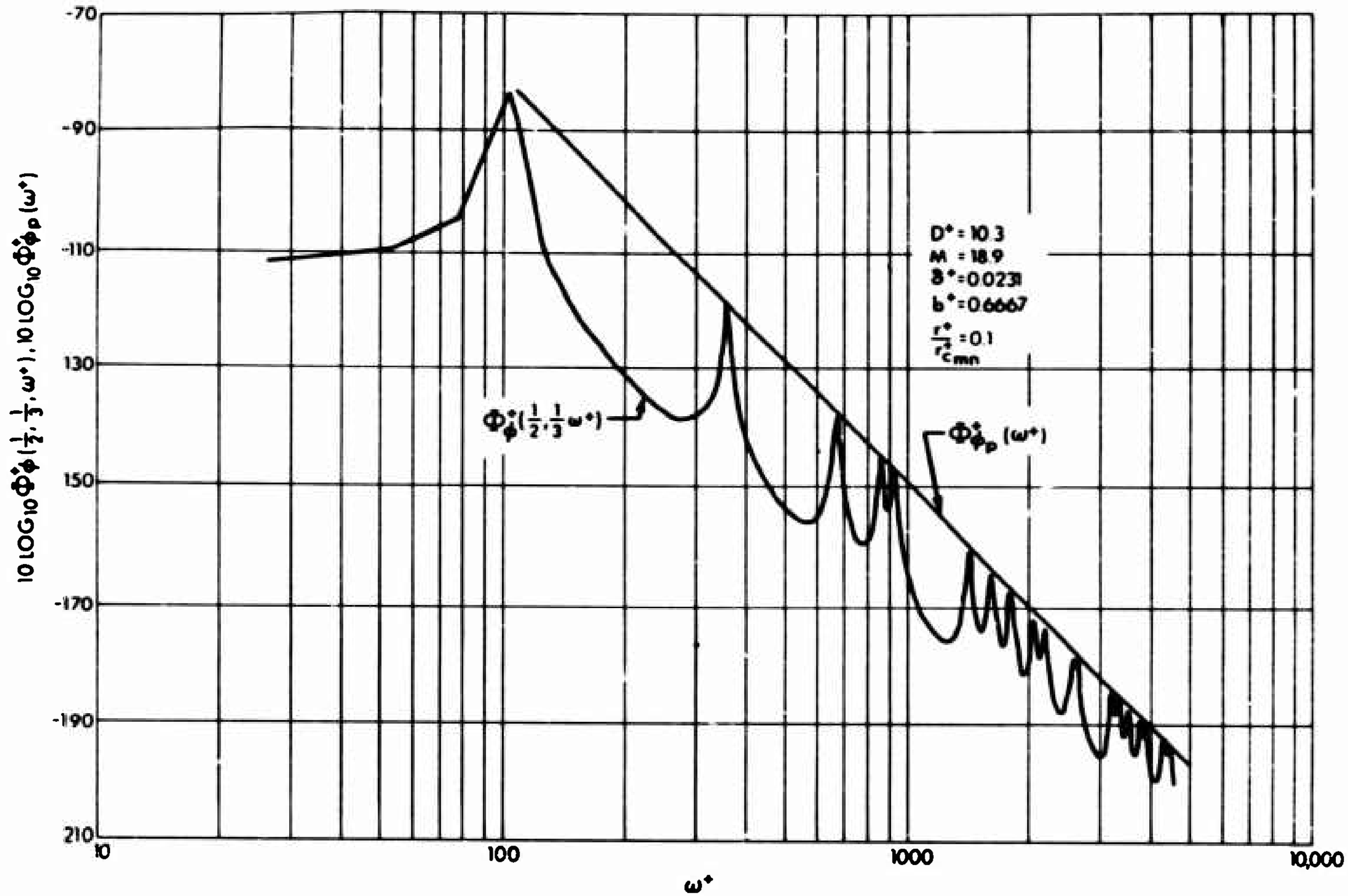

Figure 24. Comparison of Computed Dimensionless Plate Velocity Power Spectrum with Dimensionless Plate Velocity "Peak Spectrum"

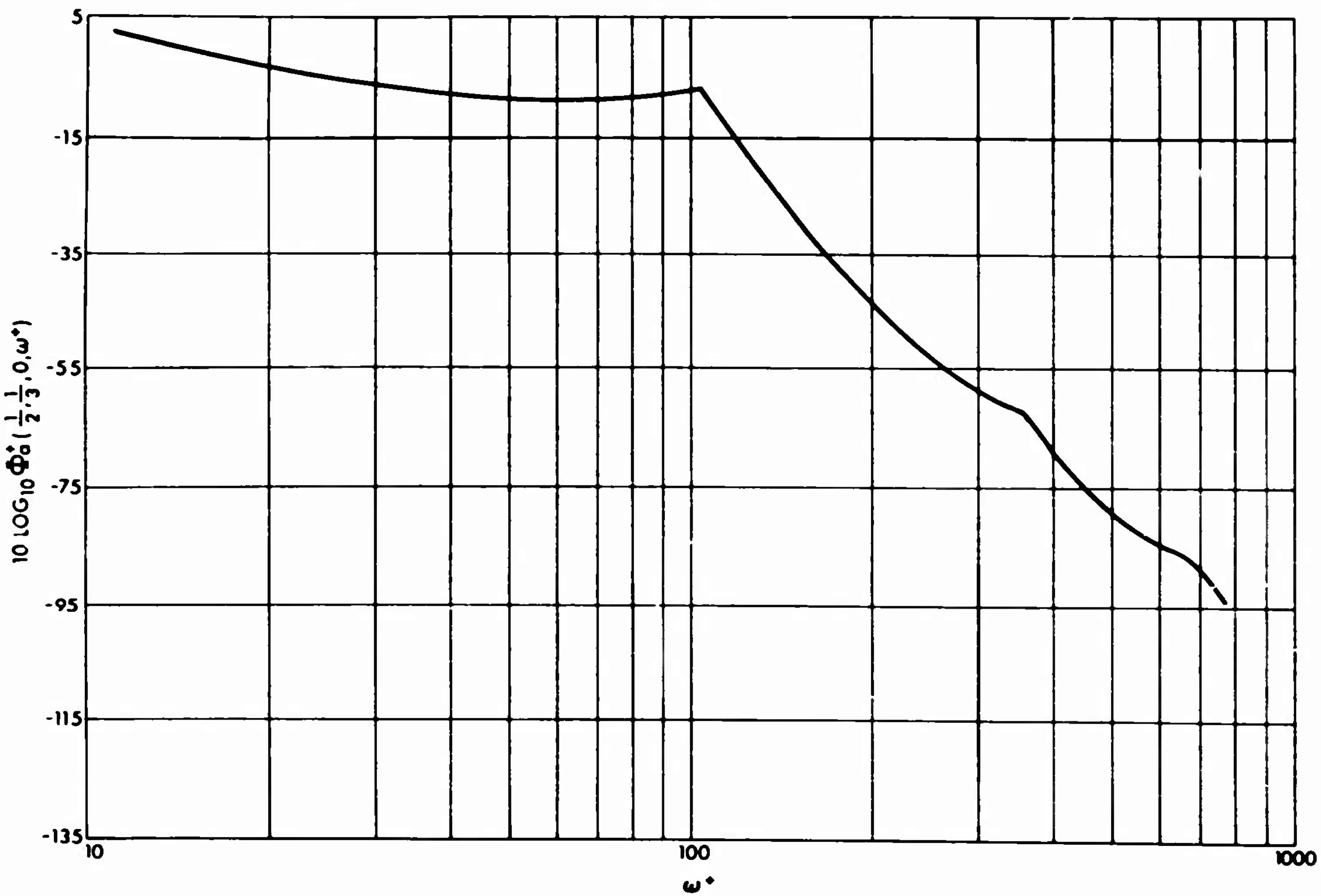

Figure 25. Computed Dimensionless Cavity Acoustic Pressure Power Spectrum at Dimensionless Cavity Coordinates (1/2, 1/3, 0) for Case 1 Parameters

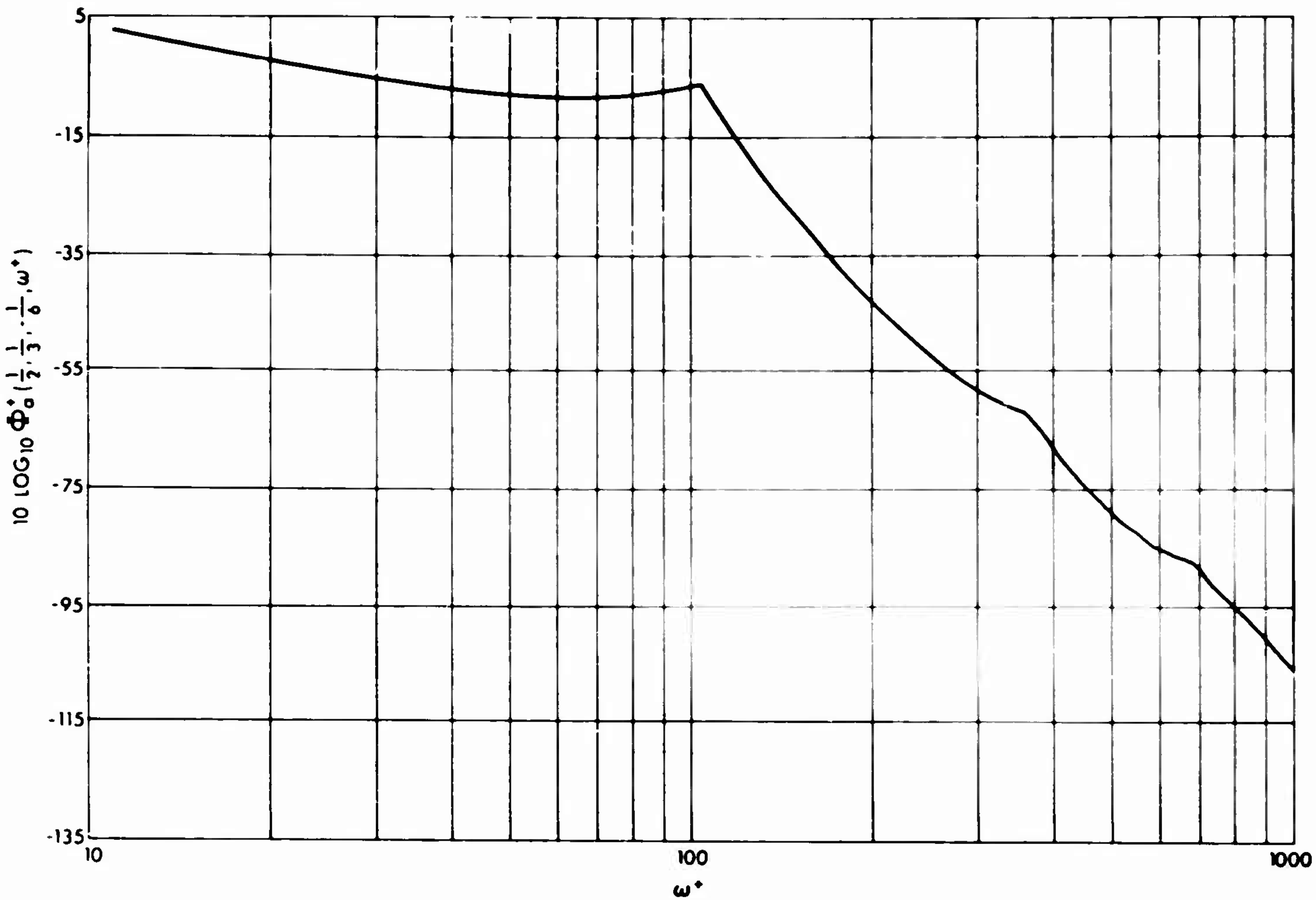

Figure 26. Computed Dimensionless Cavity Acoustic Pressure Power Spectrum at Dimensionless Cavity Coordinates (1/2, 1/3, -1/6) for Case 1 Parameters

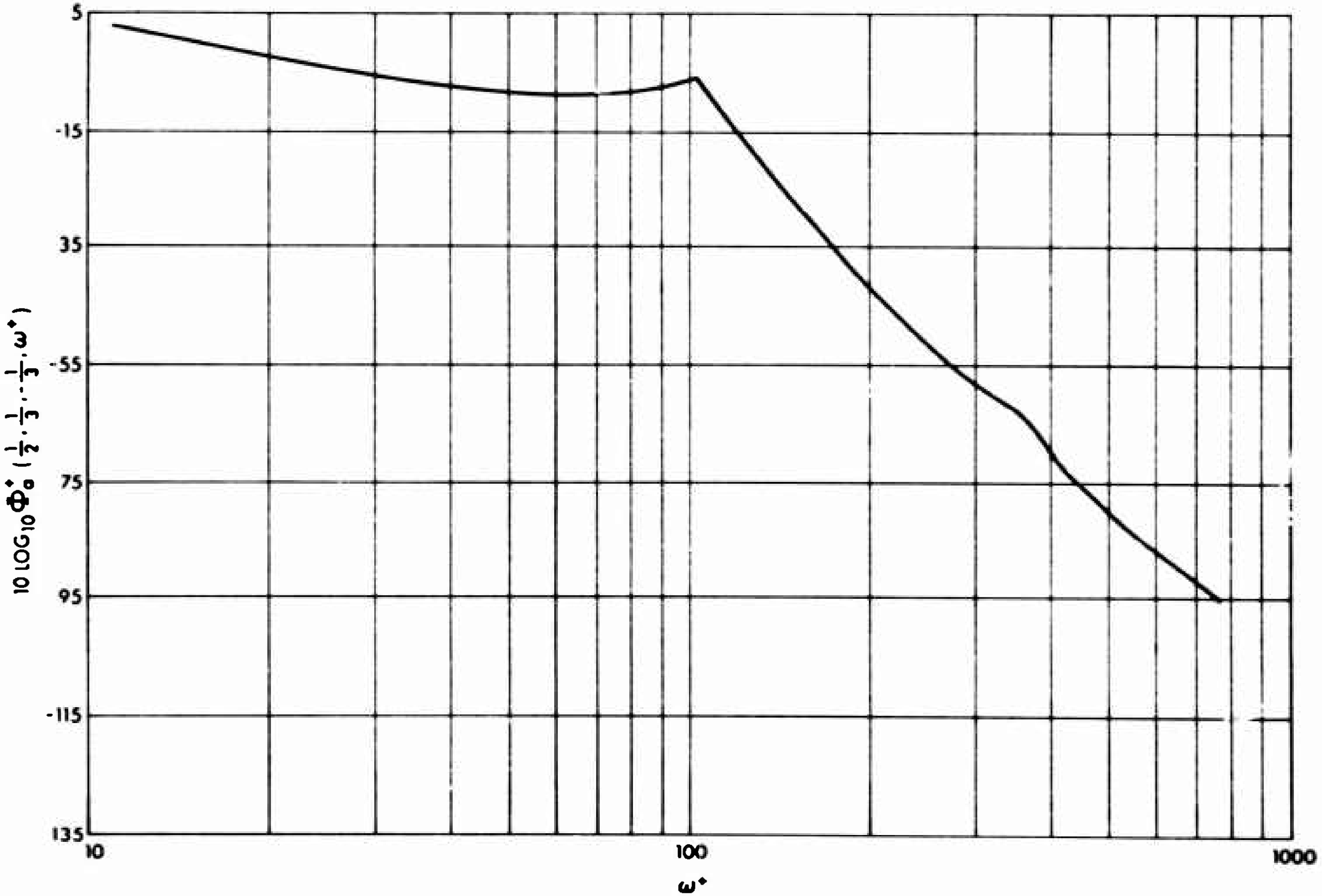

Figure 27. Computed Dimensionless Cavity Acoustic Pressure Power Spectrum at Dimensionless Cavity Coordinates (1/2, 1/3, -1/3) for Case 1 Parameters

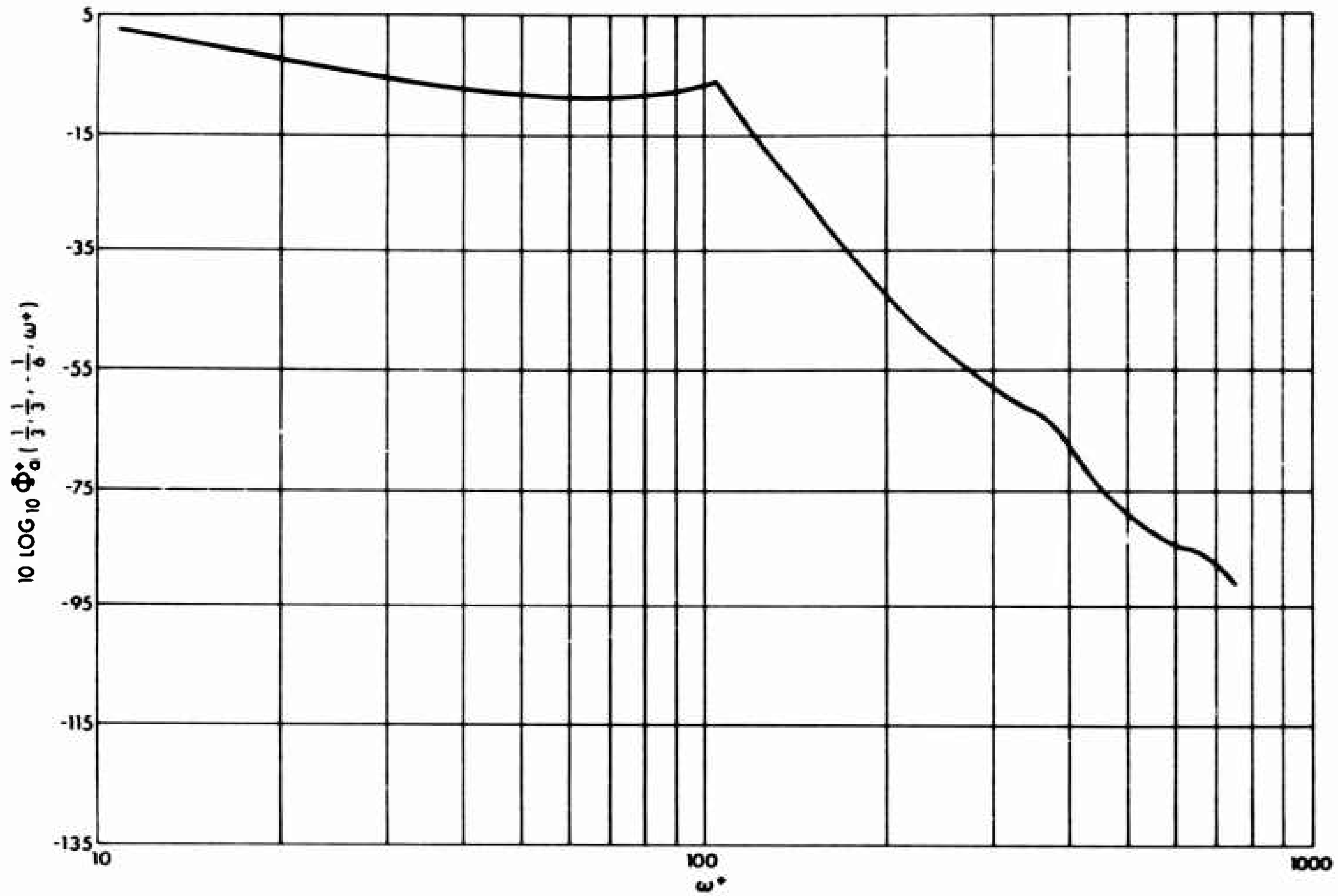

Figure 28. Computed Dimensionless Cavity Acoustic Pressure Power Spectrum at Dimensionless Cavity Coordinates (1/3, 1/3, -1/6) for Case 1 Parameters

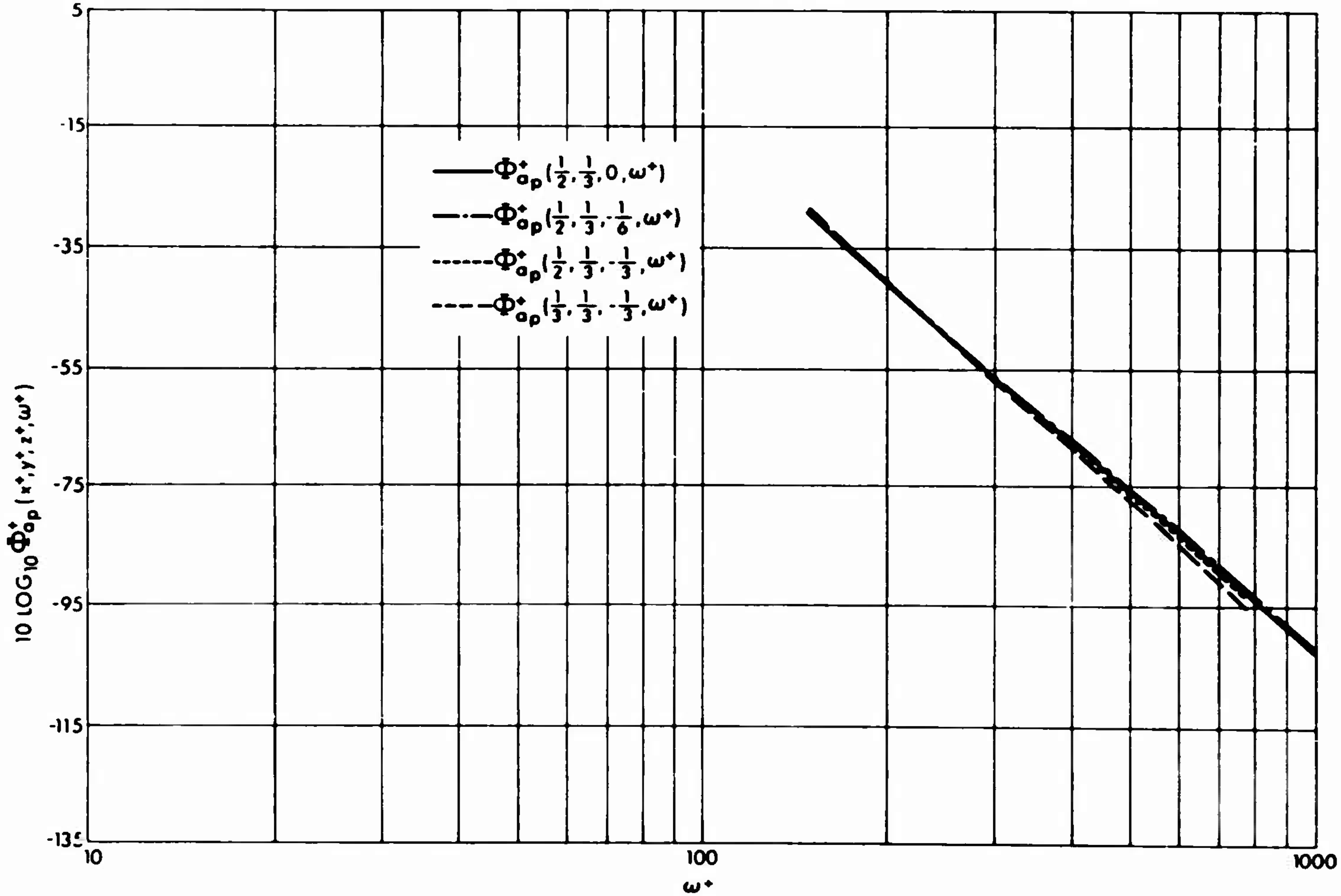

Figure 29. Effect of Cavity Coordinates on the Dimensionless Cavity Acoustic Pressure "Peak Spectrum"

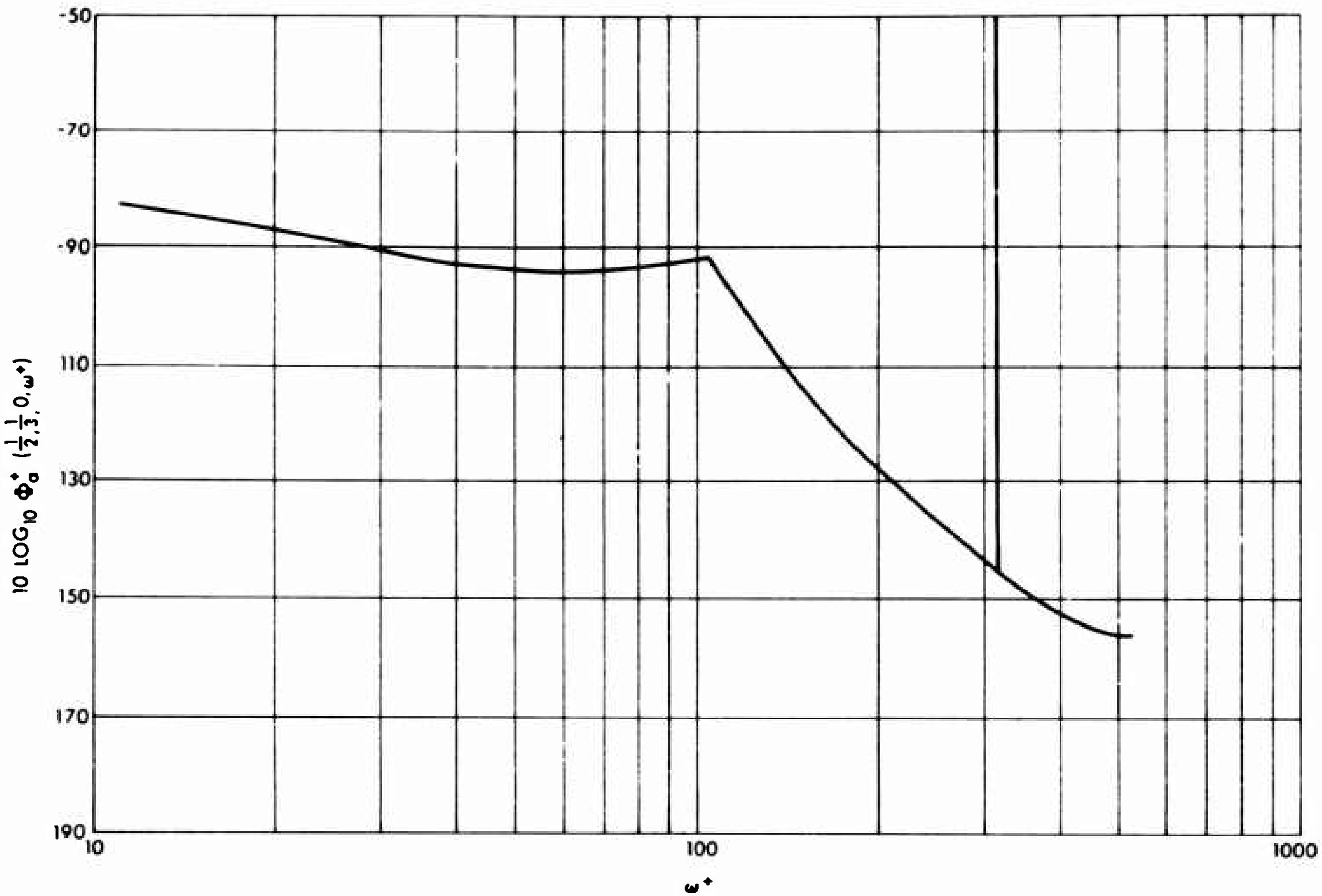

Figure 30. Computed Dimensionless Cavity Acoustic Pressure Power Spectrum at Dimensionless Cavity Coordinates (1/2, 1/3, 0) for Case 4 Parameters

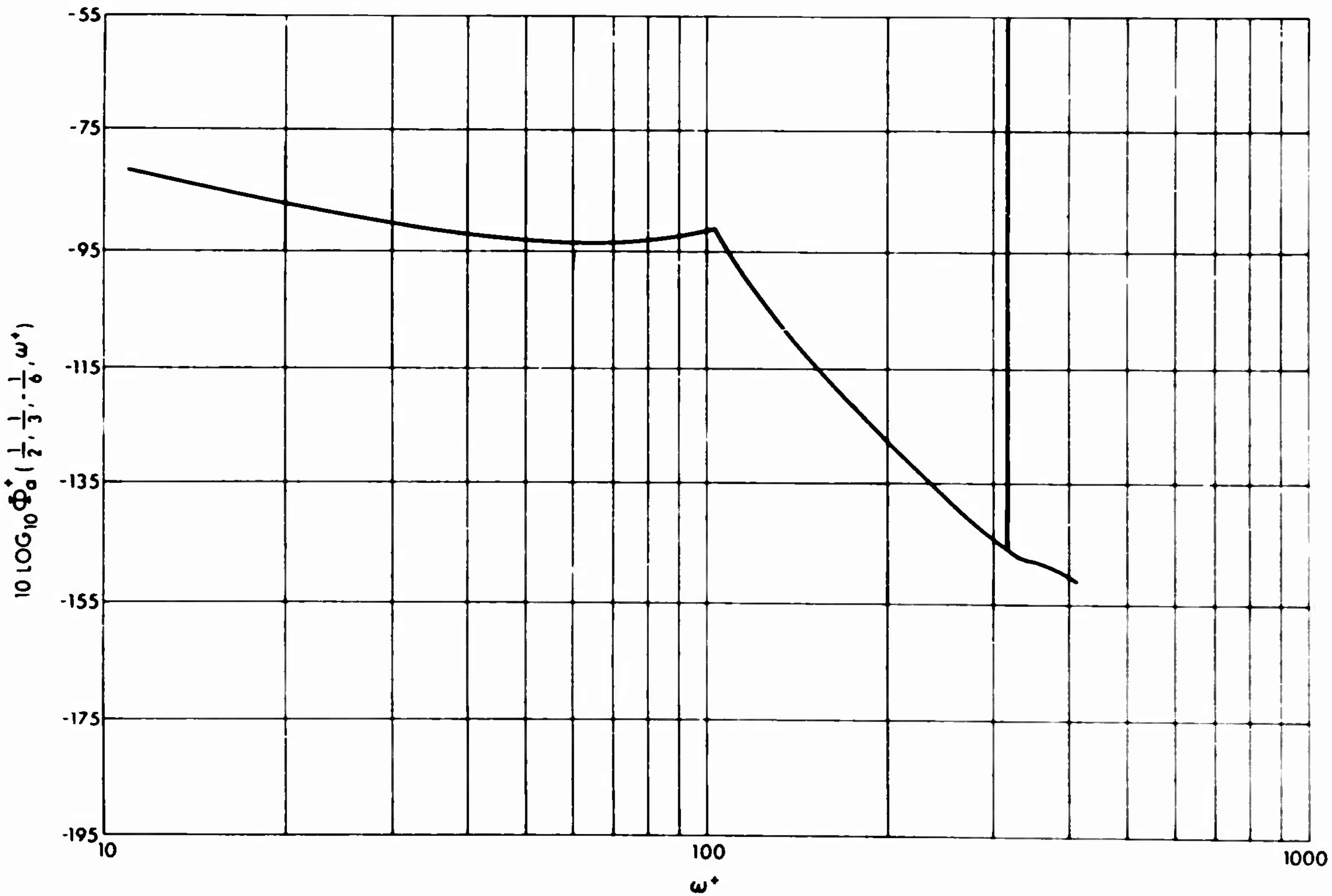

Figure 31. Computed Dimensionless Cavity Acoustic Pressure Power Spectrum at Dimensionless Cavity Coordinates (1/2, 1/3, -1/6) for Case 4 Parameters

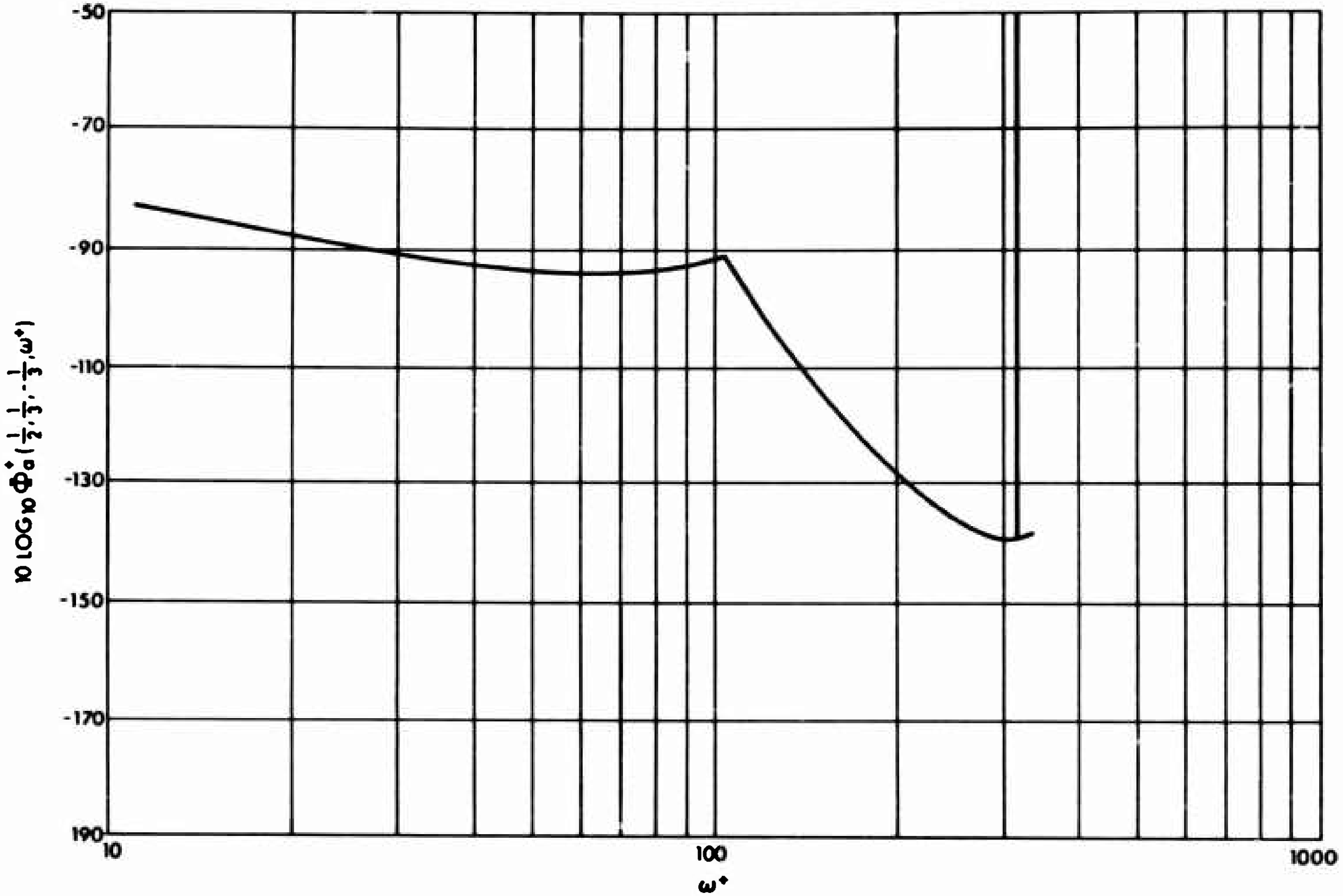

Figure 32. Computed Dimensionless Cavity Acoustic Pressure Power Spectrum at Dimensionless Cavity Coordinates (1/2, 1/3, -1/3) for Case 4 Parameters

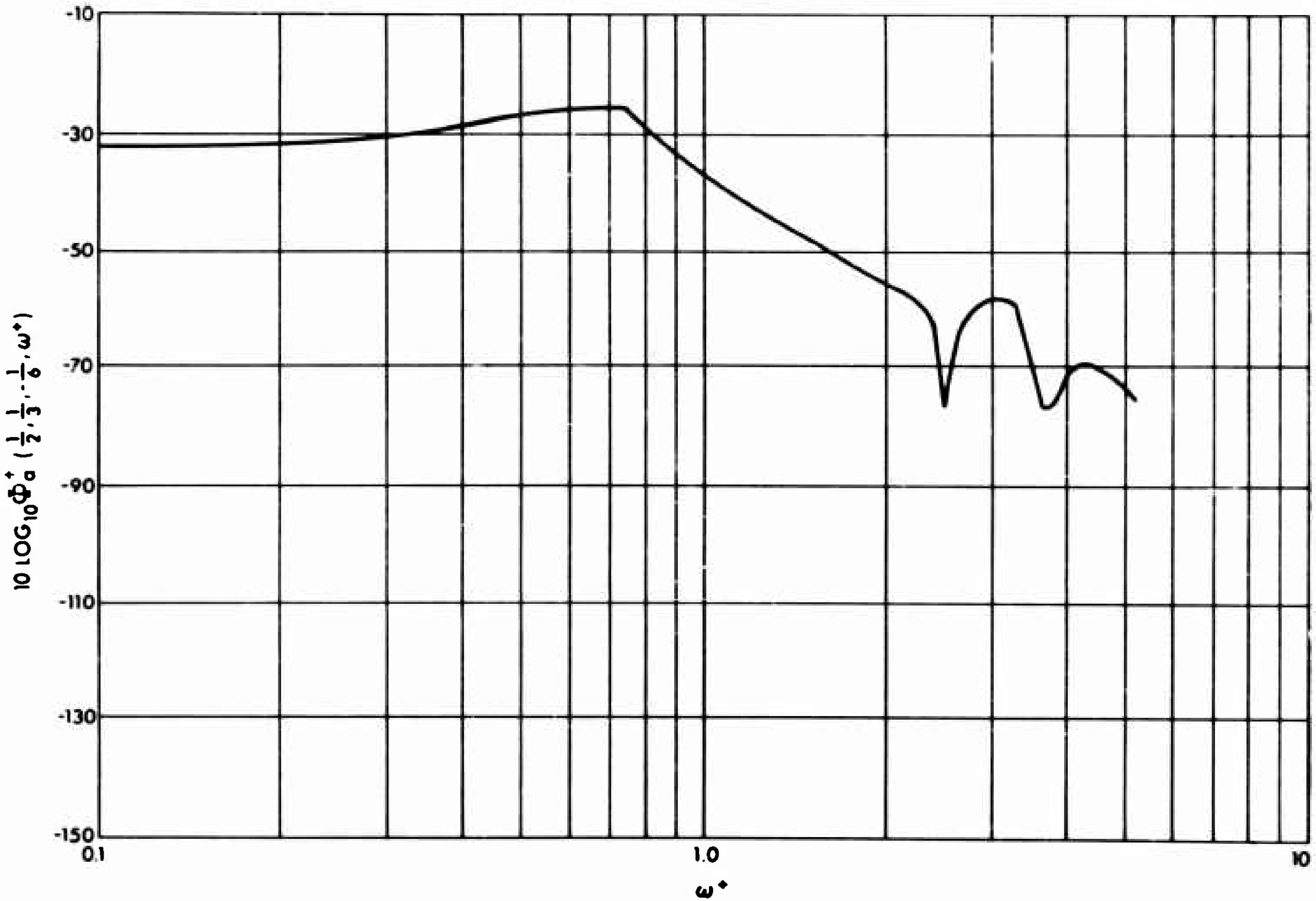

Figure 33. Computed Dimensionless Cavity Acoustic Pressure Power Spectrum at Dimensionless Cavity Coordinates (1/2, 1/3, -1/6) for Case 2 Parameters

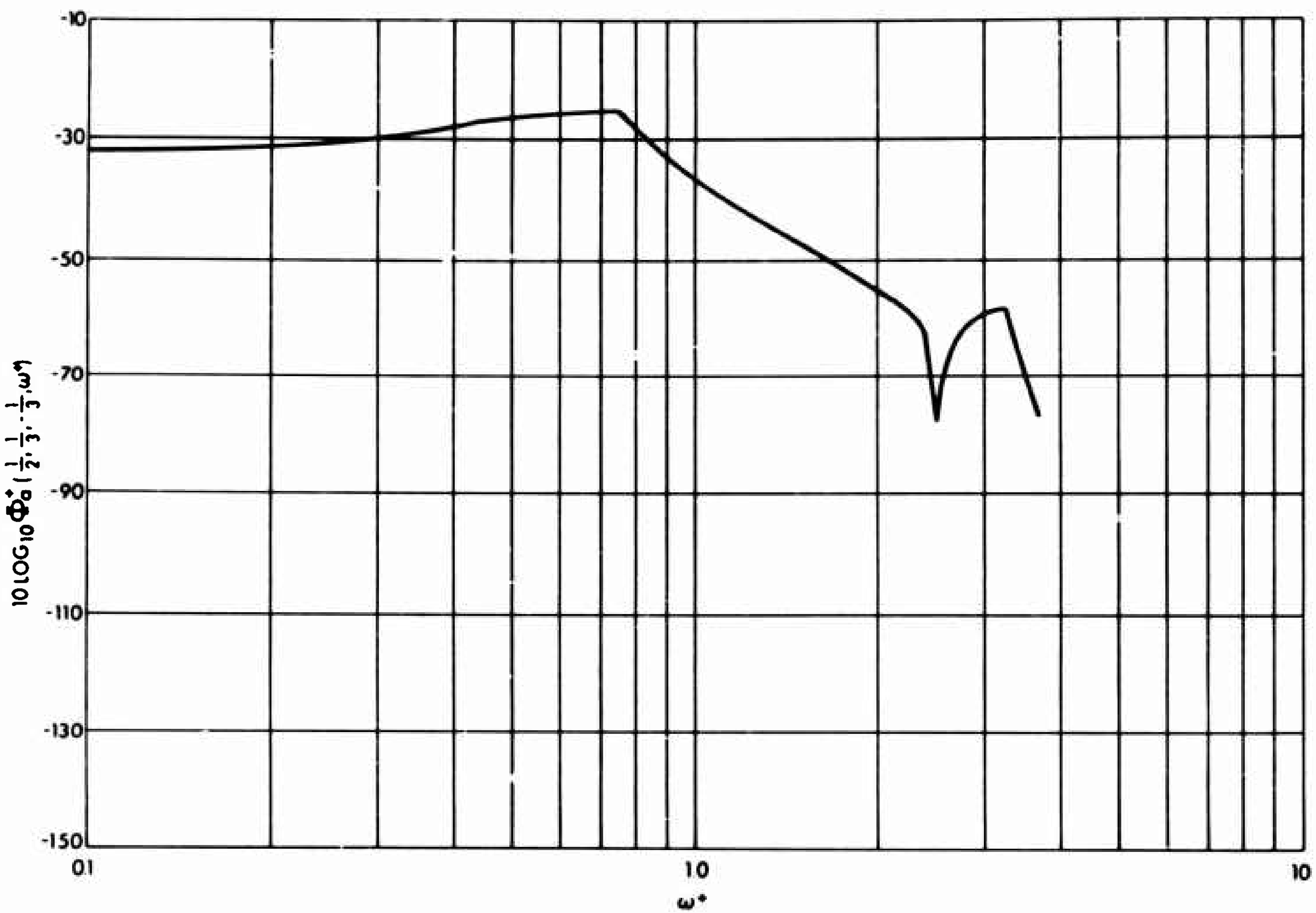

Figure 34. Computed Dimensionless Cavity Acoustic Pressure Power Spectrum at Dimensionless Cavity Coordinates (1/2, 1/3, -1/3) for Case 2 Parameters

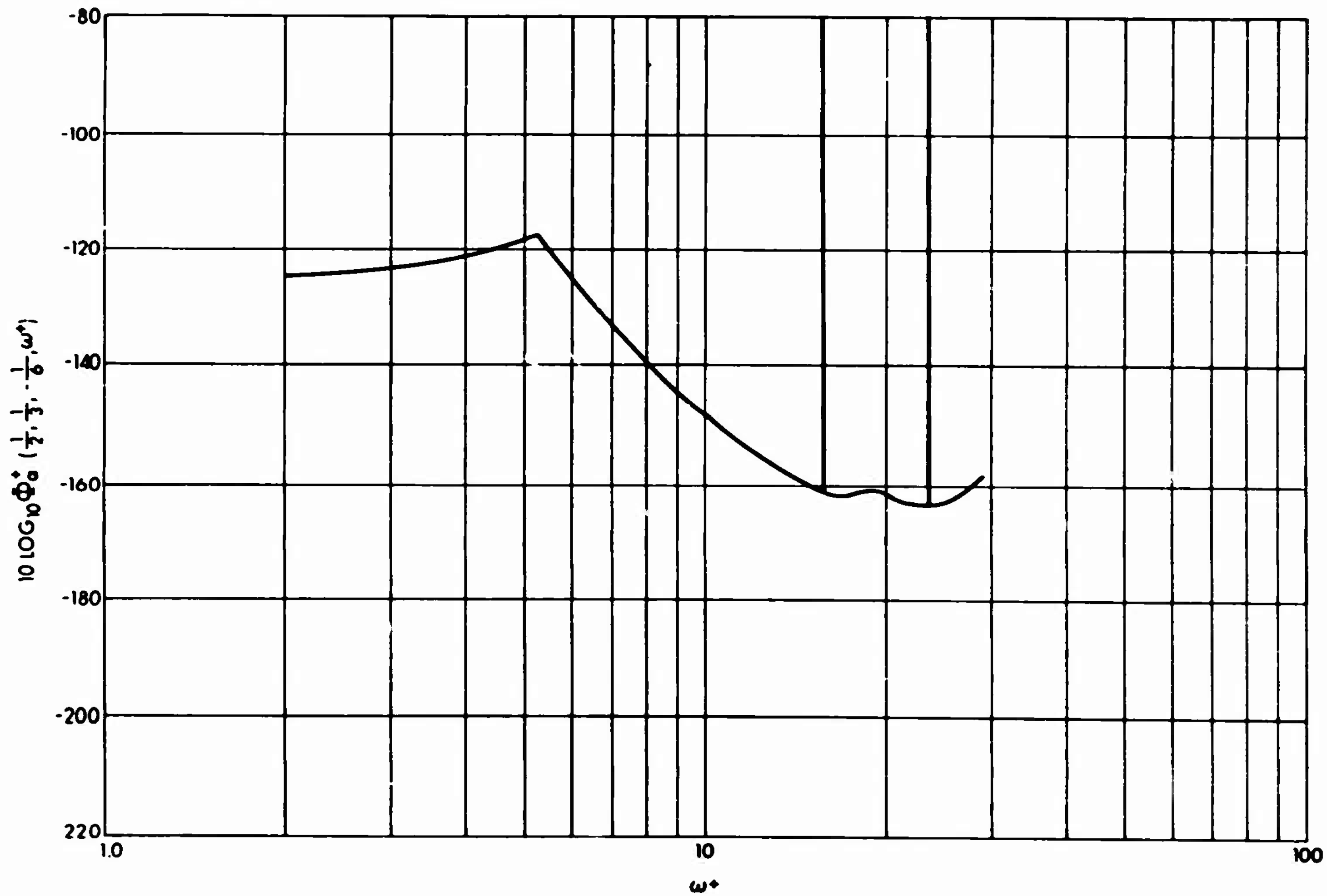

Figure 35. Computed Dimensionless Cavity Acoustic Pressure Power Spectrum at Dimensionless Cavity Coordinates (1/2, 1/3, -1/6) for Case 3 Parameters

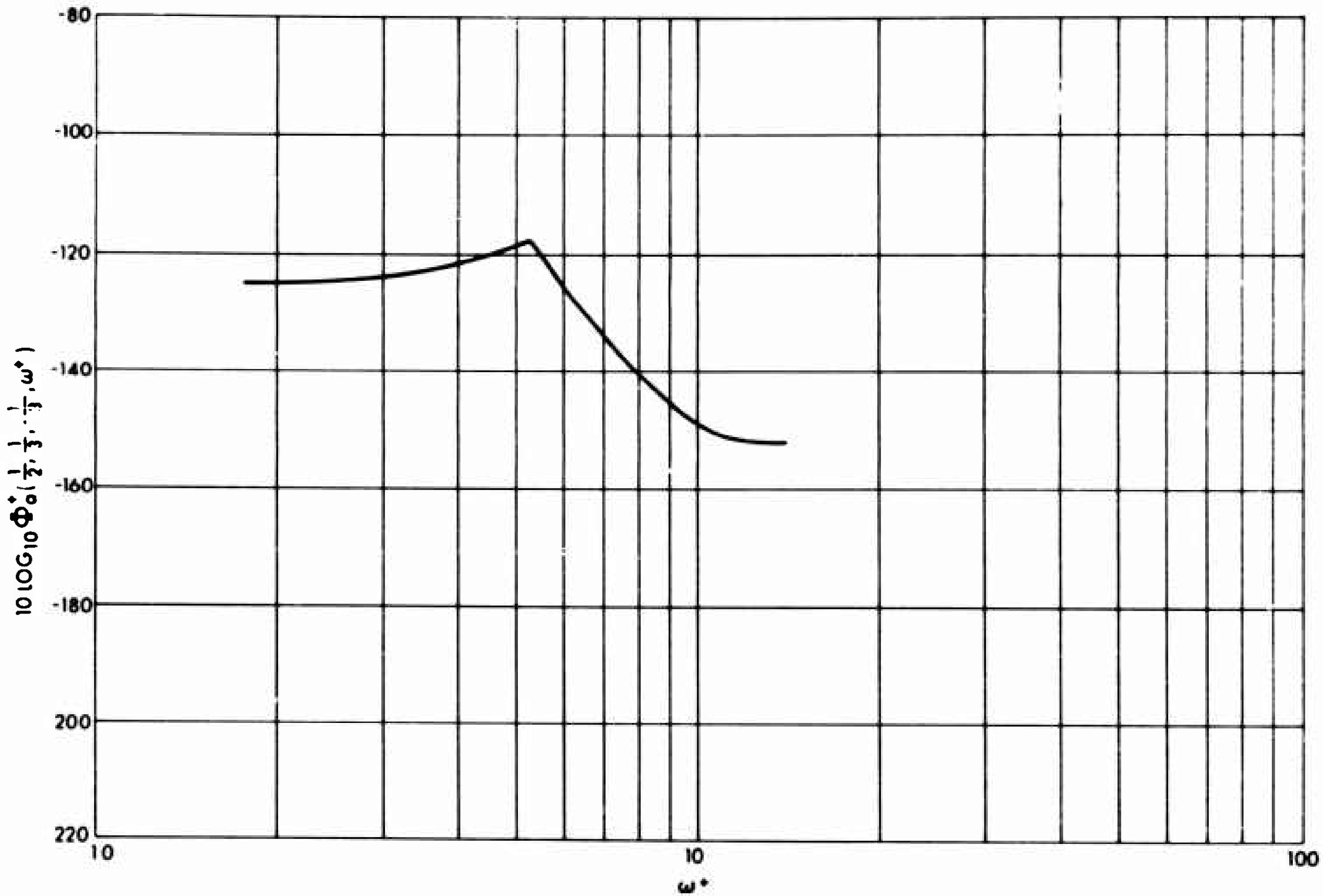

Figure 36. Computed Dimensionless Cavity Acoustic Pressure Power Spectrum at Dimensionless Cavity Coordinates (1/2, 1/3, -1/3) for Case 3 Parameters

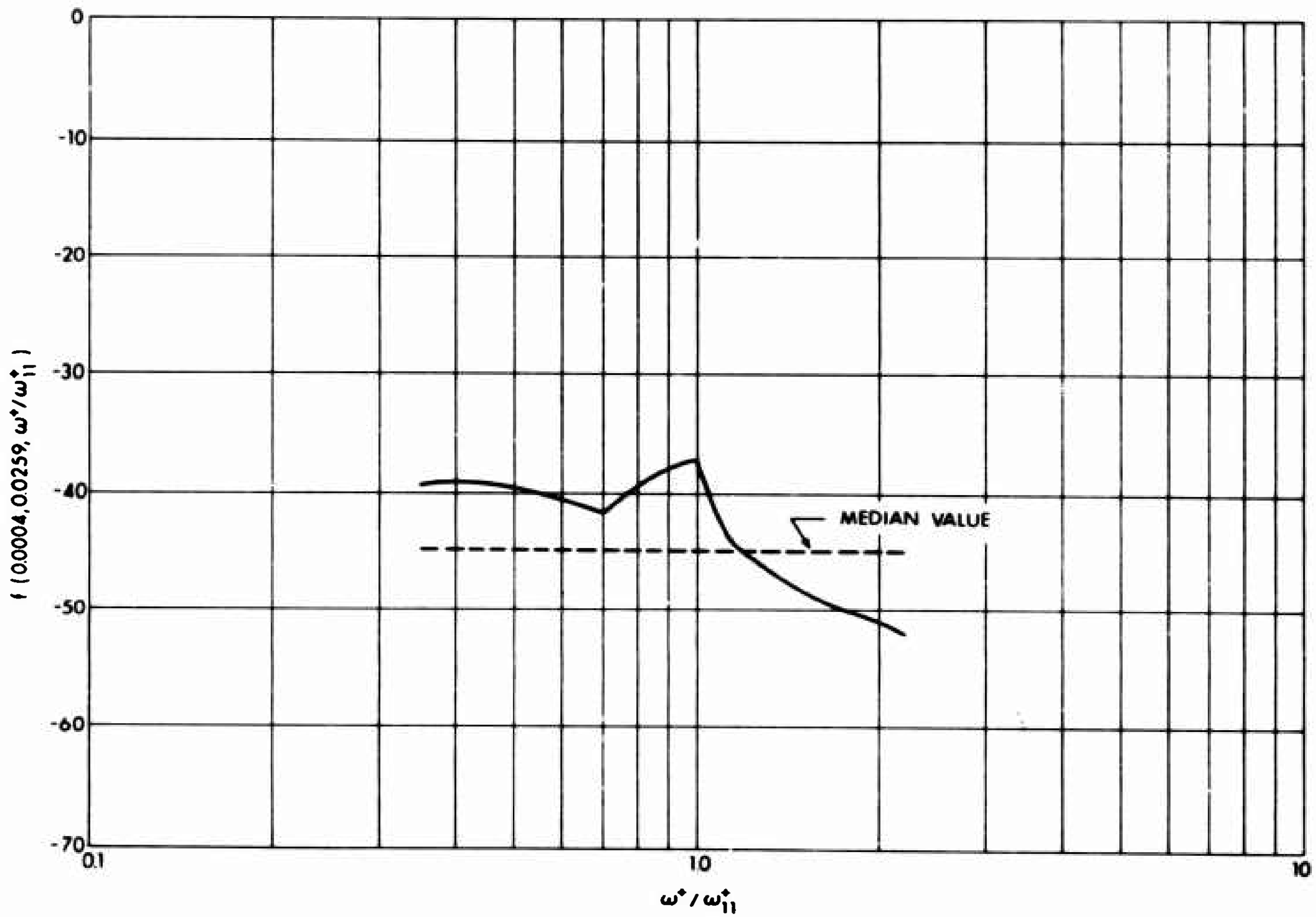

Figure 37. Effect of Plate Rigidity on the Dimensionless Cavity Acoustic Pressure Power Spectrum at Dimensionless Frequencies Below $1.932/\delta^+$

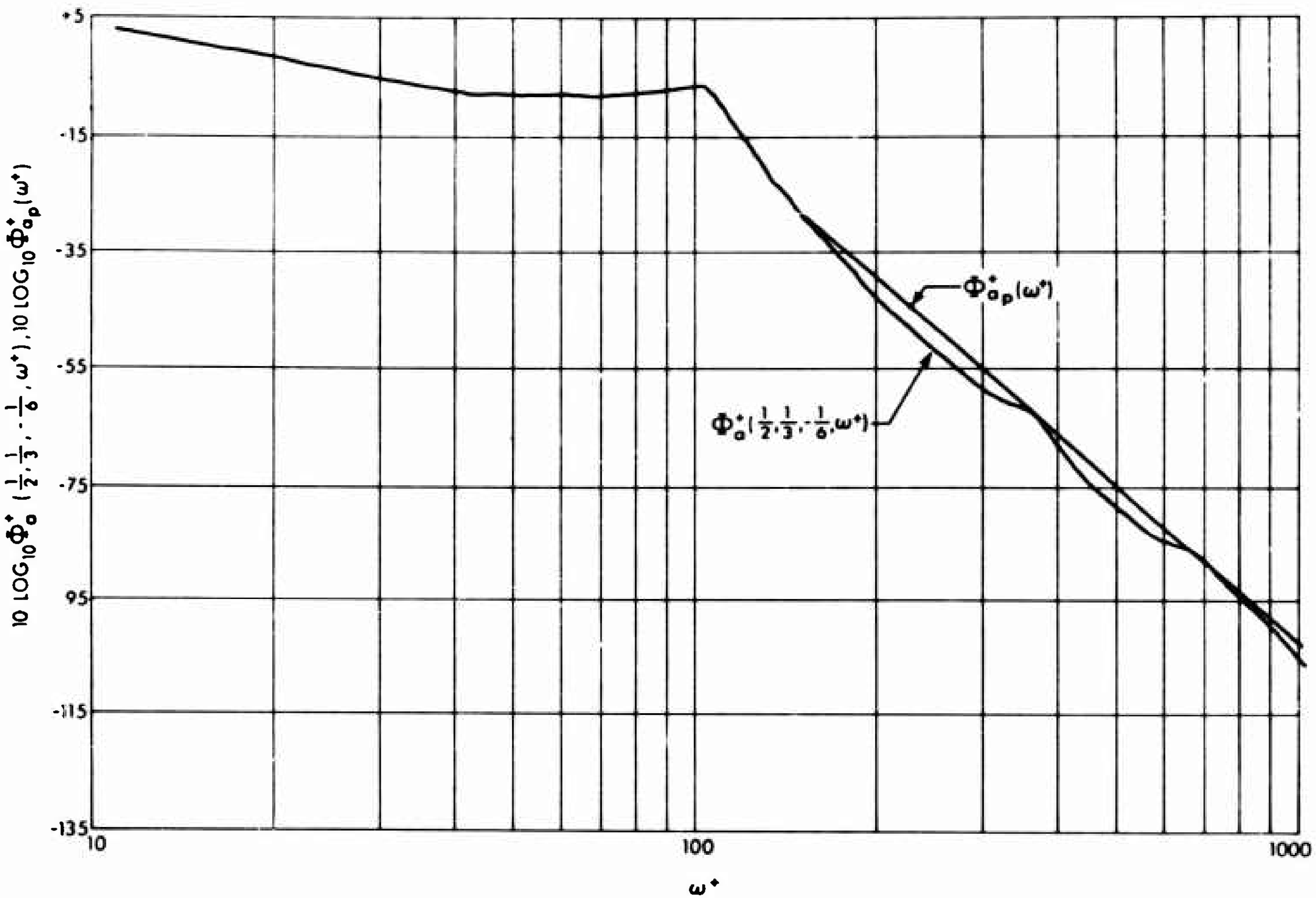

Figure 38. Comparison of Computed Dimensionless Cavity Acoustic Pressure Power Spectrum with Dimensionless Cavity Acoustic Pressure "Peak Spectrum" for Case 1 Parameters

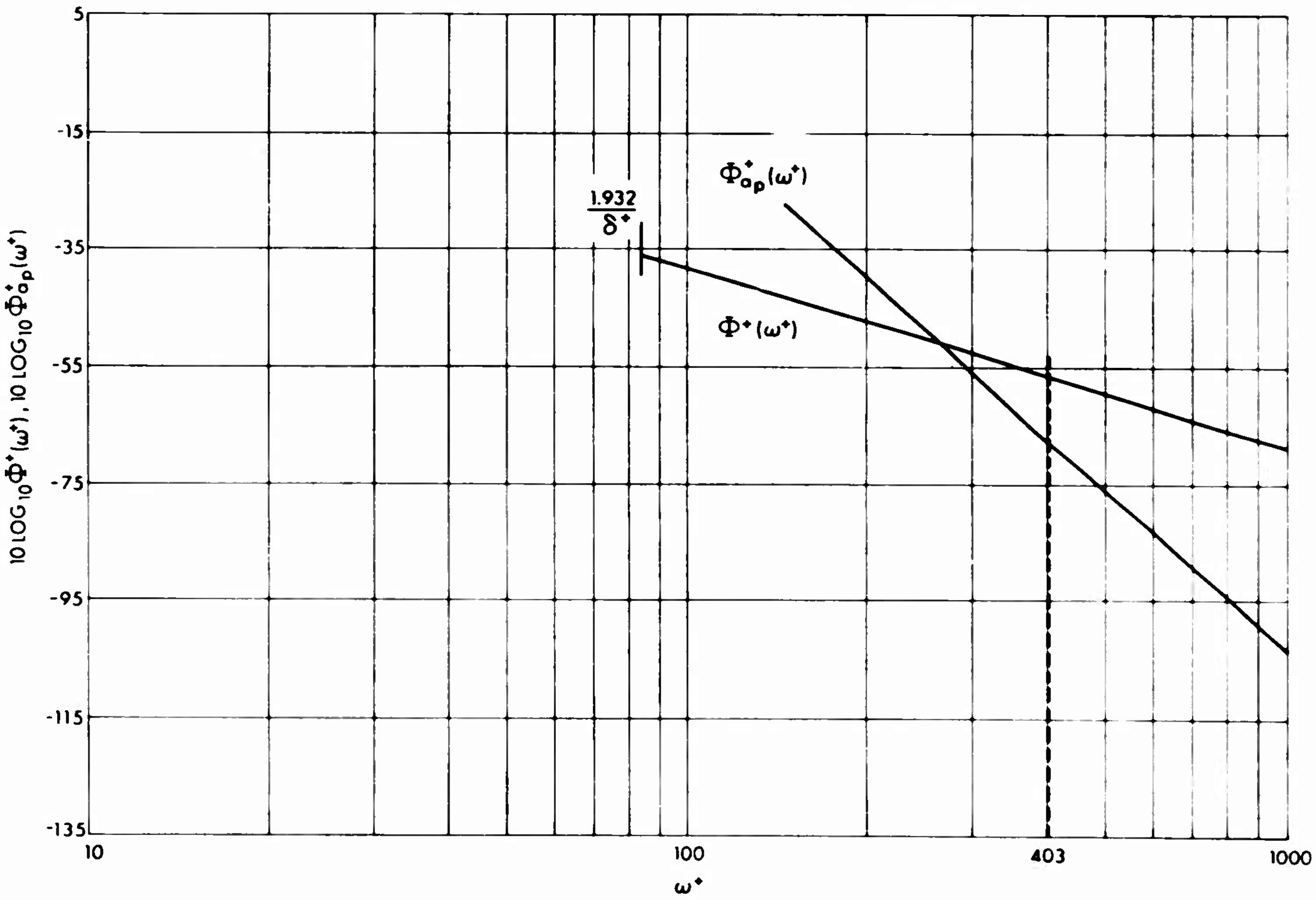

Figure 39. Comparison of Dimensionless Turbulent Pressure Power Spectra with Dimensionless Cavity Acoustic Pressure "Peak Spectrum" for Case 1 Parameters

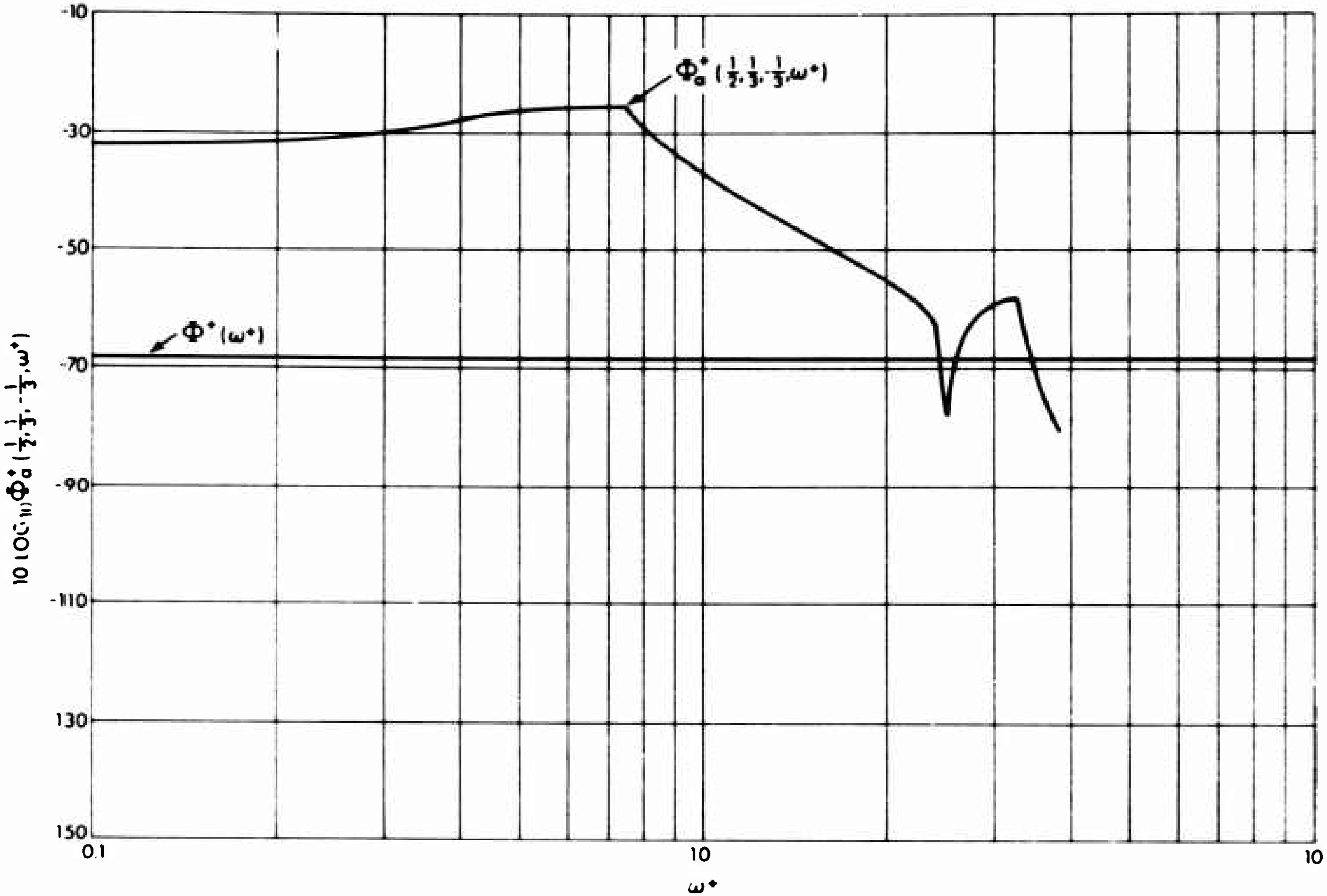

Figure 40. Comparison of Dimensionless Turbulent Pressure Power Spectra with Computed Dimensionless Cavity Acoustic Pressure Power Spectrum for Case 2 Parameters

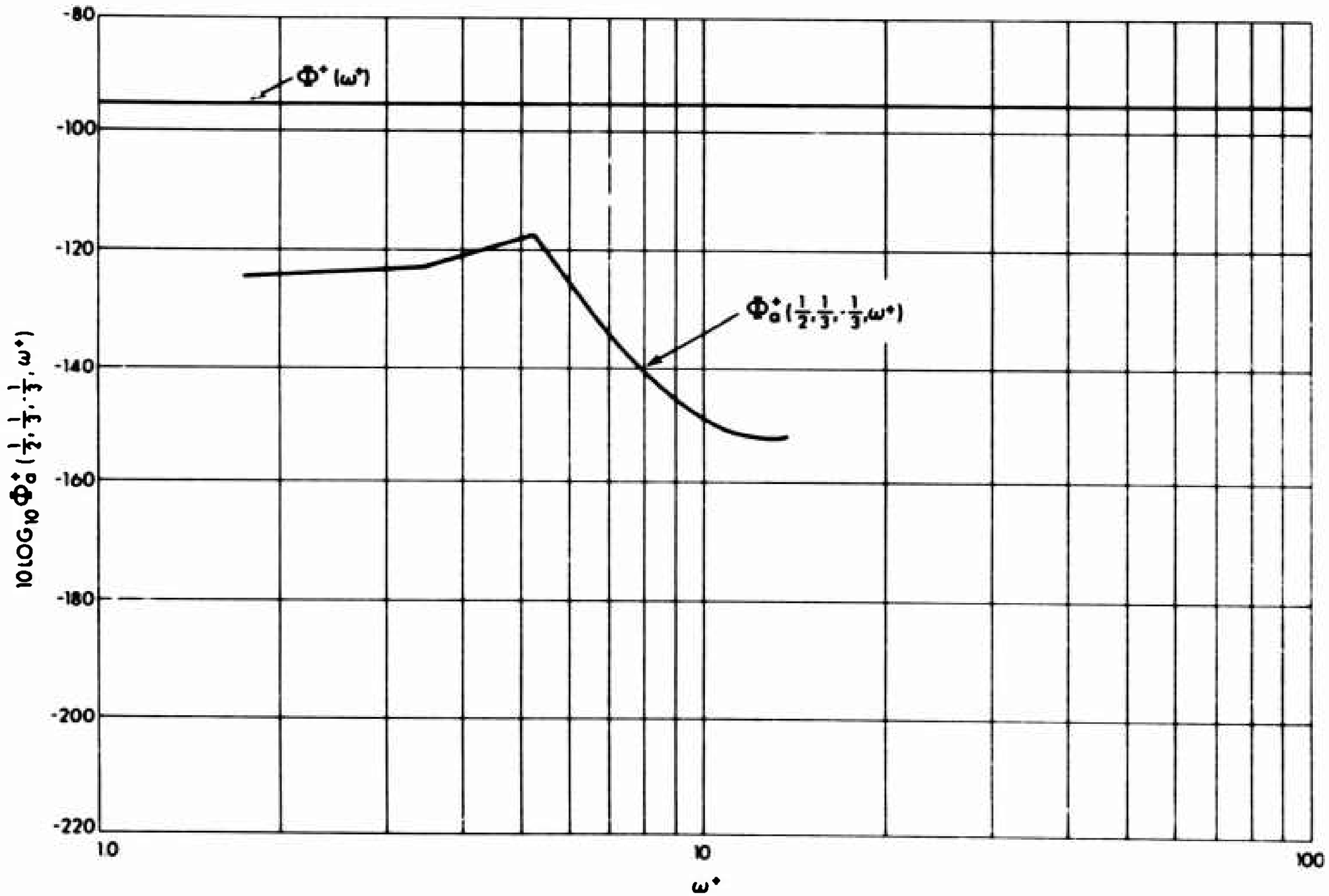

Figure 41. Comparison of Dimensionless Turbulent Pressure Power Spectra with Computed Dimensionless Cavity Acoustic Pressure Power Spectrum for Case 3 Parameters

UNCLASSIFIED
Security Classification

DOCUMENT CONTROL DATA - R & D

(Security classification of title, body of abstract and indexing annotation must be entered when the overall report is classified)

1. ORIGINATING ACTIVITY (Corporate author)
U. S. Navy Underwater Sound Laboratory
Fort Trumbull, New London, Connecticut

2a. REPORT SECURITY CLASSIFICATION
UNCLASSIFIED

2b. GROUP

3. REPORT TITLE
THE ACOUSTIC FIELD IN A CLOSED SPACE BEHIND A RECTANGULAR SIMPLY SUPPORTED PLATE EXCITED BY BOUNDARY LAYER TURBULENCE

4. DESCRIPTIVE NOTES (Type of report and inclusive dates)
Research (1966-1967)

5. AUTHOR(S) (First name, middle initial, last name)
Wayne A. Strawderman

6. REPORT DATE
11 May 1967

7a. TOTAL NO OF PAGES
153

7b. NO OF REFS
43

8a. CONTRACT OR GRANT NO

b. PROJECT NO
ZR 01101 01

c.

d.

9a. ORIGINATOR'S REPORT NUMBER(S)
827

9b. OTHER REPORT NO(S) (Any other numbers that may be assigned this report)

10. DISTRIBUTION STATEMENT
Distribution of this document is unlimited

11. SUPPLEMENTARY NOTES

12. SPONSORING MILITARY ACTIVITY
U. S. Navy

13. ABSTRACT

An analytic solution is obtained for the acoustic pressure statistics in a closed rectangular shaped cavity behind a simply supported, rectangular plate excited by boundary layer turbulence. The contribution of the cavity acoustic pressure is neglected as contributing to the plate excitation, leaving only the turbulent pressure fluctuations as the exciting force. The mathematical model for the turbulent pressure statistics is based on that of Corcos, which agrees well with experiment. A byproduct of this analysis is an analytic solution for the turbulent flow excited plate vibration velocity statistics. The plate velocity and cavity acoustic pressure statistics are expressed in the form of cross power spectral densities and power spectral densities. Dimensionless forms of the plate velocity spectral density and cavity acoustic pressure spectral density are developed.

The dimensionless plate velocity spectral density and dimensionless cavity acoustic pressure spectral density were computed, by means of a digital computer, for selected values of dimensionless input parameters. From these computed dimensionless spectra, the effects of major parameters on the plate velocity spectral density and the cavity acoustic pressure spectral density were determined.

DD FORM 1 NOV 65 1473 (PAGE 1)

S/N 0101-807-6801

UNCLASSIFIED
Security Classification

3ND PPSO 13152

14 KEY WORDS	LINK A		LINK B		LINK C	
	ROLE	WT	ROLE	WT	ROLE	WT
Vibrating Materials						
Wall Pressure Fluctuation						
Turbulent Boundary Layer						
Hydrodynamic Noise						
Turbulent Pressure						
Flow-Induced Noise						
Random Acoustics						